



POLITECNICO DI MILANO

Faculty of industrial engineering
Mechanical engineering – Production system

Evaluation of off design and dynamic performance of an ORC radial inflow turbine provided by IGV

Universitary tutor: Prof. Marco Astolfi
Company tutor: Ing. Marco Pelella

Lorenzo Marchi
ID Code 848213

Academic year 2016/2017

INDEX

1. ABSTRACT	8
2. INTRODUCTION	9
3. PROJECT PURPOSE AND DEVELOPED ACTIVITIES.....	12
4. ORGANIC RANKINE CYCLE	14
4.1. RANKINE CYCLE CONFIGURATION	14
4.2. ORC THERMODYNAMIC VIEW	16
4.3. MAIN COMPONENTS OF AN ORC SYSTEM	19
4.4. APPLICATIONS.....	19
4.5. WORKING FLUID	21
5. OREGEN™	26
5.1. ORegen™ CYCLE COMPONENTS:.....	28
5.2. ORegen™ APPLICATIONS	34
6. ORGANIC RANKINE CYCLE EXPANDER.....	35
6.1. VOLUMETRIC EXPANDER	35
6.2. TURBOEXPANDER	37
7. METHODOLOGY AND RESULTS OF THE STATIC MODEL	45
7.1. EQUATIONS OF STATE.....	46
7.2. MODEL DESCRIPTION	47
7.3. MODEL TUNING WITH CFD DATA	51
7.4. DEPENDANCE EQUATIONS	53
7.5. VERIFICATION AND COMPARISON	64
7.6. CONCLUSION	70
8. MAP CREATION	106
9. DYNAMIC MODEL	120
9.1. DATA MATCH	128
9.2. BEHAVIOR OF THE POWER RELATED TO THE IGV	90
9.3. CONCLUSION	93
10. FINAL CONCLUSIONS	94
11. APPENDIX: MASS FLOW.....	95
12. BIBLIOGRAPHY	150

PICTURE INDEX

Figure 4-1 Basic Rankine cycle	14
Figure 4-2 Supercritical and subcritical Rankine cycle	15
Figure 4-3 Rankine cycle with internal regenerative exchanger.....	16
Figure 4-4 ORC cycle on a Temperature – Entropy diagram	17
Figure 4-5 Percentage of installed applications of the ORC (Gaetano Chinnici, 2015).....	21
Figure 4-6 T-s diagram for wet fluids	23
Figure 4-7 T-s diagram for isentropic fluids	23
Figure 4-8 T-s diagram for dry fluids	24
Figure 4-9 Saturation curve of different fluids	24
Figure 5-1 GE oil&gas.....	27
Figure 5-2 ORegen™ Waste heat recovery cycle composed by: Waste heat recovery unit, oil cycle and ORC cycle	28
Figure 5-3 ORegen™ parallel oil configuration	30
Figure 5-4 ORegen™ Typical layout.....	32
Figure 6-1 Screw expander	35
Figure 6-2 Scroll expander.....	36
Figure 6-3 Turboexpander	38
Figure 6-4 Turboexpander section	40
Figure 6-5 16 blade wheel.....	41
Figure 6-6 Turbine scheme section.....	42
Figure 6-7 h-s diagram explaining turbine behavior.....	43
Figure 6-8 Velocity triangles for the wheel	44
Figure 7-1 Inlet velocity triangle	50
Figure 7-2 Graph of incidence related to the Csi wheel	54
Figure 7-3 Graph of Absolute Mach related to the Csi nozzle	56
Figure 7-4 Graph of %IGV related to the Csi nozzle	56
Figure 7-5 Graph of incidence related to the Cv wheel	58
Figure 7-6 Graph of relative Mach related to the coefficients	59
Figure 7-7 Graph of incidence related to the Cv wheel	60
Figure 7-8 Graph of incidence related to the wheel deviation angle	61
Figure 7-9 Graph of the relative Mach related to the coefficients	62
Figure 7-10 Graph of incidence related to the wheel deviation angle	62
Figure 7-11 Model vs CFD comparison	66
Figure 7-12 Model vs CFD comparison for eta	68
Figure 7-13 Model vs CFD comparison for the power.....	69
Figure 7-14 Model vs CFD comparison for the mass flow.....	69
Figure 8-1 %IGV related to Eta, changing the u/c value	111
Figure 8-2 Graph of U/C related to Tau for different inlet guided vanes opening	112
Figure 8-3 Graph of U/C related to Tau.....	77
Figure 8-4 Graph of U/C related to Tau zoomed.....	115
Figure 8-5 Graph of the angular coefficients related to the %IGV.....	116
Figure 8-6 u/c vs Tau for high and low pressure	118
Figure 9-1 Behavior of LP %IGV related to HP %IGV and Pcond= 1,36 bar	124

Figure 9-2 Behavior of LP %IGV related to HP %IGV and Pcond = 1,62 bar	125
Figure 9-3 Behavior of LP %IGV related to HP %IGV and Pcond = 2,10 bar	126
Figure 9-4 Power scheme.....	132
Figure 9-5 Graph of power related to %IGV with Pcond = 1,44	135
Figure 9-6 Graph of the mass flow related to the efficiency	92
Figure 10-1 Wheel profile.....	140
Figure 10-2 Graph of U/C related to Cp	141
Figure 10-3 Graph of IGV related to the coefficients.....	142

TABLE INDEX

Table 1 Advantages of an ORC vs steam Rankine cycle.....	18
Table 2 HP predictive model values	52
Table 3 LP predictive model values.....	52
Table 4 CSI wheel values for HP.....	54
Table 5 CSI nozzle values for HP.....	55
Table 6 CV nozzle values for HP.....	57
Table 7 CV wheel values for HP	57
Table 8 Coefficients related to the Mach	58
Table 9 Wheel deviation angle for HP.....	60
Table 10 Coefficients and average Mach values	61
Table 11 High pressure summary	63
Table 12 Low pressure summary	63
Table 15 Difference values	65
Table 19 Values for u/c = 1.....	109
Table 20 Values for u/c multiplied for 1,1.....	110
Table 21 Values for u/c multiplied for 1,2.....	111
Table 22 Values of adimensional torque for high pressure	119
Table 23 Values of adimensional torque for low pressure.....	119
Table 24 5 points of analysis.....	127
Table 25 Total power data match.....	131
Table 26 Different power values for pressure at the condenser equal to 1,4 bar.....	134
Table 27 Table of coefficients values related to the IGV	142
Table 28 Percentage difference between the mass flow calculated in different ways.....	101

ABBREVIATION INDEX

HP: High pressure
LP: Low pressure
IGV: Inlet guided vane
ORC: Organic Rankine Cycle
PLD: Pressure Let down
CFD: Computational Fluid Dynamics
WHRC: Waste Heat Recovery Cycle
WF: Working Fluid
WHRU: Waste Heat Recovery Unit
POD: Pressure Outer Diameter
TEX: Turboexpander

1. ABSTRACT

Con il presente lavoro di tesi si è voluto lavorare sul miglioramento del tool per la produzione delle mappe di prestazione dei turboespansori. In particolare il lavoro si è concentrato sulle macchine per applicazioni ORC (Organic Rankine Cycle), nelle quali sono presenti due espansori, uno di alta pressione e uno di bassa pressione.

Lo stesso lavoro ha avuto anche una ulteriore appendice relativa a macchine per applicazioni PLD (Pressure Let Down).

Data la iniziale mancanza di dati sperimentali accurati, si è ritenuto adeguato calibrare i modelli per le mappe sui risultati CFD post-processati, andando a tarare inizialmente cinque parametri di tuning, e successivamente il valore della potenza, cercando di individuare delle equazioni che descrivessero il comportamento di quest'ultimo, dipendente da altri fattori.

A monte di tutto è stata necessaria anche la validazione di un nuovo modello stazionario.

Le mappe di prestazioni ottenute sono state introdotte in modelli Hysys, sia dinamici sia stazionari, e utilizzate in un ampio range di condizioni operative.

Infine è stata eseguita una comparazione dei risultati ottenuti dal nuovo modello, con i dati di cantiere presi da un impianto ORC già installato e perfettamente funzionante.

The goal of this thesis is to work on the improvement of the tool for the production of the performances maps of the turboexpanders.

In particular the work has been focused on the turbo machinery for the ORC application (Organic Rankine Cycle), where are present two expanders, one of high pressure, and the other one of low pressure.

The ORC application produced in General Electric is called ORegenTM.

The same work has been done even on other application, as the machineries for PLD applications (Pressure Let Down).

Facing with the initial lack of experimental accurate data, I have calibrated the models for the maps on the CFD post-process results, calibrating initially five tuning parameters, and later on the value of the total power, trying to find some equations which would describe in the best way its behavior.

First of all, has been necessary the validation of a new stationary model

The performances maps obtained in this way have been introduced in stationary and dynamic models, and have been used in a huge range of operative condition.

Finally, has been done a comparison between the results obtained from the new model and the data field taken from an ORC plant actually working.

2. INTRODUCTION

The world energy consumption has risen to a level never reached before, releasing in the same process large quantities of CO₂ into the atmosphere. Current concerns over climate change call for measures to reduce greenhouse gases emissions, which will most likely include the following modifications of the current energy systems:

- A decrease in the energy intensity of buildings and industry.
- A shift from fossil fuels toward electricity, e.g. for transportation and space heating.
- Clean power generation by a massive shift toward renewable energies, comprising wind energy, PV, CSP, biomass, geothermal and large hydro.
- A reinforcement of the grid capacity and inter-regional transmission lines to absorb daily and seasonal fluctuations.

Among the proposed solutions to fulfill these objectives, the Organic Rankine Cycle (ORC) technology can play a non-negligible role, in particular for the first and the third objectives. (S. Quoilin, 2013)

The Organic Rankine cycle (ORC) is named for its use of an organic, high molecular mass fluid, with a liquid-vapor phase change, or boiling point, occurring at lower temperature than the water-steam phase change. (Siemens Organic Rankine Cycle Waste Heat Recovery with Orc, s.d.)

Looking at some experimental evaluation is possible to verify how the ORC can be a reasonable and advantageous choice for converting heat in mechanical and electrical energy.

The ORC is particularly suitable in the situations where is present heat at low temperatures (100-300 °C), that can't be used with the traditional systems. (S. Quoilin, 2013)

This is possible thank to the low boiling point, low latent heat of evaporation and high density of the organic fluids used. Then the specific heat of evaporation of the organic fluid is considered lower than that of water; this is the main reason for which the organic fluids are used in place of water for the recovery of heat from sources in the medium-low temperature range. (R. Capata, 2014)

Furthermore, the ORC is a perfect solution for the connection with renewable sources biomass energy, hot geothermal brines and solar energy in CSP plants, with consequent reduction of greenhouse gas emissions.

In the case of average temperature of the source below 250 °C, and power below 1 MW, the ORC is the best solution, having a high performance, low investment costs, reliability and being able to work even in remote places without any type of maintenance. (E. Macchi)

I'm going to focus my attention on the waste heat recovery from the industrial processes, being the ORegenTM, the Organic Rankine Cycle of GE, used for recovering waste heat of thermal plants.

The productive cycles of many energy-intensive sectors, are characterized by big quantities of waste thermal energy contained in the process flue gases. For recovering the energy of the flue gases, there could be some difficulties due to the low temperature, or due to the cyclicity of the productive process, that decreases the economy of the recovery of the energy.

For this reason are used Rankine cycle with organic fluid, characterized by higher performances compared with steam cycles. (Siemens Organic Rankine Cycle Waste Heat Recovery with Orc, s.d.)

The availability of heat that can be exploited, consists in a flow of hot gases, less frequently we speak of liquids. The heat exchange can happen directly between the thermal source and the working fluid, or indirectly.

Usually, in the case of waste heat from gases, the primary thermal source is not directly matched with the working fluid, but the heat is transferred using a thermal vector, that could be for example diathermic oil, or pressurized water or steam.

This solution brings many advantages from the point of view of the plant safety.

The thermal vector is able to transport heat at high temperature with low risk and low costs of transportation.

Instead when we treat with liquids, we have the direct exchange between the primary heat source and the working fluid of the ORC cycle.

The most interesting industrial sectors for the waste heat recovery, and electrical energy production are:

1. Cement

The production process of the cement is characterized by a huge availability of waste heat at medium/low temperature. The two main sources are the combustion gas of the furnace (250-400 °C), and the cooling air of the clinker (300°C).

2. Steel industry

The production of ferrous metals has good possibilities for what concern the thermal recovery.

The thermal heat can be obtained from, process “clean” fumes, which are due to the combustion of natural gas in ovens, or thermal treatments (low-medium temperature), or by foundry “dirt” fumes, that come from the fusion of the metal.

The productive process of this industry is less standardized, compared with the cement industry, and are present different recovery processes that are reliable.

This happens for the “clean” fumes, for temperatures higher than 400°C, while operating on the “dirt” fumes is much more complicate.

3. Glass

The glass production is, without doubts, another candidate for the application of thermal waste heat recovery systems.

From a technical point of view, the availability of gases from the fusion of gas at high temperatures (400-600 °C) can guarantee high electrical efficiencies. With the potentiality of production of electrical energy, even the energetic recover from this industrial sector could bring good results.

4. Other industrial sectors

Other interesting sectors for the heat recover are the petrochemical sectors, the production of non-ferrous material and ceramics.

More generally we can say that the Organic Rankine cycle can recover the heat from any industrial process where the thermal power available is over 3/5 MWt, translatable in an annual consumption of 20 $M\text{Sm}^3$ of natural gas. (E. Macchi)

3. PROJECT PURPOSE AND DEVELOPED ACTIVITIES

The waste-heat-recovery plants, are built both with axial turbines and radial turbines.

Axial turbines are usually projected for low ratio of pressure and high mass flows. Their design is connected to the molecular weight of the working fluid. In fact, if the fluids used have an high MW, instead of water, the turbine needs a lower number of stages. This is due to the smaller enthalpic drop.

The radial turbine is used with high pressure ratio and low mass flows. Their design allows an higher peripheral velocity.

These plants need attention in the phase of start-up and shut-down for the extreme conditions in which the expander must operate, and even for its interaction with the other parts of the plant.

Furthermore, the real gases used as engine fluid follow complicated laws.

The first objective of the work is the validation of an alternative stationary model, and the creation of performances maps for analyzing some points where the CFD is not done. Then the objective will be to find a method to model the outputs with transference function, in off-design conditions.

We will focus our attention on the Total Gas Power, trying to find its correlation with other values.

Finally, a comparison with data field obtained from experimental campaign on a real plant is performed.

Working in this way we would be able to have better information on the annual mode of operation of the plant, and we would even have the possibility of projecting it at the optimal technical-economical point.

The method I'm going to find, could be applicable for every turboexpander, of every plant.

We always start from post-processed CFD data, that for every TEX will naturally be different.

The equations I will find, must be re formulated every time, changing input data, and the correlations between the parameters, but the method will be replicable.

The Aero-thermodynamic operating prediction of the turbine is done using a not-stationary CFD 3D, and taking in consideration even the effect of the real gas and naturally the geometrical details. These calculations are of difficult elaboration, for this reason is general practice to create a CFD simulation data-base, for then enveloping a static model calibrated and validated on the CFD results (which has already been validated on a reduced number of experimental data-sets).

The performance maps, so obtained, are later introduced in Hysys model both dynamic and stationary, and used in a huge range.

In the development of the thesis the main issues that will be faced up are:

1. Analysis of the available 1D model of the turboexpander.
2. Comparison between the CFD and the 1D model results on a number of CFD simulations including design and off design conditions (for example increasing the pressure of condensation, which happens often in the real situation).
3. Validation of the methodology on the set of available CFD results
4. Calibration of a new set of equations to be introduced in the 1D model in order to create performances maps.

5. Generation of a new correlation of the nominal couple as function of parameters to be introduced in the whole ORegenTM model for off-design and dynamic simulation of the gas power plant.
6. Comparison of the results with experimental field data obtained by the real operation of an existing plant.

The turboexpander I'm going to treat and study during my work is part of a bigger waste-heat-recovery-cycle (WHRC) called **ORegenTM System**.

4. ORGANIC RANKINE CYCLE

The organic Rankine cycle presents the same configuration of a water Rankine cycle, but uses an organic fluid instead of water. Through the ORC we are able to convert heat in electrical energy using a Rankine cycle.

4.1. RANKINE CYCLE CONFIGURATION

The *basic Rankine cycle* is composed by 4 devices: pump, steam generator, turbine and condenser. In its original architecture, the operative fluid is water, but for temperature lower than 300 °C the traditional Rankine cycle with water is not performant. (S. Quoilin, 2013)

The cycle follows these transformations:

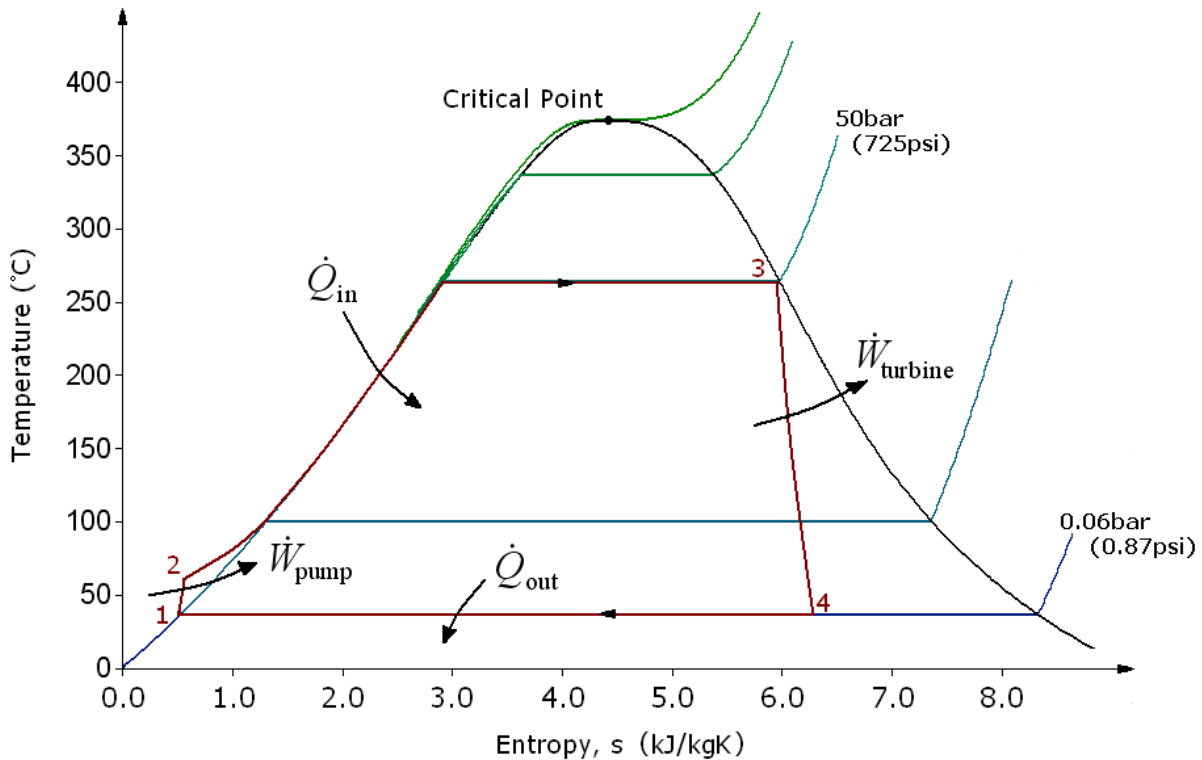


Figure 4-1 Basic Rankine cycle

There are four processes in the Rankine cycle. These states are identified by numbers (in brown) in the above T-s diagram.

- **Process 1–2:** The working fluid is pumped from low to high pressure. As the fluid is a liquid at this stage, the pump requires little input energy.
- **Process 2–3:** The high-pressure liquid enters a boiler, where it is heated at constant pressure by an external heat source to become a dry saturated vapor.
- **Process 3–4:** The dry saturated vapor expands through a turbine, generating power. This decreases the temperature and pressure of the vapor, and some condensation may occur.

- **Process 4–1:** The wet vapor then enters a condenser where it is condensed at a constant pressure to become a saturated liquid.

In an ideal Rankine cycle the pump and turbine would be isentropic, generating no entropy and hence maximizing the output. Processes 1–2 and 3–4 would be represented by vertical lines on the diagram. The Rankine cycle shown here prevents the vapor ending up in the superheat region after the expansion in the turbine, which reduces the energy removed by the condensers.

The Rankine cycle with water finds huge application in the big thermoelectrical power plants, typically powered by coal or biomass or coke.

For increasing the efficiency of these plants is used the preheat, superheat and regenerative spills for pre-heating the feed water.

Using instead the *Supercritical Rankine cycle*, is not present an evaporation interval, but the working fluid changes phase without passing through the biphasic zone. In this way the exegetical losses in the thermal exchange will be lower compared to the subcritical cycles. (Sotirios Karellas, 2014)

The cycle is called “*Transcritical*” when the critical pressure is between the minimum and maximum pressure of the cycle.

Is said “*Supercritical*” when the whole cycle is over the critical point.

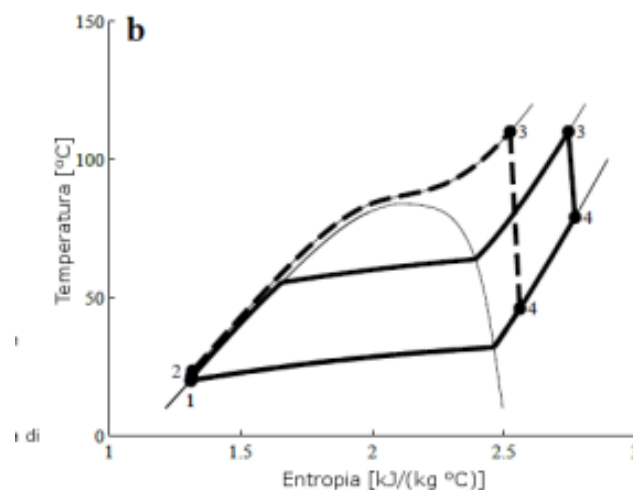


Figure 4-2 *Supercritical and subcritical Rankine cycle*

The exchangers work in a more efficient way with a supercritical. The thermal profile of source and working fluid are generally coupled in a better way.

Inserting a regenerator, we have a *Rankine cycle with internal regenerative exchanger*.

This cycle is used when is inserted a dry fluid; the regenerator allows to improve the thermal performance, even if the higher total cost must be taken in consideration.

It consists in an heat exchange from the fluid in the steam phase, going out from the turbine, to the fluid in the liquid phase which must be heated from the condensation temperature to the evaporation temperature. (Pedro J. Mago, 2007)

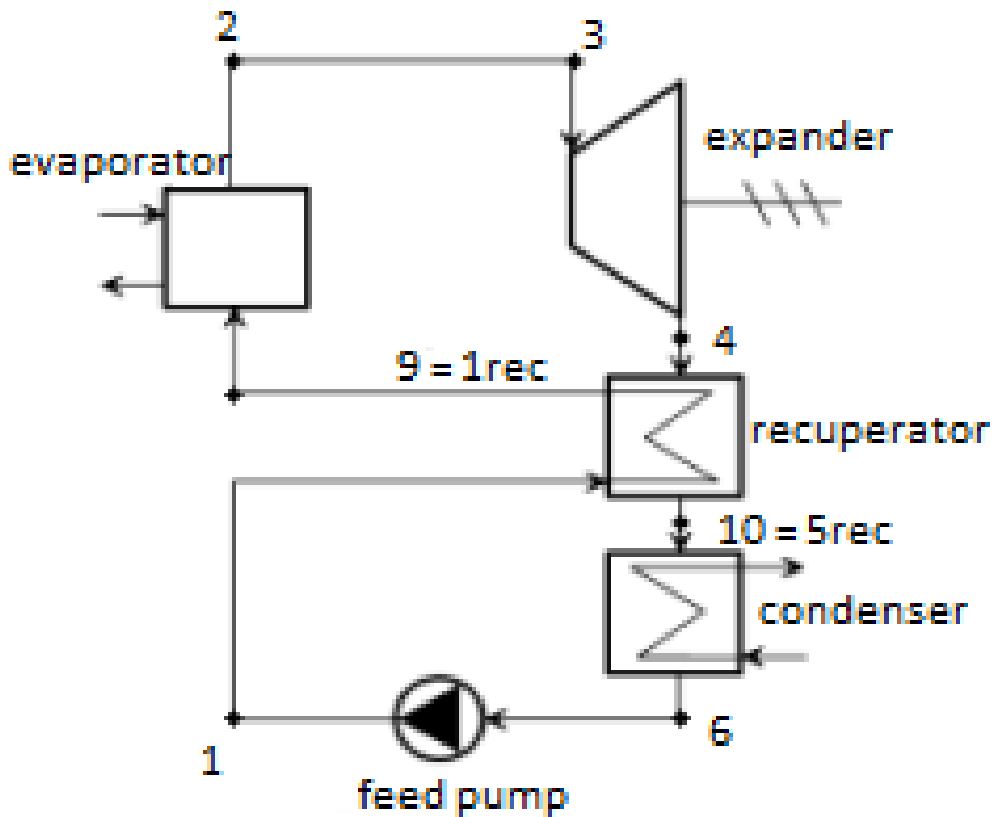


Figure 4-3 Rankine cycle with internal regenerative exchanger

Rankine cycle with re-overheating has never been analyzed with organic fluid, even if is common in the case of water cycle. It's always used in the big power plants.

Rankine cycle with binary fluids. Until now we have treated cycles with pure fluids, but some configurations work even with binaries mixtures.

Actually, the research is evaluating the possibility of introducing particular mixed fluids, with variable temperature of evaporation, in order to reduce the ΔT of the heat exchanger, and to increase the efficiency of the cycle. (Ghasemi, 2013)

4.2. ORC THERMODYNAMIC VIEW

The Rankine cycle is a thermodynamic cycle extremely diffused to produce electrical energy which converts heat in power. The classical cycle works with water fluid, which is heated, and the steam is expanded in the turbine.

The ORC is an application where is used an organic fluid as working fluid, instead of water, for producing energy.

The history of the Organic Rankine cycle (ORC) development spreads from the early 19th century until the ORC power systems became a substantial niche market in the 21st century power industry. (E. Macchi M. A., 2016)

The first organic fluid used substituting water was “nafta”, in 1883. Along the years were introduced solutions which use mixtures.

Nowadays, in the world, exist various applications for producing different power plants.

The cycle is composed by 4 phases, that in the hypothesis of an ideal thermodynamic cycle can be described as:

1. Isentropic compression
2. Isobar heating
3. Isentropic expansion
4. Isentropic cooling

The real cycle is far from the ideal one, because of the presence of pressure drops, and others dissipation phenomenon, due to the fact that the expansion and the compression are not anymore isentropic.

We can describe it in this way:

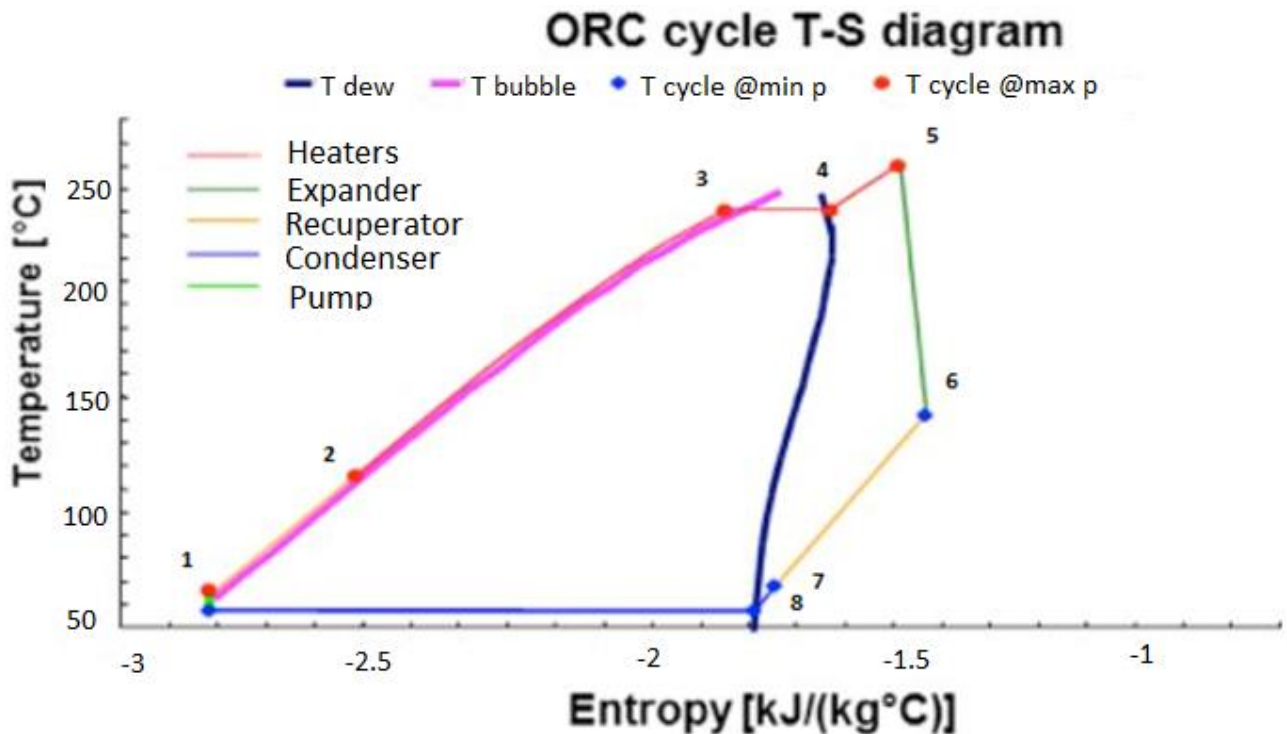


Figure 4-4 ORC cycle on a Temperature – Entropy diagram

1. The working fluid (WF) is pumped into a series of heat exchangers where it is heated (1-3), using a pre-heater, vaporized (3-4), using an evaporator, and slightly superheated (4-5) with a heater, even if this is not always necessary.

2. Subsequently the Working fluid passes through a Turboexpander (5-6), where its pressure and temperature decrease and the useful work is extracted.
3. Since the temperature at the end of the expansion (6) is considerably higher than the condensation temperature, the exhaust vapor flows through the recuperator (6-7).
4. Finally, the Working fluid is condensed using a Condenser (7-8-1). In the ideal cycle, the expansion is isentropic and the evaporation and condensation processes are isobaric.

In the real cycle, the presence of irreversible processes, decreases the cycle efficiency. Those irreversible situations mainly occur:

- During the expansion: Only a part of the energy recoverable from the pressure difference is transformed into useful work. The other part is converted into heat and lost. The efficiency of the expander is defined by comparison with an isentropic expansion.
- In the heat exchangers: The Working fluid path ensures effective heat transfer but causes pressure drops that decreases the amount of recoverable power from the cycle.

ADVANTAGES ORC	ADVANTAGES STEAM RANKINE CYCLE
<ul style="list-style-type: none"> • Lower Inlet Temperature in the turbine • Lower evaporation pressure • Higher condensation pressure • No water treatment • Low cost and higher safety since the plant operates with lower temperatures and pressures • Recover of the heat at low temperature • Boiler without recycling • Higher density of the fluid • Lack of erosion due to the absence of liquid in the final phases of the expansion • High reliability, and low need of maintenance • ORC plant is safe, due to the presence of diathermic oil, which is a thermal vector fluid at high boiling point and not toxic. 	<ul style="list-style-type: none"> • Higher Efficiency • Low cost of the fluid • Fluid “environmental friendly” • Fluid chemically stable

Table 1 Advantages of an ORC vs steam Rankine cycle

4.3. MAIN COMPONENTS OF AN ORC SYSTEM

Expander

Depending on the volumetric flow, different type of expanders are used.

For small power volumetric expanders are preferable, while in the case of big electrical power, are used axial or radial turboexpanders.

In particular the radial turbine with radial outflow turbines are preferred in case the fluid is due to high volumetric variation during the expansion.

The significant advantage of radial outflow turbine is:

1. a flow direction from a smaller to a bigger radius corresponds to an area increase of the flow path which is helpful for expanding organic fluids with high volume flow ratios. (Weis, 2015)

The axial instead is used when there is an application that needs the use of a medium-big sized machine. The radial centripetal expander is used with low flows and big pressure drop.

Furthermore, if the working fluid is characterized by a high molecular weight, the expander must work at low peripheral speed and with minimum mechanical stresses.

Feed pump

Usually are used centrifugal and hydrodynamics pumps, avoiding in this way the contact between the fluid and the air, guarantying so a higher reliability. Typically, a centrifugal pump would be used in a large-scale ORC as the flow and pressure requirements could easily be matched. A small ORC requires a much lower flow rate with the same pressure.

Heat exchanger

The heat exchanger most used is the model Shell &Tubed. In the Organic Rankine cycle, usually there are 3 heat exchangers:

The first one through which is introduced the heat in the cycle, the recuperator, and the condenser. The condenser is a very important component which can influence the overall system performance regarding the heat sink of thermodynamic cycle. (R. Capata, 2014)

4.4. APPLICATIONS

The features of the fluid permit to exploit small enthalpy gap at medium-low temperature, where the Rankine cycle with steam would be limited. The technology of the steam Rankine cycle is not particularly performant for temperatures below 350 °C, while at the same temperature with an organic fluid the performances keep being at a good level. This happens because the inlet temperature in the ORC expander is usually lower than 350-400°C, while in the steam Rankine cycle the inlet temperature of the turbine must be higher than 450°C.

This causes an increase of the thermal stresses in the boiler, and on the vane, and an increase of the costs. (S. Quoilin, 2013)

The possible applications are a lot, but the most promising fields are:

- **Geothermal plants**

The geothermal is showed up as rocks, water or hot steam, and are available over a broad range of temperatures. Could be at high temperature ($>180^{\circ}\text{C}$), medium ($100\text{-}180^{\circ}\text{C}$) or low temperature ($<100^{\circ}\text{C}$). The actual technological lower bound for power generation is about 80°C : below this temperature the conversion efficiency becomes too small, and geothermal plants are not economical. (Gaetano Chinnici, 2015)

We can even distinguish between “dry” and “wet” geothermal depending on the quantity of steam present at well head.

The ORC is perfectly adapted for this kind of application. However, is to keep in mind that for low-temperature sources, the efficiency is low, and depends strongly on heat sink temperature.

- **Waste heat recovery**

The potential offered by this category (waste heat recovery cycle), is huge and involves different sectors as the industrial one, the domestic sector and the transportation one.

The heat can be recovered by the air, hot gases, exhaust fumes, steam of process and even solids.

The thermal levels can be distinguished in low ($<150^{\circ}\text{C}$), medium ($150\text{-}400^{\circ}\text{C}$) and high ($>400^{\circ}\text{C}$).

- **Biomass power plant**

The biomasses have different origins, as for example wood, waste products of agriculture, waste of animal origins and urban solid waste.

Biomass is widely available in a number of agricultural or industrial processes such as wood industry or agricultural waste. Among other means, it can be converted into electricity by combustion to obtain heat, which is in turn converted into electricity through a thermodynamic cycle. The cost of biomass is significantly lower than that of fossil fuels. (Gaetano Chinnici, 2015)

The problem of high specific investment costs for machinery, such as boilers, are overcome due to the low working pressures in ORC power plants. Another important advantage is the long operational life of the machine due to the characteristics of the working fluid.

The ORC process also helps to overcome the relatively small amount of input fuel available in many regions because an efficient ORC power plant is possible for smaller sized plants.

- **Solar thermal power**

Solar energy is the biggest renewable source on the earth. The sun supplies to earth a power of 1000 W/m^2 and an energy of $3,9 \cdot 10^6$ EJ/year.

The exploitable potential with the technologies, nowadays is of $1500\text{-}50000$ EJ/year.

The available technologies are the solar photovoltaic and thermal panels. The ORC allows power generation at lower capacities and with a lower collector temperature, and hence the possibility for low-cost.

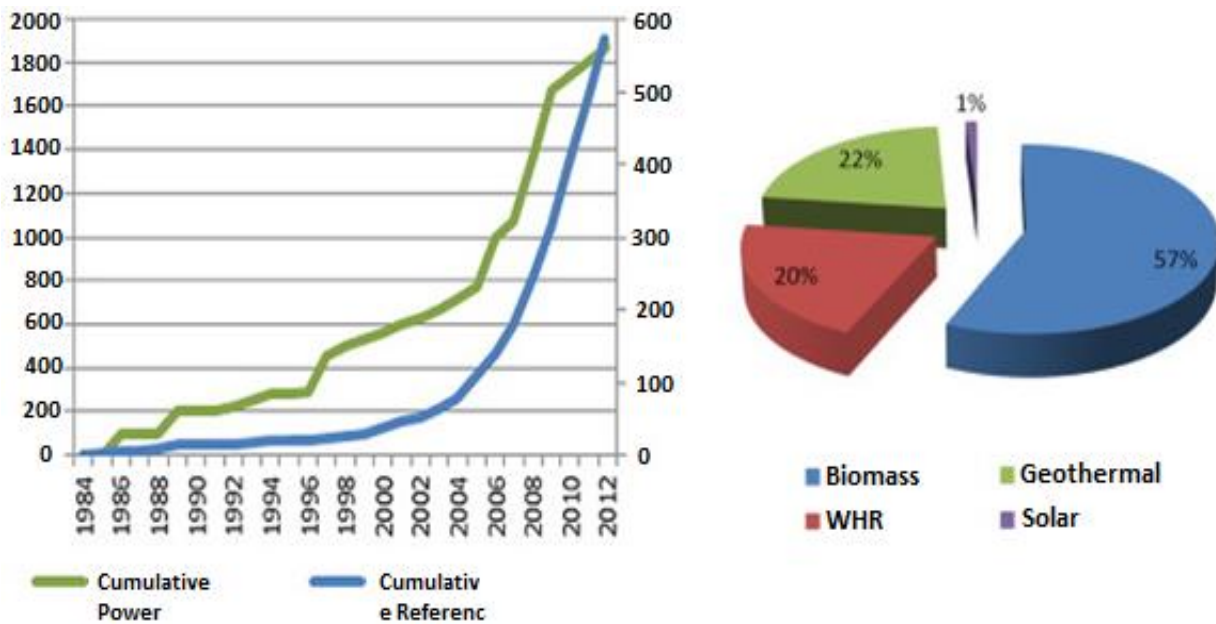


Figure 4-5 Percentage of installed applications of the ORC (Gaetano Chinnici, 2015)

4.5. WORKING FLUID

The selection of the working fluid is of crucial importance for the maximization of the efficiency of an organic Rankine Cycle. There are some characteristics that must be respected.

The efficiency of an ORC plant strongly depends on the physic and thermodynamic features of the fluid. The main features are:

- **Critical temperature**

The expansion ratio is strongly connected to the critical temperature, and particularly the pressure ratio increases with the increase of the critical temperature. Once we know the evaporation temperature, and the condensation temperature, the efficiency of the system is strongly influenced by the critical temperature.

- **High density**

To have a high-density fluid is important both for the liquid phase and for the steam phase, for increasing the efficiency and decreasing the costs.

Is particularly important at low pressure, so at the end of the expander, because these fluids permit to reduce the volumetric flow, with important advantages in term of size of components, and pressure drops in the exchangers.

- **Molecular weight**

The molecular weight of organic fluid is always higher than the one of water (18 kg/Kmol).

Having a fluid with higher molecular weight, permit to work at higher temperatures, and so is possible to reach higher efficiencies.

Actually, pressures play a big role, Moreover Δh evaporation decreases, and mass flow rate soars. This is particularly advantageous in the plants that use low condensation pressures, because permits to reduce size and complexity of the expander, and even of other components.

- **High thermal conductivity**

Fluids with good conductivity realize better heat exchange coefficients in the exchanger.

- **Low viscosity**

A low viscosity both of liquid and of the vapor phase is necessary for maintaining low pressure drops in the expanders and in the pipes, high heat transfer coefficients and low friction losses in the heat exchangers. (Quolini, 2012)

- **Thermal stability**

While the water does not have any problem of stability at high temperatures, the organic fluid can have some problem. For this reason, must be stabled a maximum process temperature.

- **It must not be toxic and corrosive, for interacting with the lubricants and materials**

The inflammability index is used for indicating the inflammable features of a fluid. There are even some chemical and toxic indexes, as for example ASHRAE (America society of heating, refrigerating and air-conditioning engineers) which indicate some features as corrosion and toxicity. Fundamental is even the chemical stability. Almost every fluid suffers of a deterioration and a chemical composition at high temperatures. For this reason, a working fluid will be used in a ORC plant only if its chemical stability temperature is higher than the maximum temperature of the cycle, and well below the unstable condition. (Hung T.C., 1997)

Than naturally the fluid must be compatible and not react when in contact with the materials of the plant, and with the lubricants. (Chen H., 2010)

- **Low cost and reliable**

No organic fluid could compete with water under these aspects, anyway the economical aspect strongly depends on these two aspects. The organic fluid must be easy to find, and at the same time must have a reasonable price.

- **Freezing point**

For avoiding problems in the pipes, and generally in the plant, the freezing point must be lower than the lowest temperature reached in the cycle.

- **Low environmental impact**

For what concern the environmental impact, exist some important indexes as GWP (global warming potential) and ODP (Ozone depletion potential), that indicate how much the fluid would influence the global warming and the ozone depletion in the case it would be released in the atmosphere. (D.J., 1983)

Some working fluids, as R11, R113 and R114 manifest higher thermodynamic performances, even if have high ODP and GWP, while other fluids as R245fa and R245ca are the most environment-friendly working fluids for engine waste heat-recovery applications. (E. Macchi M. A.)

Other fluids as for example R141b, even if it has good thermodynamic performances is forbidden from 2010, R123 will be prohibited in 2020 and R-22 in 2030 in the whole world. (E. Macchi M. A.) (Ramaija, 2012)

- **Saturation curve of steam in the T-s diagram must be positive**

Concentrating on the slope of the saturation curve we can divide the type of fluid.

If the slope is negative ($dT/ds < 0$), the fluid can be catalogued as *wet*, if it's positive ($dT/ds > 0$) we are speaking of dry fluid, while if the slope is infinite we are working with isentropic fluid.

The wet fluids as water, need to be super-heated before entering in the turbine, for avoiding that at the end of the expansion the steam quality would be too small.

Furthermore, low values of quality are to avoid, because having liquid drops in the steam part could damage in an irreparable way the turbine, decreasing so the efficiency and reliability of the cycle.

With isentropic and dry fluids, there is no need of superheat, and for this reason are preferable in the choice of the fluid for the ORC cycles.

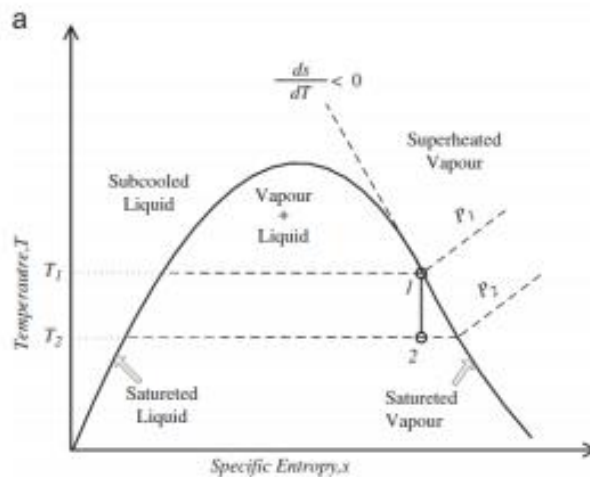


Figure 4-6 T-s diagram for wet fluids

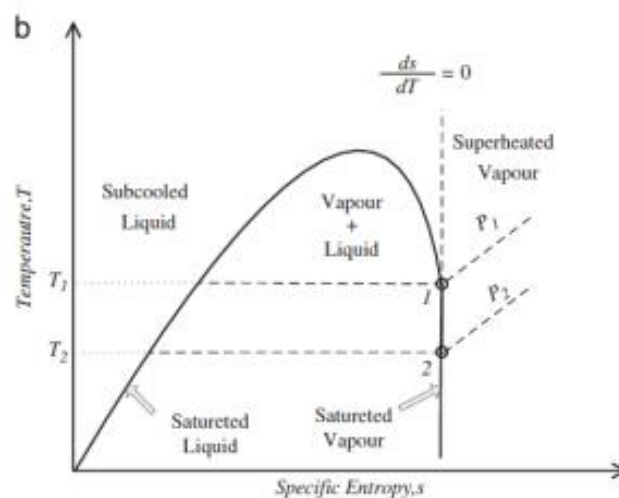


Figure 4-7 T-s diagram for isentropic fluids

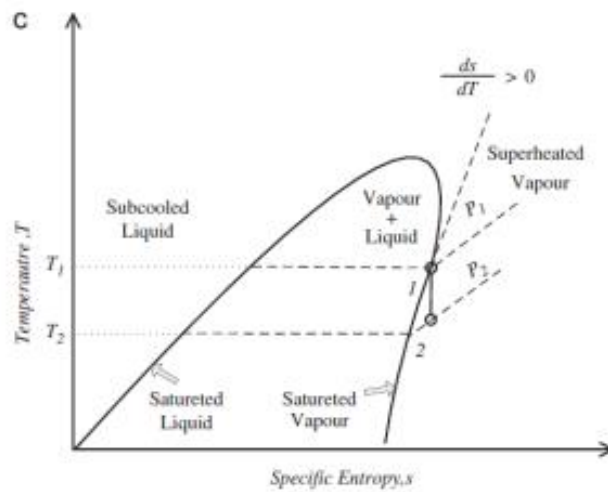


Figure 4-8 T-s diagram for dry fluids

Especially isentropic fluids are the better choice, because apart from staying saturated for the whole expansion, permits even to avoid the presence of a recuperator for decreasing the gas temperature. (D.J., 1983)

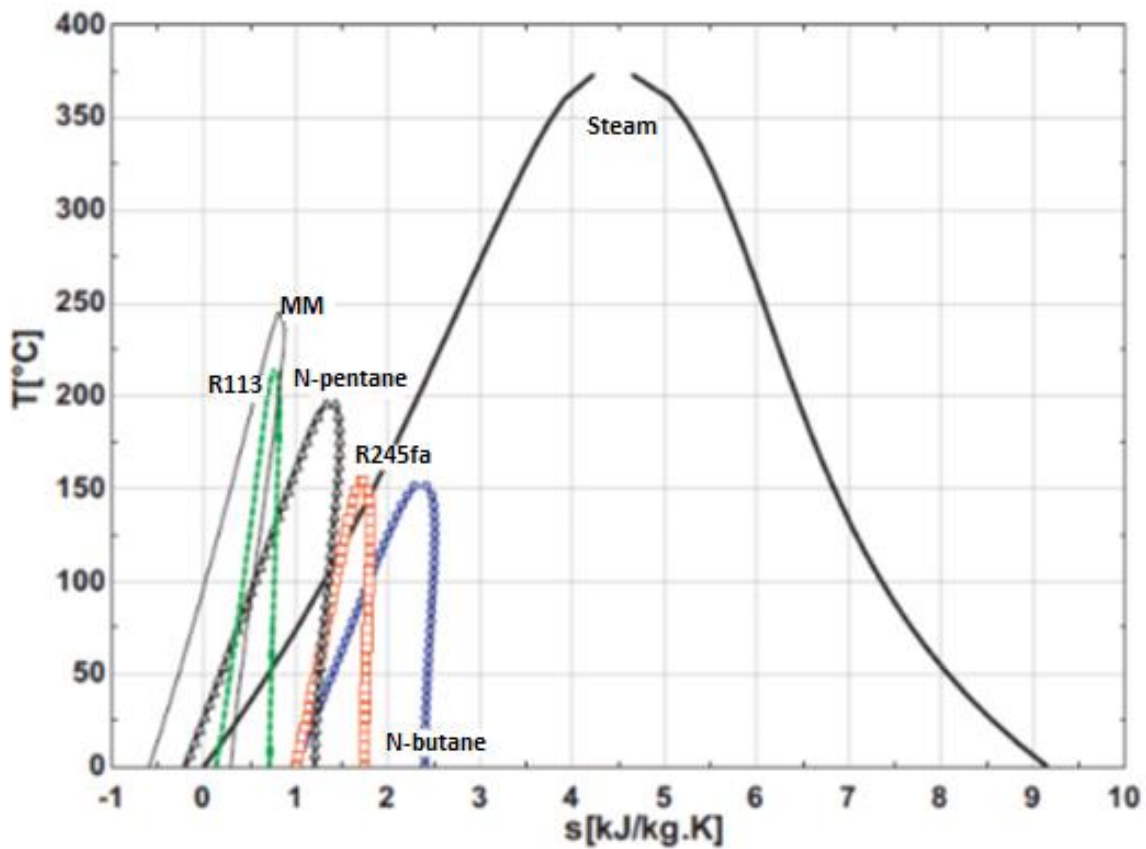


Figure 4-9 Saturation curve of different fluids

As we can see from this picture the organic fluid has a lower critical point, compared with the steam critical point, and the slope of the saturation curve is substantially different. (E.H. Wang, 2011)
(Kang, 2013)

5. OREGEN™

ORegen™ is the Organic Rankine cycle (ORC) produced by General Electric; a thermodynamic superheat cycle that recovers waste heat from gas turbine exhaust and converts it into electric energy, using cycle-pentane as working fluid. Through the ORC we are able to convert heat in electrical energy using a Rankine cycle, which uses an organic substance with high molecular weight as working fluid. (General Electric, s.d.)

Just a short overview on General Electric in Italy.

General Electric (GE) is an American multinational conglomerate corporation incorporated in New York and headquartered in Boston, Massachusetts.

As of 2016, the company operates through the following segments: Aviation, Current, Digital, Energy Connections, Global Research, Healthcare, Lighting, Oil and Gas, Power, Renewable Energy, Transportation, and Capital which cater to the needs of Financial services, Medical devices, Life Sciences, Pharmaceutical, Automotive, Software development and Engineering industries.

General Electric is present in our country since 1921, with an amount of 11500 dependents which operate in 7 divisions in 38 head offices.

- GE Oil & Gas, located in Florence, is the most important sector both for its size and for being the head quarter for many products. Other factories in Italy are in Massa, Talamona, Bari, Casavatore e Vibo Valentia. Oil & Gas was born after the acquisition from ENI of the society “Nuovo Pignone”. Its production goes from compressive system for the extraction, refining and transportation of oil and gas, as centrifugal compressors, centrifugal pumps and steam and gas turbines.
- Avio Aero, is a sector of GE aviation which operates in the design, production and maintenance of components and systems for the civil aviation and for the air force. It’s the excellence center of the whole group in the field of transmissions and for what concerns low pressure turbines. In Italy, has more than 4 000 dependents in the main factory in Torino, and in Brindisi and Pomigliano d’Arco (Napoli).
- GE Healthcare, located in Milano, working in the biomedical sector. It commercializes and assists diagnostic machineries as: TAC, PET, X-Ray, ultrasound, resuscitation devices and contrast liquid.
- GE Energy, that since 1957 produces gas generators. Principally it takes up the cogeneration from renewables.
- GE Capital is a banking group which offers financial services to the companies, leasing and factoring.
- GE Transportation System of Florence, which operates in the rail signaling field.
- GE Industrial Solution, composed by:
 - GE Power Protection, located in Agrate and Chiuduno (BG), which operates in the field of electric boards in low and medium tension.
 - GE Lighting, which operates in the illumination sector.
 - GE Appliances, which operates in the domestic electrical appliances field.

NUOVO PIGNONE

Nuovo Pignone is the main company of the Group “GE Oil and Gas”, and entered in the General Electric world 20 years ago, in 1994, when GE decided to invest in the manufacturing competences and in the technological and innovative capabilities of the Italian Company.

Nuovo Pignone represents for the group “GE oil and Gas” the world excellence center for the gas turbines, compressors and pumps. In Italy, it counts 5300 workers split in 6 productive plants as shown in figure 5-1.

- Firenze
- Massa
- Bari
- Vibo Valentia
- Talamona (SO)
- Casavatore (NA)



Figure 5-1 GE oil&gas

After 20 years from the acquisition (1994-2014), GE Oil & Gas had grown up 20 times in terms of orders while Nuovo Pignone has grown up seven times. (General Electric, s.d.)

5.1.OREgen™ CYCLE COMPONENTS:

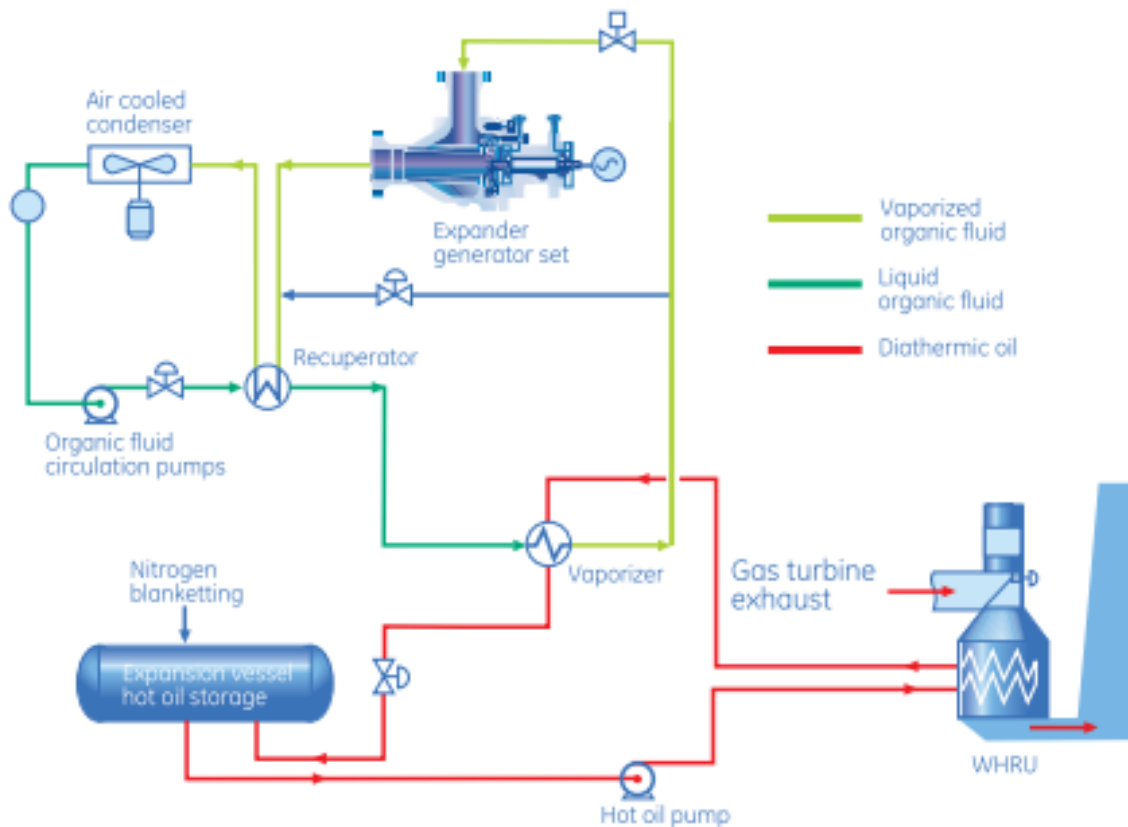


Figure 5-2 ORegen™ Waste heat recovery cycle composed by: Waste heat recovery unit, oil cycle and ORC cycle

- ✓ **TURBINES:** The flue gases come from turbines. Can be three out of four existing turbines (three in operation and one in standby), or even two out of three turbines. It depends on the plant.
- ✓ **WASTE HEAT RECOVERY UNIT:** The gases pass through a waste-heat-recovery-unit, one for each turbine, where they release the heat to the thermal oil system.
- ✓ **THERMAL OIL SYSTEM:** The Thermal oil system is a closed loop circuit to transfer the heat recovered from the gas turbines flue gases to the ORC system. The temperature and

the mass flow of the oil are regulated, and then it's sent to the evaporator. It's composed by:

- ***Thermal Oil circulation pumps***

Thermal oil pumps, or hot oil pumps as they are otherwise known, are designed for the movement of heat-transfer oil under high temperature conditions.

- ***Thermal Oil emergency pump***

Is a pump used in case of emergency, only when the other pumps, for some reasons won't be working.

- ***Thermal Oil cleaning filter***

This device has the function of cleaning the thermal oil. This function is fundamental, because an incorrect cleaning of the thermal oil could involve problems of sliding in the pipe.

- ***Thermal Oil expansion vessels and distribution***

An expansion vessel is a small tank used in closed heating systems. From this vessel than will start even the distribution of the thermal oil.

- ***Waste heat recovery unit bundle***

Fundamental for the heat transfer from the thermal oil to the organic fluid. Through this device we can heat the cyclopentane. The bundle consists of several serpentes arranged in tube rows perpendicular to the flue flow.

To ensure the mechanical integrity of the tubes, the relevant skin temperature should be lower than the design temperature. So, when the hot flue gases pass through the bundle, the tubes must be cooled.

✓ **WORKING FLUID ORC SYSTEM:** The ORC system is a closed loop circuit which convert thermal energy to power output. The Organic Rankine cycle main equipment are:

- ***Working fluid circulation pump*** → Consists of three centrifugal pumps, two working pumps and one in standby. The circulation pumps take suction from the condensate collector and deliver working fluid flow to the heat exchangers. Each pump discharge line is provided with an automatic recirculation valve to ensure that required minimum flow is ensured through the pump at all times.
- ***Recuperator*** → Its special purpose is the energy recovery from the heat exchanger.
- ***Heat exchanger*** train composed by:
 1. ***Preheaters*** → They preheat the liquid flow close to the saturation liquid curve.
 2. ***Evaporator*** → Performs the phase change from liquid to vapor of the WF flow.
 3. ***Superheater*** → Used for increasing the temperature of the gas.
- ***Turboexpander unit***

- **Condensing system** that consist of:
 1. Air cooled condenser → Performs the phase change from vapor to liquid of the WF coming from the TEX outlet.
 2. Condensate collector.
 3. Non-condensable gases removal system.
- **Drain system** → Collects and removes the liquid WF from the vapor side and recovers it back to the liquid side. Liquid formation in the vapor side is quite normal because of the heat release to the ambient.
- **Storage system** → The working fluid storage system provide an accumulation volume to storage working fluid quantity to make up possible working fluid leakages, and to storage the working fluid content inside a vessel be subject to maintenance. The storage system consists of a storage vessel and a transfer pump (air-operated pump powered by compressed air).

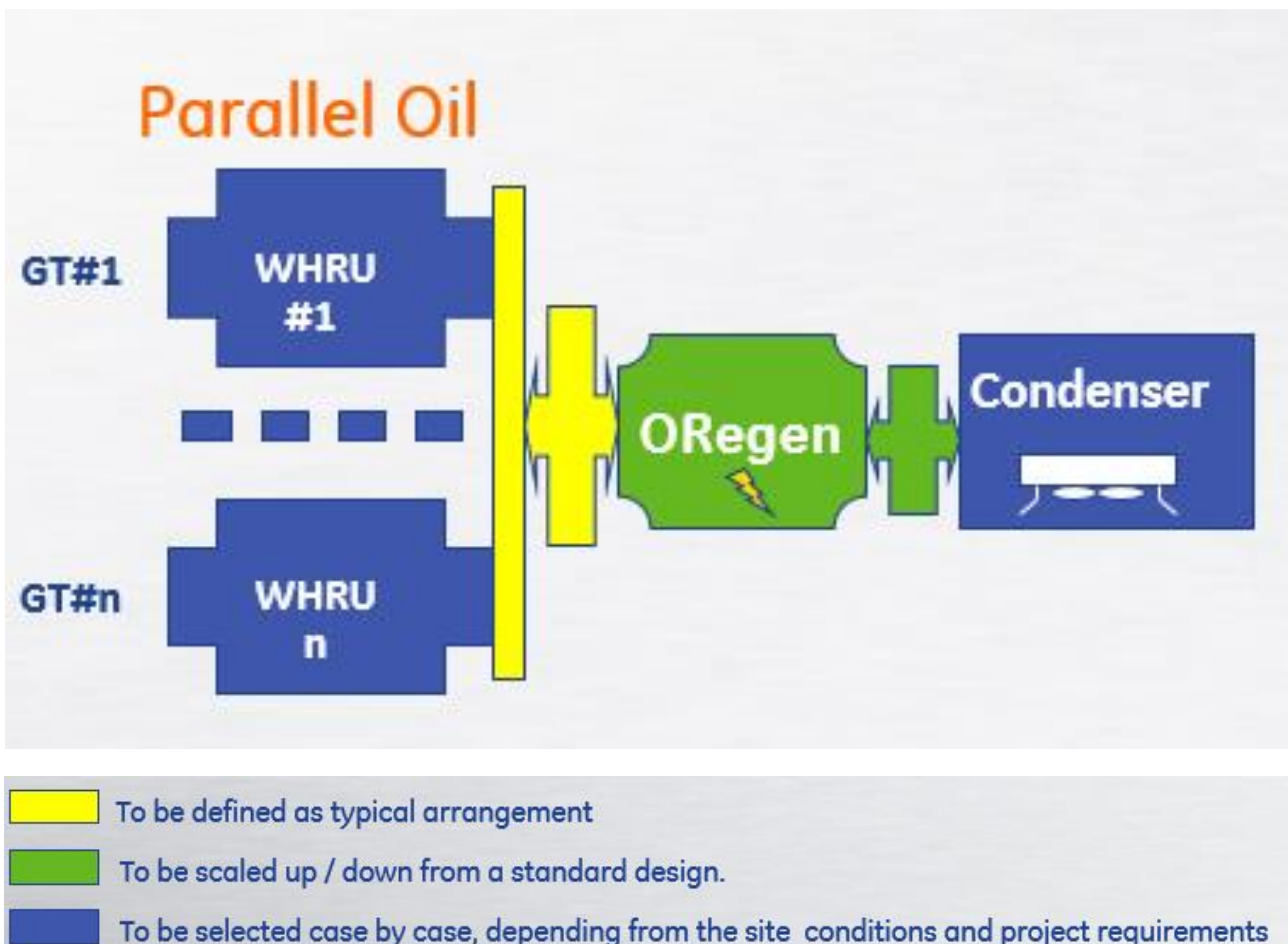


Figure 5-3 ORegen™ parallel oil configuration

The Oregon™ technology is designed to receive the heat input from gas turbine (in the plant I'm analyzing a technology which receives the heat from 3 out of 4 turbines), resulting in a power production. (Burrato, 2012)

In the figure 5-3, both the condenser and the waste heat recovery unit are painted of blue. This means that these devices change case by case.

For what concern the condenser, can change its design, and the refrigerant fluid, that can be air or water or other fluids.

Even the waste heat recovery unit change. Can change the number of heat exchangers, or the type of exchanger or otherwise the cycle of the heat exchanger.

When the first intermediate loop is used, the heating source and the working fluid are not in direct contact.

Thermal oil is used as a thermal vector.

The diathermic oil and the organic fluid allow low temperature heat sources to be exploited efficiently to produce electricity over a wide range of power output, from a few Megawatt up to 17 Megawatt per unit.

ORegen™ Typical Layout

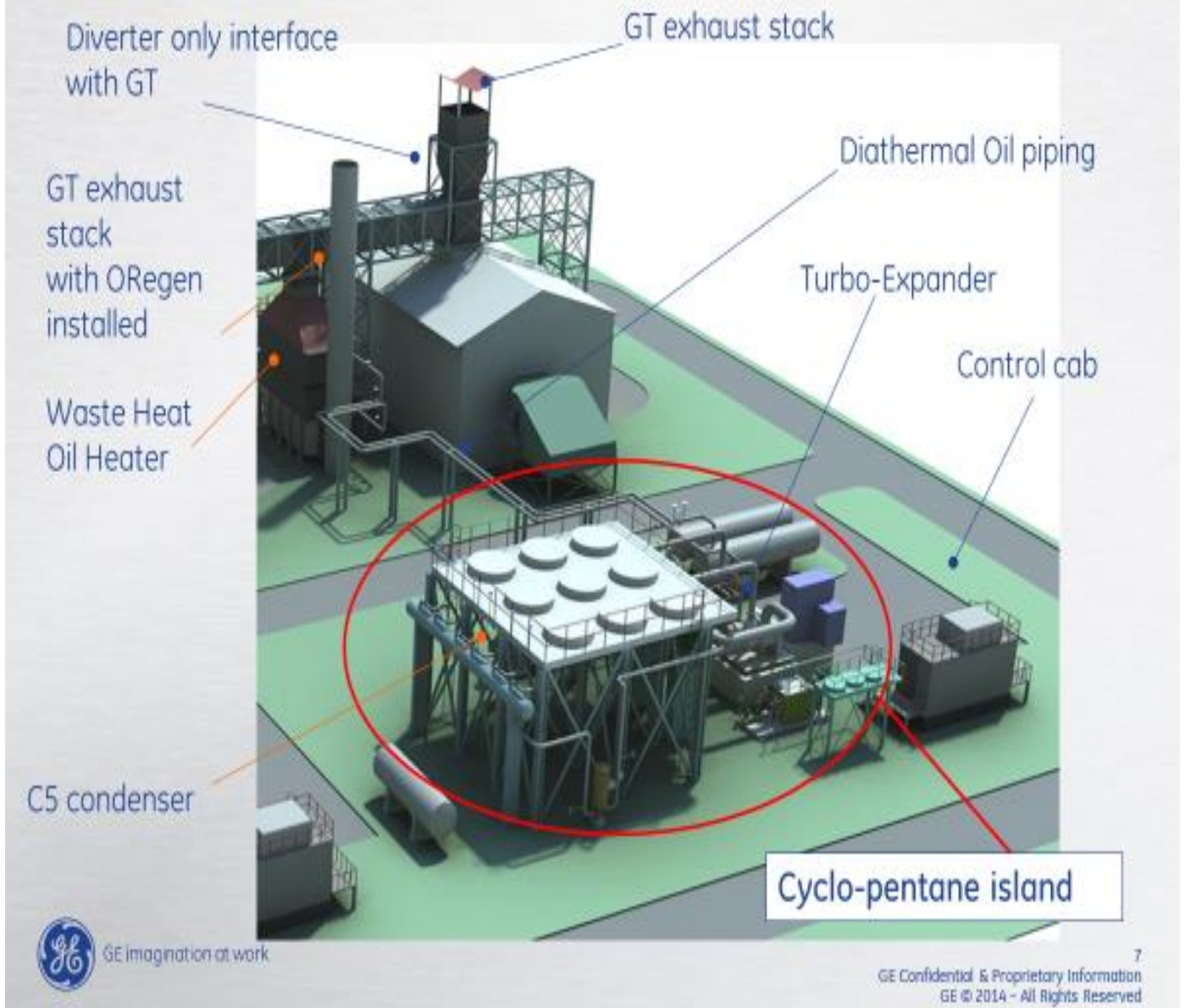


Figure 5-4 ORegen™ Typical layout

In the ORegen™ application the organic fluid used is composed by:

- Cyclopentane 95%
- i-pentane 0,75%
- n-pentane 0,75%
- 2-Mpentane 3,50%

Cyclopentane is a highly flammable hydrocarbon, both in liquid and vapor state; being the flash point very low, air exposures forms explosive mixture: the relevant lower explosion limit is 1.5% (lowest volume concentration of cyclopentane in air capable of producing a flash of fire in presence

of an ignition source), and the relevant upper explosion is 8.7% (highest volume concentration of cyclopentane in air capable of producing a flash of fire in presence of an ignition source).

The analysis highlighted Cyclopentane as the most suitable fluid for this type of application, giving fair on high performance in all categories.

The advantage of cyclopentane is that provides a good efficiency over a broad waste heat temperature interval ranging from about 400 C° to more than 500 C°. (Burrato, 2012)

Its main features are:

- Boiling point: 49.3 °C
- Freezing point: -94°C
- Molecular weight: 70,62
- Flash point: -37 °C
- Appearance: Clear, colorless liquid
- No corrosion issue on plant equipment

The selection criteria for the hot oil considers the parameters of minimum pumpability temperature and operability range.

Low minimum pumpability temperature also allows the use of hot oil in very cold climates, limiting winterization activities to the minimum.

Features of the diathermic oil are:

- Low freezing point and high temperature stability, which allow higher cycle temperature and higher efficiency.
- High heat of vaporization and density.
- Low environmental impact.
- No additional EHS considerations.
- Low cost.

The selection of oil and working fluid is critical for the product development.

Possible ORegen™ applications extend to every climate, from extreme cold locations with temperature well below -20C°, to extreme hot temperatures, that we can meet in desert or tropical locations.

Using cyclopentane as working fluid, and a suitable diathermic oil we can ensure the application of the ORegen™ in every location.

One of the main advantages of the ORegen™ is the non-presence of water. This feature makes this technology perfect for dry areas and for locations without water or very cold places.

Water is becoming, year after year, an increasingly precious resource in many places and it may be difficult and expensive to supply the quantity of water required by combined cycle.

Another point that make the ORegen™ perfect for extreme locations, is that there is no need of constant presence of an operator at the site, but it can be remotely controlled.

Another important advantage is the layout flexibility.

This feature is fundamental for an installation on an existing unit, where the space close to the machine often is very crowded with balance-of-plant equipment.

The only equipment that has to be mounted near the plant is the waste-heat-recovery unit, and the only interconnections are the oil piping which can be mounted easily in a crowded plant.

Compared with the traditional cycle, this ORC has several advantages:

- High efficiency of the cycle for heat sources with low temperature.
- Low solicitation of the turbine due to the low tangential velocity.
- Low vaporization pressures even close the critical point.
- Expansion always in the zone of superheated steam. In this way, there is no humidity that could damage the turbine.
- Low cost, and higher safety because we are working at lower pressures and lower temperatures.
- Long life and low maintenance.
- No emission.

Obviously, there are even some disadvantages, as for examples the high investment costs, since this is a new technology.

5.2. ORegen™ APPLICATIONS

Have been already sold different ORegen™ systems all over the world, and is continuously being developed.

There are different types of product line:

- ORegen™ for output power between 5 and 17 MW.
- Mini ORC for output power between 0.5 and 2 MW.
- Micro ORC for output power of 125 kW.

One system has been sold in Canada on a pipeline station; it recovers the waste heat of three gas turbines in a gas compression station, generating approximately 17 MW.

Two of the three turbines run continuously, while the third is on stand-by.

Another one has been sold in Brunei on a powergen station, and recovers the waste heat of four gas turbines, 3 running constantly and one in standby. Even this system generates an amount of 17 MW.

Finally, a third one has been sold in Thailand on a pipeline station

ORegen™ can recover waste heat from the exhaust of gas turbines operating at variable loads of 50 percent to 100 percent in mechanical drive or power generation applications. (Burrato, 2012) (Gas.)

6. ORGANIC RANKINE CYCLE EXPANDER

This chapter presents the main expander architectures commonly used in ORC power system.

The performances and the costs of an ORC system depend mainly on the operative condition of the plant, from the working fluid and from the size of the components.

The expanders for the ORC system can be classified in:

- Volumetric expander
- Turboexpander

6.1. VOLUMETRIC EXPANDER

The volumetric expanders are more suitable in low grade heat and waste heat engines for smaller size, and can work with a biphasic fluid. (Muhammad Ihram, 2015)

Anyway, the continuous need of lubricant, the technical difficulties and the friction losses are negative keys for its marketing.

The volumetric expander can be divided in:

- Screw expander

These expanders are characterized by two helicoidal counter rotating rotors. These types of expanders have good performances for high power. (I. Papes, 2015)

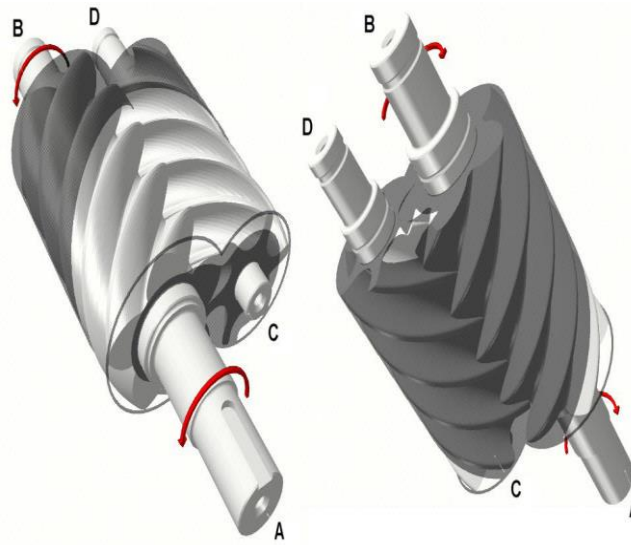


Figure 6-1 Screw expander

- Scroll expander

A scroll expander uses the expansion of a vapor pocket through two concentric scrolls to produce shaft rotation. It has a fixed volumetric ratio with two involutes curves orientated in different directions and 180° out of phase. One scroll is fixed, while the other one orbits. High pressure fluid enters the suction port and expands steadily. The expansion ends when the fluid is discharged at low pressure and temperature. (R. Capata, 2014)

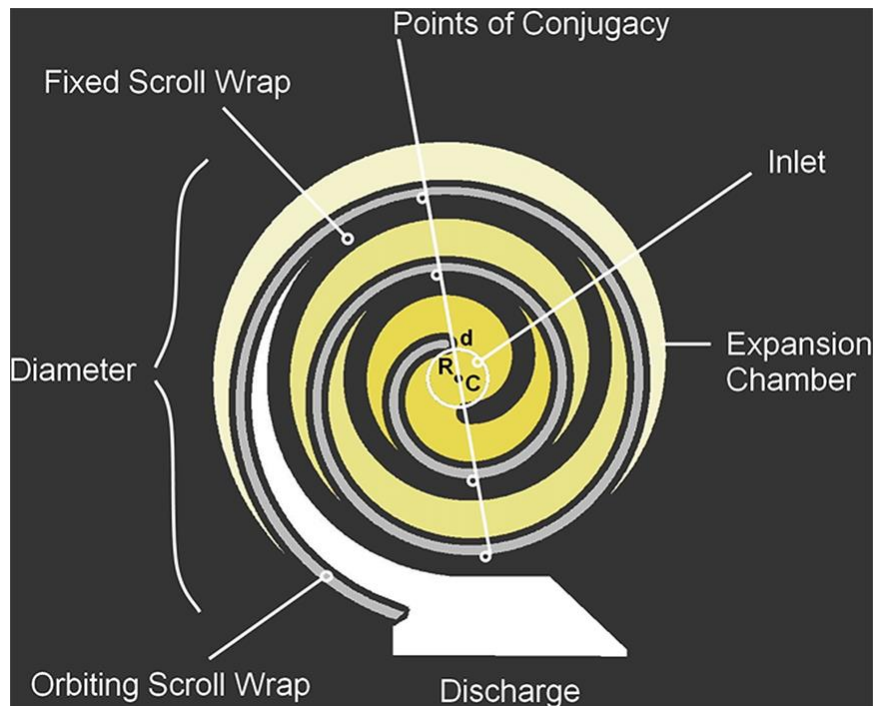


Figure 6-2 Scroll expander

- Vane expander

This type of expander is constituted by a rotor with slots, where vanes can slide with a linear motion. The vanes isolate volumes. During the rotor rotation, the volume, between the vane and the outer casing, increases, permitting the expansion of the fluid, until it reaches the discharge section. The geometry and the material of the vanes have an important role in the performances of the expander. The low density of the vane material gives a better performance, allowing to use less lubricant. (M. Imran, 2016)

These expanders have higher losses and dispersions, compared with the other volumetric expanders, and even a lower isentropic efficiency.

- Piston expander

The cycle of operation of this expander is constituted by three phases:

- 1) "Suction" The piston is in the top dead point, the suction valve opens and the fluid enters at high temperature and high pressure.
- 2) "Expansion" once closed the suction valve, the fluid pushes the piston until it reaches the bottom dead point.
- 3) "Discharge" once the piston reaches the bottom dead point, the discharge valve is opened, the fluid is discharged and the piston goes back to the top dead point.

These expanders are used in the CHP systems (combined heat and power) of low size, and in the refrigeration cycles. (Oudkerk, 2015)

6.2. TURBOEXPANDER

A turboexpander, even called turbo-expander or expansion turbine, is a radial or axial flow turbine, through which a high-pressure gas is expanded to produce work that is often used to drive a compressor or generator.

The choice between radial flow or axial flow, depends on the size of the system, the mass flow and the pressure ratio.

Axial turbine, usually, are projected for low ratios of pressure and high mass flows.

The design of the expander depends strongly on the molecular weight of the fluid used; if organic fluids with a high molecular weight are used, instead of water, having in this way a lower enthalpic drop, the turbine will have a lower number of stages.

Radial turbines instead are used when the pressure ratio is high and the mass flow is low. Their design permits a higher peripheral speed, compared to the axial turbine. They guarantee a good efficiency and are even more robust, as the gas or vapor expand through the turbine. (E. Macchi M. A.)

Turboexpanders can also be characterized as modern rotating device that convert the pressure energy of a gas or vapor stream into mechanical work. (Block, 2001)

If chilling the gas or vapor steam is the main objective, the mechanical work so produced is often considered a byproduct. Otherwise if pressure reduction is the main objective, then heat recovery from the expanded gas is considered a beneficial byproduct.

Nowadays turboexpanders do this either by recovering energy from cold gas (cryogenic type) or from hot gases at temperatures of over 1,000 degrees. Current commercial models exist in the power range of 75 kW to 25+ MW, so many applications are possible.

Changing market conditions, accentuated by growing environmental awareness on a global scale, are improving market receptivity for the turboexpander.

Machinery manufacturers, quick to sense this market potential, have developed design features within their turboexpander ranges that offer user-friendly features, promoting ease of maintenance and operation, and aid design optimization

For many years, turboexpanders have been used in cryogenic processing plants to provide low-temperature refrigeration. Power recovery has always been of secondary importance, but the number of power recovery applications is steadily increasing. Large and small demonstrations plants are operating, or are about to begin operation.

Some of these plants were built to study, or minimize, potential problem areas for new, large power plants in the planning stage. (Block, 2001)

A turboexpander expands process fluid from the inlet pressure to the discharge pressure in two steps:

1. first through variable inlet guided vanes
2. through the radial wheel.

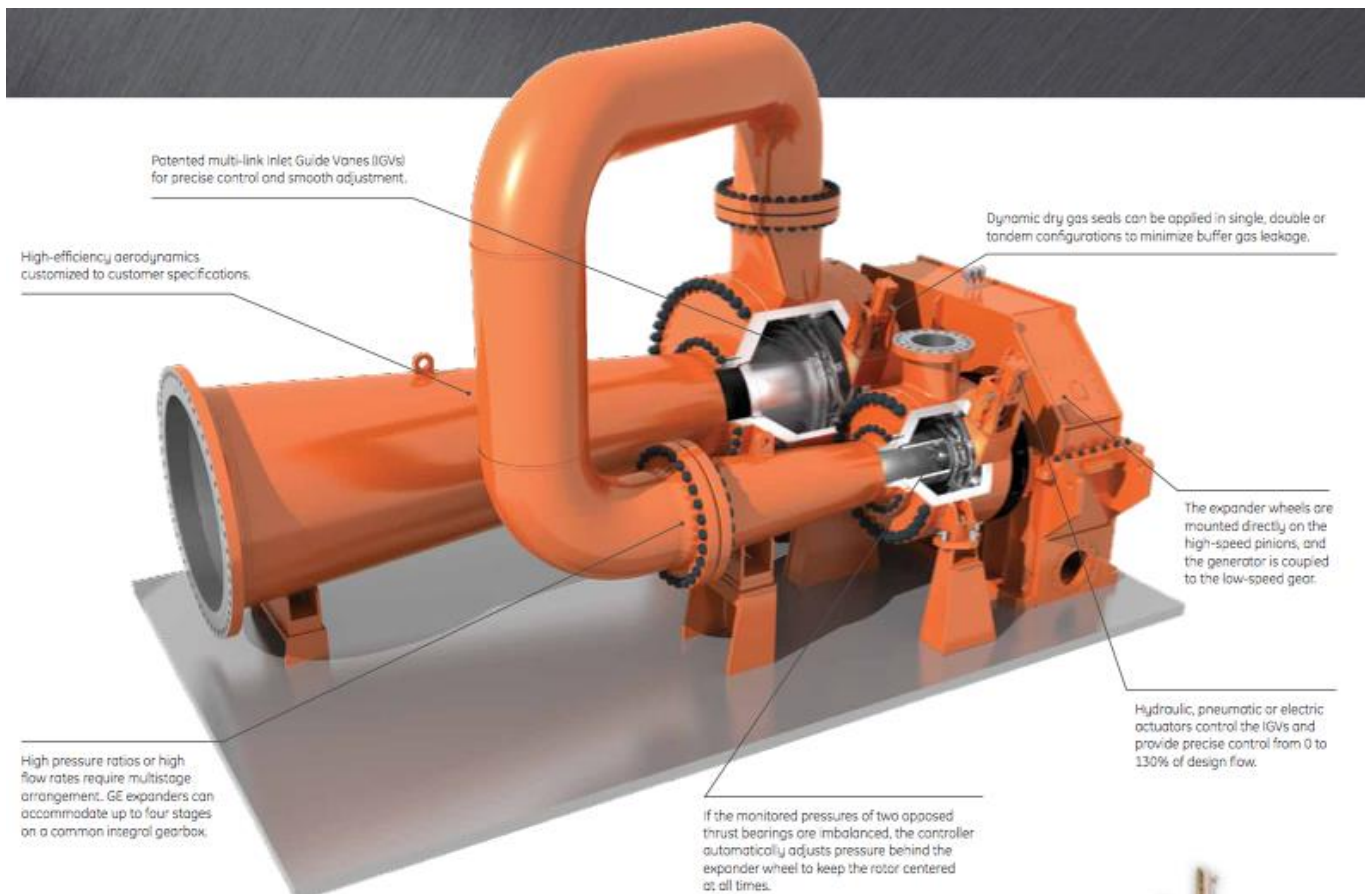


Figure 6-3 Turboexpander

As the accelerated process fluid moves from the inlet guided vanes to the expander wheel, kinetic energy is transformed into useful mechanical energy; it's done extracting energy from the process fluid and cooling it down.

The mechanical energy is available to drive other process equipment, the generator.

The turboexpander-generators are used in a wide range of applications, including:

- Oil & Gas processing Natural Gas Liquids (NGL) plants, Liquefied Petroleum Gas (LPG) recovery; tail gas treatment; GasTo-liquids (GTL); Integrated Gasification Combined Cycle (IGCC)
- Liquefaction and purification of gases on air treatment plants
- Petrochemicals: hydrogen, nitrogen and ammonia purification; ethylene production
- Pressure Let Down (PLD) on pipeline
- Geothermal power generation (e.g. Organic Rankine Cycle, Kalina and direct steam)
- Waste-heat recovery (WHR) and Combined Heat and Power (CHP)
- Ocean Thermal Energy Recovery (OTEC) (General Electric)

In the ORC cycle the turboexpander is composed by 2 expanders in a row, the first one is a high pressure (HP) expander, while the second one is a low pressure (LP) expander; in this cycle are

used 2 expanders because delta-pressure (ΔP) between the inlet of the HP and the outlet of the LP is high.

The shaft of every expander is connected to a wheel chain, which is connected to another central wheel (situated between HP wheel chain and LP wheel chain), which transmits the couple to the generator. The three wheel chains are all situated in the integral gearbox, and have different centrifugal speed.

For what concern the plant I'm going to analyze:

$$\omega_{HP} = 10180 \text{ rpm}$$

$$\omega_{LP} = 4950 \text{ rpm}$$

$$\omega_{CENTRAL WHEEL} = 15000 \text{ rpm}$$

The dimension of the wheel chain is naturally connected to the value of the angular velocity ω .

So naturally, higher the velocity, smaller will be the dimension of the wheel chain.

The organic fluid enters in the nozzle of the high pressure expander, goes out the diffuser and then passes through the low pressure expander.

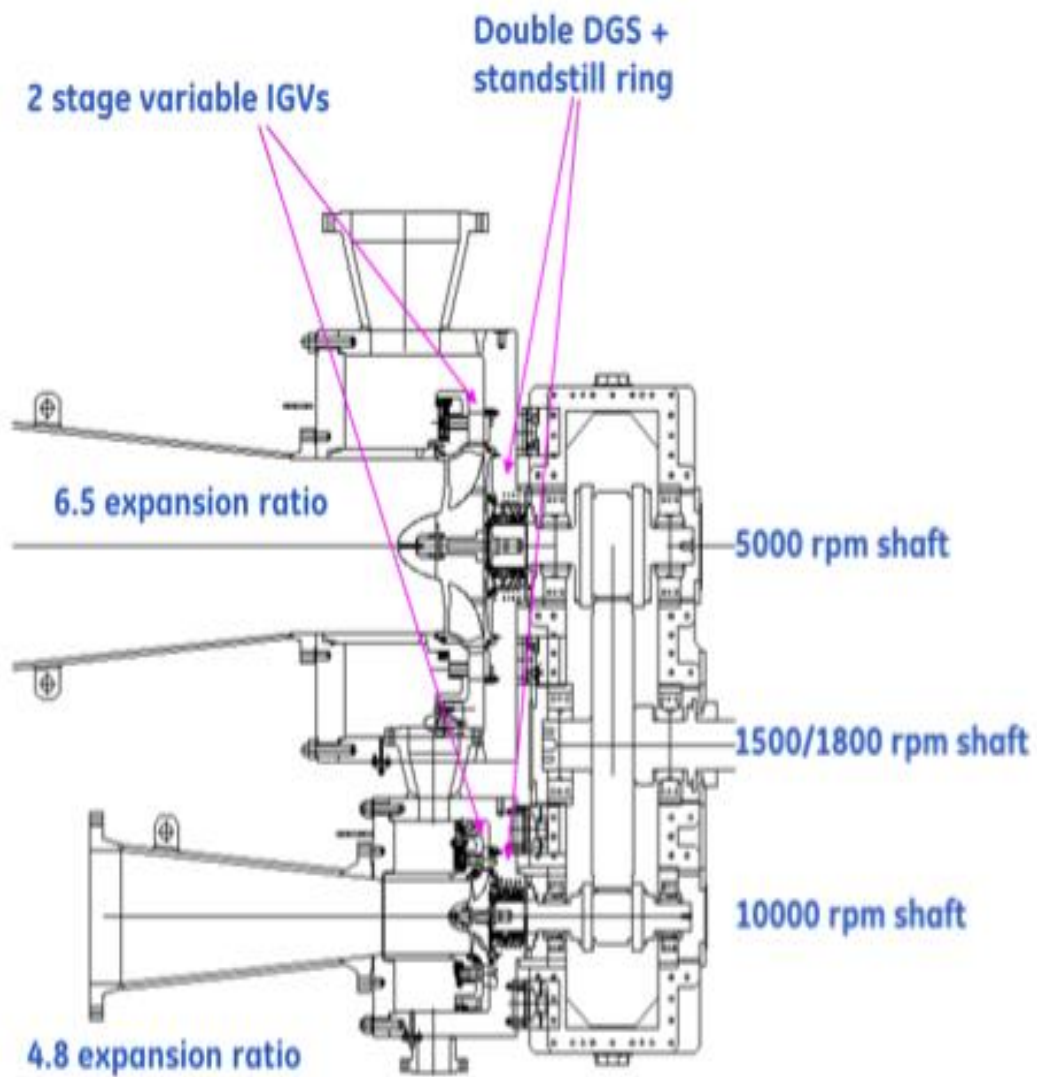


Figure 6-4 Turboexpander section

For every expander with variable geometry, there is a convergent-divergent nozzle with variable inlet guide vanes, a radial wheel and a diffuser.

The percentage of opening of the IGV influences the mass flow of the gas, and naturally even the velocity.



Figure 6-5 16 blade wheel

In the nozzle, the fluid enters with a certain subsonic velocity. Along the convergent stretch the fluid accelerate until the throat section where the value of Mach (M) is equal to 1. The Mach value is equal to 1 because the nozzle is choked, it means that the quantity of mass flow is blocked.

$$M = \frac{v}{a}$$

M= Mach number

v: Speed

a: Speed of sound

After the throat, the section becomes divergent and so the fluid goes on accelerating. For this reason, the velocity at the outlet of the nozzle is higher than the velocity at the inlet, and the pressure naturally decreases, because it follows the Bernoulli's equation.

$$p + \rho \frac{v^2}{2} + \rho * g * h = const$$

p: Pressure

ρ : Density

v: Speed

g: Gravity acceleration

h: Height

Using this type of nozzle, we are able to exploit the total enthalpic drop available.

Even passing through the wheel we have a decrease of the pressure, and a following increase of the velocity.

Finally, there is the diffuser, that permits to recover the Kinetic energy.

Between the inlet and the outlet of the diffuser there is a decrease of the velocity due to the increase of the Area. This is easily deducible by the continuity equation.

$$\dot{m} = \rho * v * A$$

A: Area

The process of the expander, from the beginning when the fluid enters in the nozzle, until when it goes out of the wheel is represented in the next figure:

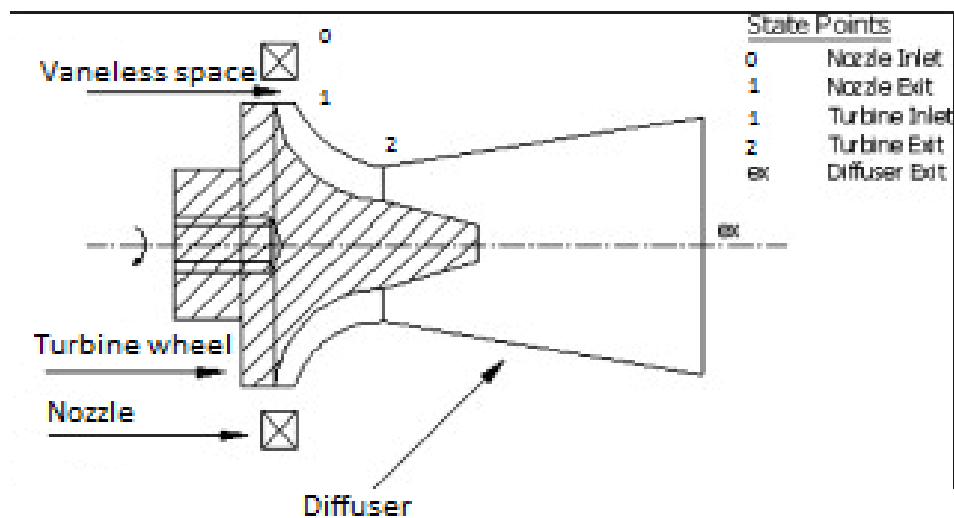


Figure 6-6 Turbine scheme section

For what concern the thermodynamic point of view:

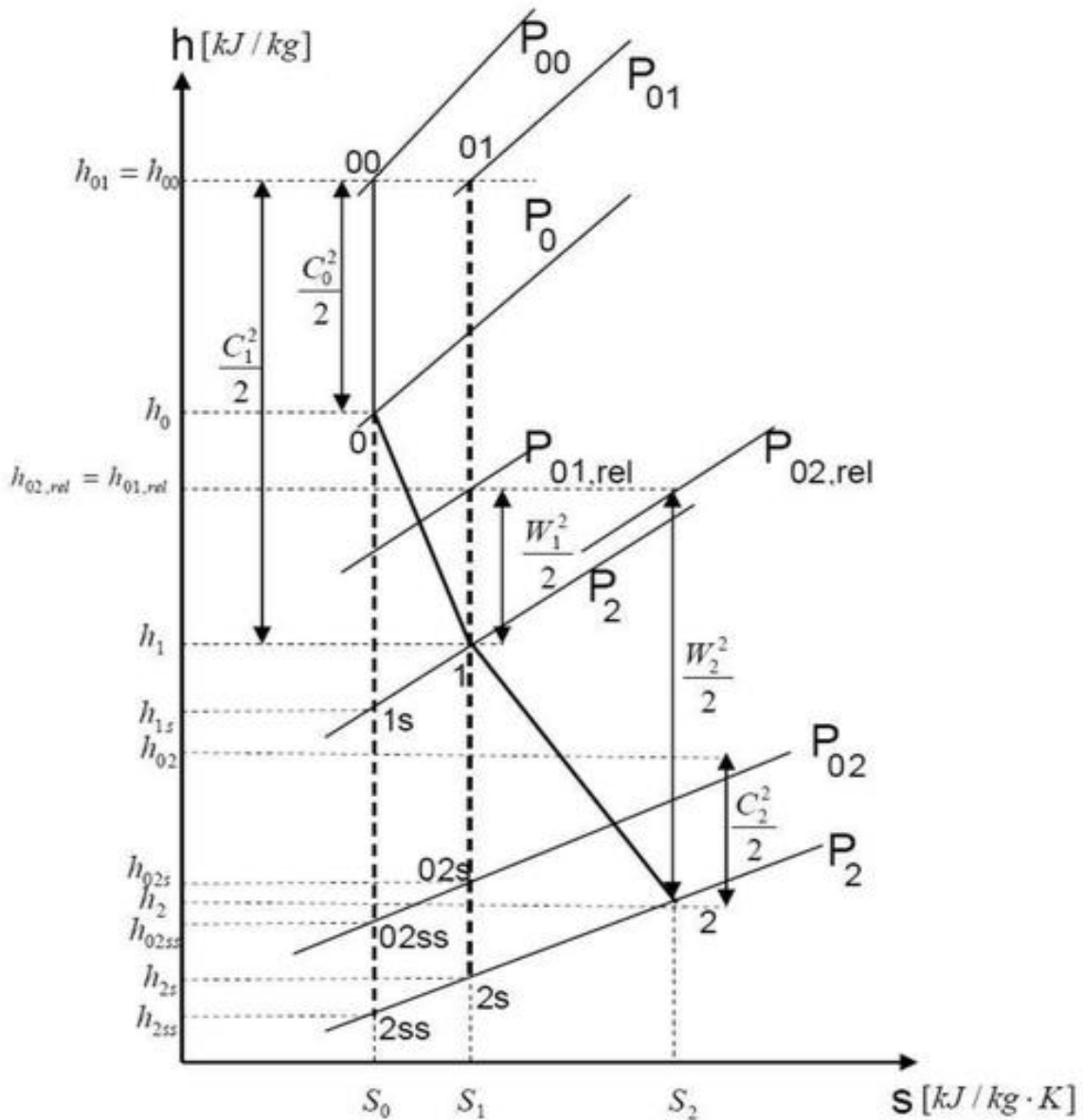


Figure 6-7 h-s diagram explaining turbine behavior

Starting from the top we can see h_0 , the enthalpy at the inlet of the nozzle, h_1 the enthalpy between the nozzle and the wheel and h_2 which is the enthalpy at the exit of the wheel.

At the inlet, the fluid has a static pressure P_0 and an absolute velocity v_0 , and in this way, we can calculate the total enthalpy h_{00} .

The gas expands and accelerate till c_1 .

Later the gas enters in the wheel where the relative velocity increase from w_1 to w_2 , and the absolute velocity decreases.

In this drawing is not present the diffuser, which recovers kinetic energy, but is present the point “00”, which is the input of the flange. Are indicated both “static” and “total” enthalpy.

$$h_{01} = h_1 + \frac{c_1^2}{2}$$

h_{01} : total enthalpy between nozzle and wheel
 h_1 : static enthalpy between nozzle and wheel
 c_1 : Absolute velocity at the output of the nozzle

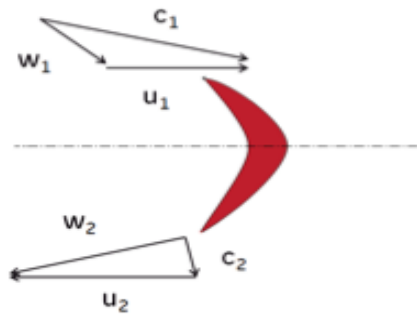


Figure 6-8 Velocity triangles for the wheel

c , w and u are the three velocities, respectively at the inlet of the nozzle (0), at the exit of nozzle-inlet of the wheel (1), and at the output of the wheel (2).

c : Absolute velocity
 w : Relative velocity
 u : Tangential velocity

For analyzing what happens in the wheel we must introduce the rothalpy, and highlight that it's constant between the nozzle and the wheel.

$$I_1 = h_1 + \frac{w_1^2}{2} - \frac{u_1^2}{2} = h_2 + \frac{w_2^2}{2} - \frac{u_2^2}{2} = I_2$$

7. METHODOLOGY AND RESULTS OF THE STATIC MODEL

The model has been designed using a software called Aspen Hysys, an energy industry's leading process simulation software that is used by top oil and gas producers, refineries and engineering companies for process optimization in design and operations.

As said before, the primary objective of the work is the improvement of the tool to produce performances maps of the turboexpander, and validation of an alternative model for analyzing some points where the CFD is not done.

A model was already present, that was used for designing the turboexpander, but it was a simple and easy model.

For this reason, the same model was previously used both for static and dynamic condition.

The problem was that this simple model didn't describe the behavior of the turboexpander perfectly in every period.

So, we have designed a new model, more complicate, but at the same time much more complete that works naturally, as the previous one, both in nominal and off-design condition.

The hypothesis of the model are:

1. Model designed for a perfect gas, with corrections for a real gas. It means that the properties of the real gas have been linearized, in every section of the model, for being described as a perfect gas. For example, this has been done changing the value of the density between wheel and nozzle.
2. Small variation of the density (ρ) in the wheel.
3. The value of Δh can be written as $\frac{\Delta P}{\rho}$ (the compressibility effects are negligible in the wheel).
4. In the previous model wasn't designed the diffuser, and the pressure at the outlet of the wheel was assumed equal to the pressure at the outlet of the diffuser. Now with the introduction of the diffuser the pressure at the outlet of the wheel, and at the outlet of the diffuser are different.

We have added the diffuser to the previous model, and the three components of the expander are connected by several solvers that are used for reaching the convergence.

Each component represents an expansion with an assigned efficiency, and is schematized in this way in the software.

For improving the model, are even introduced expanders which simulate the steps between 1-static and 01-rothalpic, 2-static and 02-abs-total and 2-static and 02-rothalpic. To reach the solution, a solver is required at each step.

In the first case, between 1-static and 01-rothalpic, the solver controls that the I_1 calculated using the formula of the rothalpy(in the page below), would be equal to the one obtained in the model with the thermodynamic laws, for what concerns the high pressure expander.

The second solver instead regulates the value of h_{02} calculated using the thermodynamic laws, and calculated using the formula, would converge, while the third one regularizes the I_2 .

We have a total of six solvers, and in the case the values regularized by each solver, wouldn't be the same, thanks to the them, the software goes on calculating until the two values converge.

Is present even another device, always schematized as an expander in the model, that calculates the wheel adiabatic efficiency, and the total efficiency.

This static model works as a map generator, so its result is a point. Changing the percentage of inlet guided vane opening, or the value of u/c , we have different results, that we can combine and create a map.

7.1. EQUATIONS OF STATE

The software I'm using, as said, is called Hysys and works using different equation of states (EoS), which are different and gives different final results.

In thermodynamic, an equation of state is a constitutive law which describes the state of the substance under some physics condition. It provides a mathematical relation between 2 or more variables as temperature, pressure or volume. (Peng, 1986)

These equations are fundamental for the description of the properties of fluids and solids.

The easiest equation is the equation of perfect gas, even known as *Clapeyron-equation*.

$$Pv = nRT$$

P: Pressure

v: Volume

n: Number of mole

R: Gas constant

T: Temperature

Another equation of state is the **Van Der Waals equation**, which has been the first equation to be developed after the Clapeyron one (Waals, 1988), and provides a better description of the gaseous state for high pressures, and near the liquefaction point. In this equation is fundamental the use of the parameters "a" and "b", which are respectively the attractive parameter and the covolume.

$$\left(P + \frac{a}{V^2}\right)(V - b) = RT$$

a: Attractive parameter

b: Covolume

Another equation widely used is the **Redlich-Kwong (RK) equation**.

It was introduced in 1949, and was considered a great improvement compared to the Van Der Waals equation. (Soave, 1972) When Redlich and Kwong proposed their celebrated equation of state, they were interested in developing a good equation only for gases. Not a single application to liquids can be found in Redlich-Kwong original paper.

The RK equation improved in a quantitative sense the predictions of VDW equations, which stopped giving good results when the pressure overcame 200 bar.

In particular, this equation is able to describe well the behavior of gases at high pressures.

$$P = \frac{RT}{V - b} - \frac{a}{\sqrt{TV}(V + b)}$$

Another important equation, widely used is the **Peng-Robinson equation**. As the RK equation is much more precise than the previous ones, having in the formulation more parameters, and is a quantitative equation too.

While the RK equation provides better results for gases at high pressures, the PR equation gives better results in the liquid-steam region. It is even better in providing the liquid density for many fluids, the non-polar ones.

The Peng-Robinson EoS has become the most popular equation of state for natural gas systems in the petroleum industry. This happened because, comparing the performance of the PR and the SR, the results are pretty similar, except for a slightly better behavior of the PR EoS at the critical point. A slightly better performance around critical conditions makes the Peng Robinson somewhat better suited to gas/condensate system. (D. Y. Peng, 1976)

$$P = \frac{RT}{V - b} - \frac{a\alpha(T)}{V^2 + 2bV - b^2}$$

The thermodynamic equation used in this case, as in the static model is the **Zudkevitch-joffe** equation, a cubic equation.

This equation is substantially a modification of the Redlich-Kwong EoS. The purpose of the modification was to improve predictions of the RK equation in the saturated vapor region up to the critical point while retaining a relatively simple form to make analytical relations for derived properties possible.

This equation approximates better the behavior of the cyclopentane, even better than the Peng-Robinson equation.

The equation doesn't approximate exactly every single field of temperature and pressure, but is thought to be sufficiently precise.

7.2. MODEL DESCRIPTION

The model works using an algorithm, and naturally needs some input data, for calculating the output.

In Input, we have geometrical data, and the boundary conditions.

In order to validate the code on the CFD data available, five tuning parameters are calibrated as function of both geometrical and thermodynamic data.

GEOMETRICAL DATA

- **A design nozzle** (nozzle area)
- **A wheel** (wheel area)

- **D1** (inlet wheel diameter)
- α_1 (output angle of the nozzle)
- $\beta_{2,av}$ (average metallic angle, at the output of the wheel)
- $\beta_{1,b}$ (metallic angle at the input of the wheel)
- **D2 shroud** (outlet diameter of the shroud)
- **D2 hub** (outlet diameter of the hub)

BOUNDARY CONDITION

- **P00** (initial pressure condition)
- **T00** (initial temperature condition)
- **Mw** (molecular weight)
- **P3** (pressure condition at the end of the diffuser)

OUTPUT CONDITION

- \dot{m} (mass flow)
- η (yield)
- **P** (power)

TUNING PARAMETERS

- ξ **nozzle** $\frac{P_{00}-P_{01}}{P_{00}-P_1}$

This parameter indicates the loss coefficient of the nozzle, for the non-reversible expansion process from the inlet of the nozzle until its throat.

- ξ **wheel** $\frac{P_{01rot}-P_{02rot}}{\rho \frac{\omega^2}{2}}$

This parameter indicates the loss coefficient of the wheel, which is the main loss of the expander, for the non-reversible expansion process from the throat of the nozzle until the throat of the wheel.

- **Cv nozzle** $\frac{A_{eff\ nozzle}}{A\ nozzle}$

This tuning parameter specifies the flow coefficient of the nozzle, from the inlet of the nozzle until its throat.

- **Cv wheel** $\frac{A_{eff\ wheel}}{A\ wheel}$

This parameter indicates the flow coefficient that flows from the throat of the nozzle until the throat of the wheel.

- **Wheel deviation angle**

This parameter indicates the difference angle between the blade and the flow that passes over it.

$$A_{eff} = A * \eta$$

The efficacy area is the ideal geometrical area, multiplied for all the different deviation from the ideality value.

Why are chosen these 5 values as tuning parameters?

Every component of the expander (nozzle and wheel) is characterized by the yield, and by the efficacy area.

For defining these values, we have to act on the losses and on the flow coefficient.

For this reason, we have chosen ξ nozzle, ξ wheel, C_v nozzle and C_v wheel as tuning parameters.

Later, we need a correspondence related to the angle, for understanding with which angle the flow goes out from the wheel; more negative is this angle, higher will be the power.

So, through these 5 values, we are able to define the output of the model: power (through the wheel deviation angle), mass flow and yield (through the coefficient flow and the effective area).

For what concern the losses coefficient, as suggested by GE expert, we haven't used any type of correlation, this choice has been done taking in consideration several things.

We know the field of validation of the correlations, but being outside it we can't use them.

We are going to use the CFD post-processed data because in those data are present the effects of the gases, so we know what is its behavior.

We always must remember that we are not using an ideal gas, but a real one.

Furthermore, we haven't used the correlations because the enthalpic drop is high, and the compressibility Factor (Z) is different from 1.

The nozzles are supersonic, and the big part of the losses derives from not-stationary phenomenon, which are the interaction of the shocks between nozzle and wheel. Even for this reason there are no correlations about this type of phenomenon. The losses correlations are principally for subcritical phenomenon.

Furthermore, the CFD is representative of the measures, it has a good accuracy and has always behaved as expected.

Treating the different type of losses, we can see that the efficiencies losses of a turbine can be considered as the sum of these 4 different losses:

- **Profile losses** → Due to the dissipation of the mechanical energy in the boundary layer, which develops along the surface fluid-profile, for the effect of the viscosity.

- **Annulus losses** → Losses that happen inside the boundary layer adherent to the cylindrical surfaces of the turbine. They are even caused by the viscosity.
- **Secondary losses** → Connected to the presence of tridimensional components of velocity inside the interblade channels.
- **Losses connected to the extremity** → Losses due to the clearance between the rotor and the box, and between the stator and the hub. (K. K. Botros, 2015)

The losses of the nozzle are caused by friction, while the wheel losses are caused by friction and incidence (due to the increase of the boundary layer). (Benson, 1965)

The incidence is a fundamental value and is equal to the metallic angle (β_{1b}) minus the inlet relative angle (β_1), and it's used for understanding if the direction of the gas is aligned with the vanes.

$$incidence = \beta_{1b} - \beta_1$$

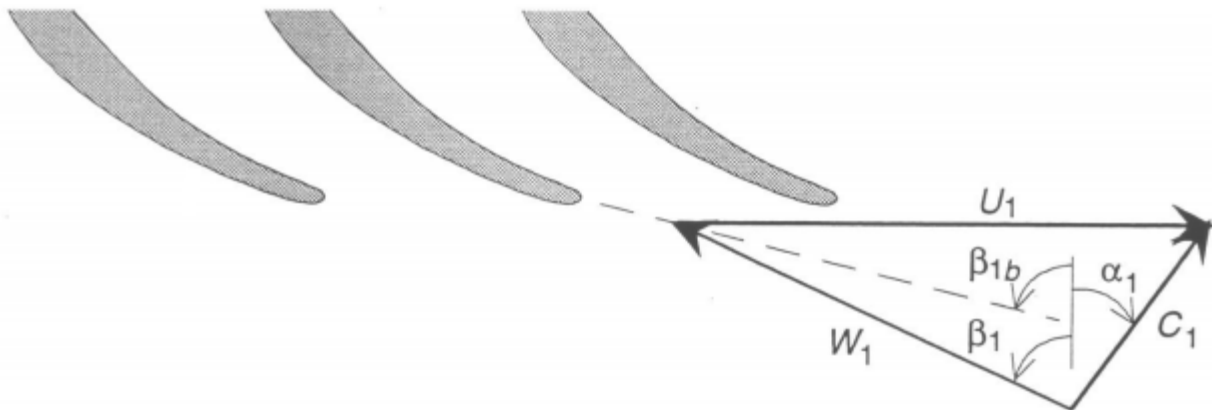


Figure 7-1 Inlet velocity triangle

With the presence of these losses, the efficiency of the system will naturally decrease, but won't create any damage to the expander.

Later, I have used some CFD data and have calibrated the output values of the model, tuning the 5 calibration factors.

The CFD data are fundamental, are the primary source of the work. We used them for obtaining the values of the tuning parameters in the static model.

The tolerance that we keep on the comparison of the outputs between CFD and the model is of 3%. A better accuracy is not necessary because Hysys is not a program created for minimizing the error. We have not used an optimization algorithm because the model, that is already complicate due to the presence of several solvers, with the presence of an algorithm would have crashed frequently.

For what concern the CFD post-processed data, I have used 9 points of the High-Pressure expander and 9 points for the Low Pressure expander.

The 9 points have 3 different Counter pressures (static pressure at the exit of the wheel) and the nozzle has 3 different rotations; in this way there are 9 different situations.

$$\text{Counter pressure} = P_2 = 178 = 0,178 * P_{00}$$

Naturally the 9 points in HP are different from the 9 points in LP.

HP

LP

Counter pressure: 178 188 208

Counter pressure: 132 142 162

Nozzle rotation: Low Design High

Nozzle rotation: Low Design High

For the high pressure expander, the design point is the one with counter pressure equal to 188, and nozzle rotation equal to 0. For the LP instead, counter pressure 142, and nozzle rotation equal to 0. The three different nozzle rotations are equivalent to three different percentage of inlet guided vane opening.

For what concern the high-pressure expander the nozzle rotation corresponds to an aero percentage opening of the HP equal to [123,4 ; 100 ; 75,93]. For the low-pressure instead it corresponds to [124 ; 100 ; 73].

These data were chosen cause had the best numerical values, and the range between every counter pressure was sufficiently high for considering the 3 points valuables for the construction of the model.

7.3. MODEL TUNING WITH CFD DATA

Initially, using the CFD post-processed data, I have validated the stationary model. So once inserted the input values (geometrical data and boundary conditions) in the map generator, I have tuned the calibration parameters for obtaining the same output values (efficiency, power and mass flow).

Here the steps I have followed:

- Insert the initial values P_{00}, T_{00}, P_2 .
- Compare the mass flow, and settle it changing the %IGV.
- Change the value of “ $\eta_{wheel\ tot - tot}$ ” until the value of P_1 will be equal to the one of the CFD.

- Change the incidence.
- Compare the value of the power, changing the wheel deviation angle.

Naturally the values of the CFD and the ones of the model will be the same.

The values obtained from the predictive model, for the HP and LP are the sequent, and are unique.

They are unique because, apart from comparing the output values between the CFD and the model, I'm going to check even the intermediate pressure (POD = P1).

HP	Csi wheel	Csi Nozzle	Cv nozzle	Cv wheel	Wheel deviation angle
178	0,329	0,082	0,976	0,91	7,3
188	0,353	0,083	0,976	0,9	7,5
208	0,377	0,086	0,976	0,88	9,1
178-2	0,261	0,1	0,976	0,905	3,7
188-2	0,253	0,1	0,976	0,89	3,7
208-2	0,278	0,1	0,976	0,886	4,9
178+2	0,426	0,119	0,976	0,9	15
188+2	0,439	0,119	0,976	0,96	15,2
208+2	0,416	0,125	0,976	0,89	18,5

Table 2 HP predictive model values

LP	Csi wheel	Csi Nozzle	Cv nozzle	Cv wheel	Wheel deviation angle
132	0,283	0,107	0,971	1,015	4,2
142	0,303	0,107	0,971	1,025	5
162	0,332	0,108	0,971	1,04	7,1
132-2	0,248	0,098	0,971	1,19	4,6
142-2	0,238	0,1	0,971	1,08	5,5
162-2	0,254	0,1	0,971	1,04	6,3
132+2	0,529	0,132	0,971	1,05	5,7
142+2	0,492	0,136	0,971	1,12	4,4
162+2	0,558	0,139	0,971	1,12	6,5

Table 3 LP predictive model values

7.4.DEPENDANCE EQUATIONS

Later, once found all the values of the tuning parameters, I have created some performances maps where the tuning parameters were written as function of other values, as %IGV, Incidence or the relative Mach number. In this way, the performances maps, could have been used for other points where the CFD data were not available.

The values chosen for settling the parameters are chosen for precise reasons:

The inlet guided vanes control the gas mass flow.

When the inlet guided vane is closed (percentage equal to 0), the mass flow of the gas that passes is equal to 0, while when the vanes are totally open the mass flow is the highest.

If I gradually increase %IGV, the Δp of the wheel will increase, while the Δp of the nozzle will be lower. So, we will have less impacts between nozzle and wheel. This leads a better yield and so even less losses.

In our case being the nozzle chocked, changing the opening of the inlet guided vane, the mass flow doesn't change, so we can assume that the C_v nozzle keeps always the same value.

The other factor that affects the losses is the incidence. There are some losses which are not connected to the incidence, as for example the profile losses, and others, as the secondary losses, which are strictly connected with it.

Even the Mach influences the losses coefficients and the flow coefficients, but in such a light way that as we will see later its dependence can be avoided. (Sunetra Sarkar, 2013)

Finding the equation, I won't have to change every time manually the tuning parameters, but just changing some values they will be set correctly.

I have analyzed every factor both for HP and LP, but I'll show here only the HP case.

✓ *CSI WHEEL*

Analyzing the values of the ξ wheel for every point, both HP and LP, I've catalogued them looking firstly at the Mach relative value, and later at the incidence value.

Firstly, I've divided the values in 3 groups:

- Relative Mach $> 0,42$
- Relative Mach $< 0,4$
- $0,4 < \text{Relative Mach} < 0,42$

Then, for every group, I put in a row the values from the smallest to the biggest.

	Incidenza	Relative Mach	Csi wheel
208	-6,448	0,345	0,377
208+2	12,02	0,284	0,416
188+2	17,7	0,386	0,439
208-2	-20,3	0,409	0,278
188	-0,380	0,406	0,353
178+2	17,27	0,413	0,420
188-2	-16,94	0,422	0,253
178-2	-15,02	0,431	0,261
178	2,512	0,426	0,329

Table 4 CSI wheel values for HP

Finally, I graphed the incidence with the ξ wheel.

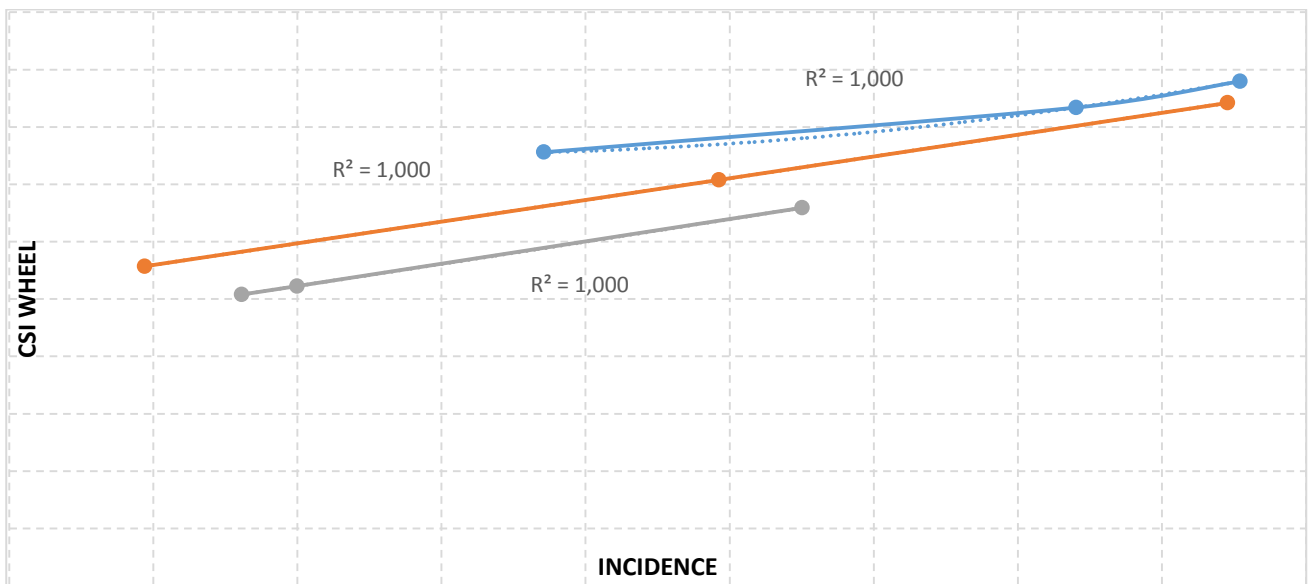


Figure 7-2 Graph of incidence related to the Csi wheel

As we can see from the drawing, the 3 lines graphed of the ξ wheel values respect the incidence, seem to be linear.

So we can affirm that the behavior of the ξ wheel can be described by the incidence, and we use the medium graph equation as “reference equation”.

$$0,000000057 * i^2 + 0,00379197 * i + 0,35524390$$

✓ *CSI NOZZLE*

For what concern the ξ nozzle we have ordered the values from the smallest to the biggest, and divided them in 3 groups.

	Abs. Mach at wheel inlet	Csi Nozzle	%IGV
178-2	1,242	0,082	75,93
188-2	1,227	0,083	75,93
208-2	1,201	0,086	75,93
178	1,333	0,1	100
188	1,306	0,1	100
208	1,241	0,1	100
178+2	1,385	0,119	123,4
188+2	1,365	0,119	123,4
208+2	1,27	0,125	123,4

Table 5 CSI nozzle values for HP

Then I graphed the ξ nozzle respect the absolute Mach and the incidence. What we can observe from the drawing is that there is no dependence between the coefficient loss and the absolute Mach, while there is a linear dependence with the percentage of the inlet guide vanes.

So, we can describe the ξ nozzle behavior only using the opening percentage of the inlet guided vanes.

The equation is calculated making an average of the coefficients of the three equations.

In this case, we are not choosing the medium line, as done in the previous case, because the three lines are really near each other, and the medium point is the same for all the lines. So we can simply make the average.

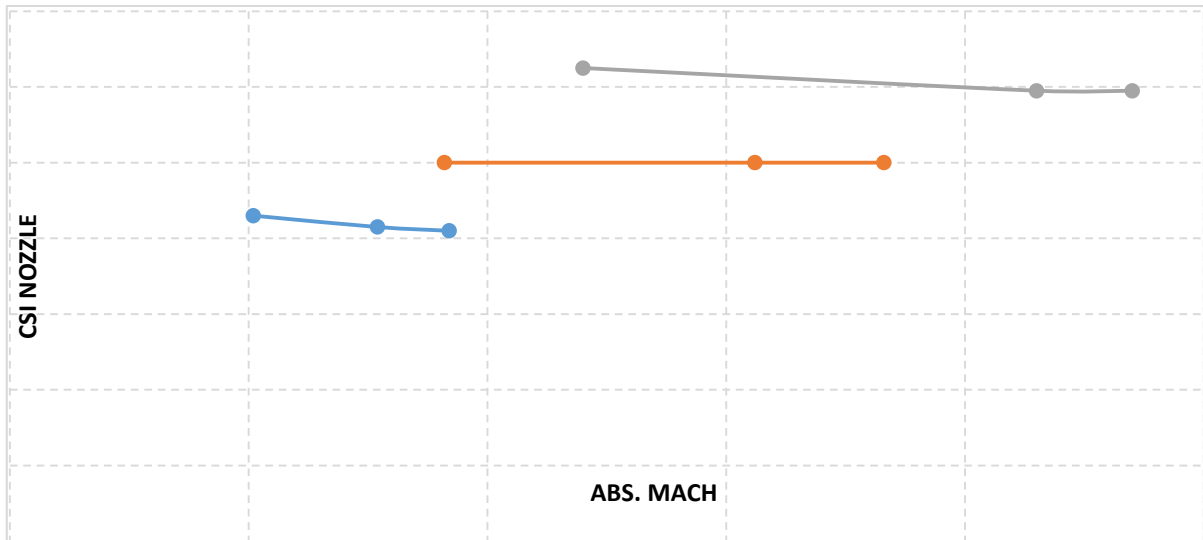


Figure 7-3 Graph of Absolute Mach related to the Csi nozzle

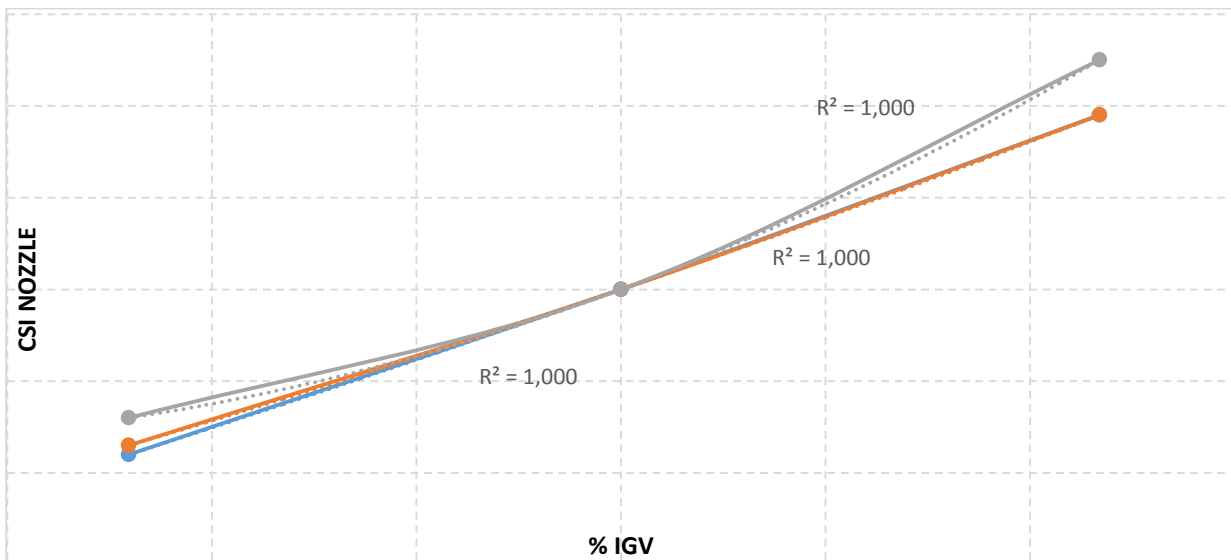


Figure 7-4 Graph of %IGV related to the Csi nozzle

$$0,000004333 * IGV^2 - 0,0001333 * IGV + 0,067166667$$

✓ CV NOZZLE

The value of this parameter is constant for the same geometry. It is constant because the nozzle is choked.

The flow coefficient goes from the beginning of the nozzle, to the throat area of the nozzle (where the Mach is equal to 1), and can be considered uniform in that area.

Despite the %IGV opening, the losses and the mass flow until the throat is almost always equal.

For this reason, for all the High-Pressure and Low-Pressure cases, the values of the flow nozzle coefficient for the different points will always be the same.

	Incidenza	Coeff. Flow nozzle	%IGV
178	2,512	0,976	100
188	-0,380	0,976	100
208	-6,448	0,976	100
178-2	-15,02	0,976	75,93
188-2	-16,94	0,976	75,93
208-2	-20,3	0,976	75,93
178+2	15,3	0,976	123,4
188+2	17,7	0,976	123,4
208+2	12,02	0,976	123,4

Table 6 CV nozzle values for HP

✓ *CV WHEEL*

For the CV wheel values, we use the same approach we have used for the CSI wheel. So, we will have:

	Incidenza	Relative Mach	Cv wheel
208	-6,448	0,345	0,88
208+2	12,02	0,284	0,89
188+2	17,7	0,386	0,96
208-2	-20,3	0,409	0,886
188	-0,380	0,406	0,9
178+2	17,17	0,413	0,9
188-2	-16,94	0,422	0,89
178-2	-15,02	0,431	0,905
178	2,512	0,426	0,91

Table 7 CV wheel values for HP

So, I make the graph of the parameter with the incidence.

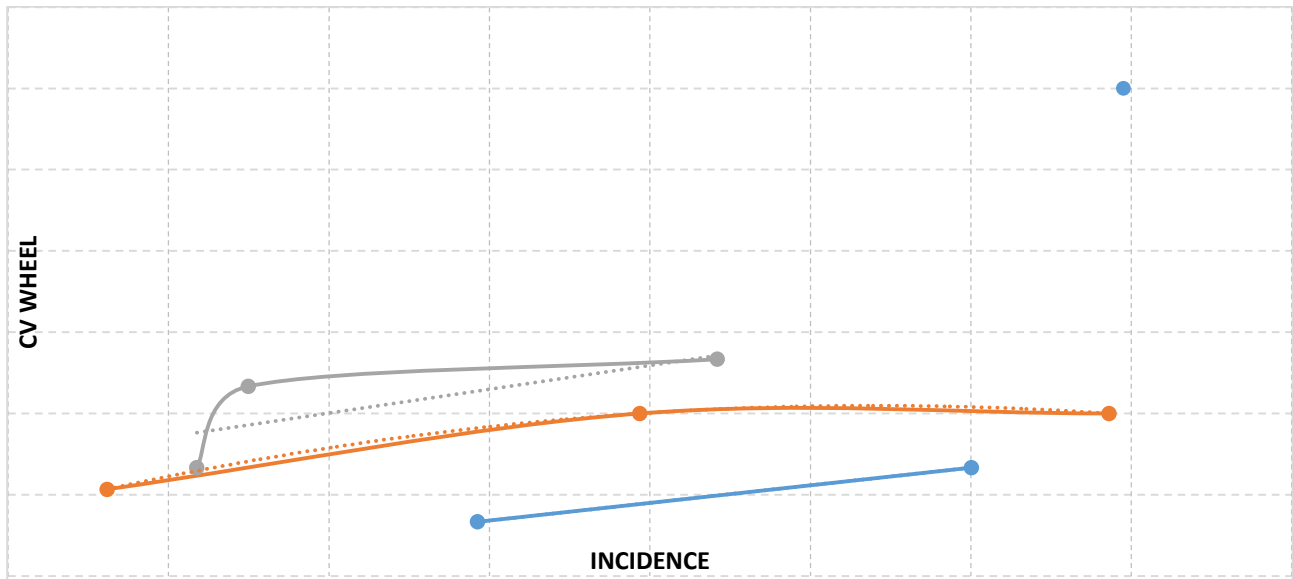


Figure 7-5 Graph of incidence related to the Cv wheel

As we can see, in this graph there is a strange point, 188+2, which has a value of Cv, really high compared to the others.

We can affirm looking at its behavior, that is a strange point, and for this reason is not part of the graph, but only represented as a single point. This point corresponds to an opening percentage of the inlet guided vane equal to 70.

The points with %IGV equal to 70 are the most difficult to study because the opening of the inlet guided vanes is small, so we could even avoid that point from the graph, not being the calibration accurate.

Anyway, apart from the incidence, we can relate the tuning parameter even to the Mach value.

For doing a new chart with the double dependence, I use the values of the three lines, and the average of the Mach relative values.

	C1	C2	C3
0,338	0,0004	0,0021	0,845
0,409	0,00001	0,00031	0,900
0,426		0,00073	0,908

Table 8 Coefficients related to the Mach

Once created the table, I make the chart connecting the coefficients with the relative Mach.

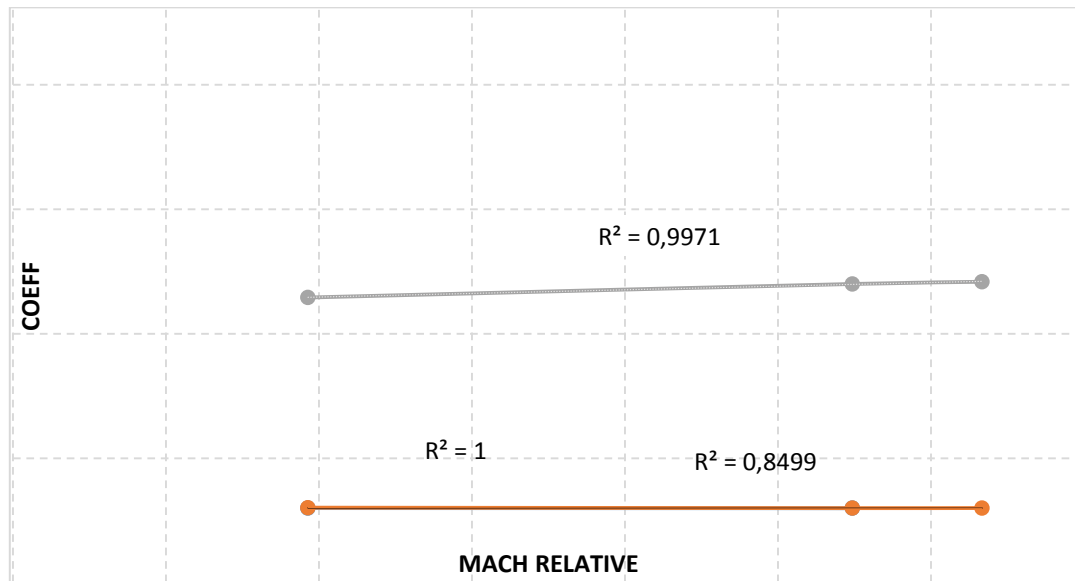


Figure 7-6 Graph of relative Mach related to the coefficients

The final equation will be:

$$(-0,0091 * M + 0,0036) * i^2 + (-0,0193 * M + 0,0086) * i + (0,7313 * M + 0,5985)$$

This type of equation could give some problems, because the values of the coefficients are close to zero, and this can give a lot of problem once that the equation will be inserted in the Hysys model. In fact, being the equation on the border between positive and negative, just a little change in the model could “crash” it, not making converge the parameters.

For this reason, we can avoid the dependence of the Mach, not being a strong dependence, and limit the dependence just with the incidence.

Doing so I will take only the medium line of the figure 7-5, and I will take in consideration just that equation.

This simplification, authorized and shared by my colleagues, has been done taking in consideration the small value of the coefficients we are treating (they all have values between 0,88 and 0,96).

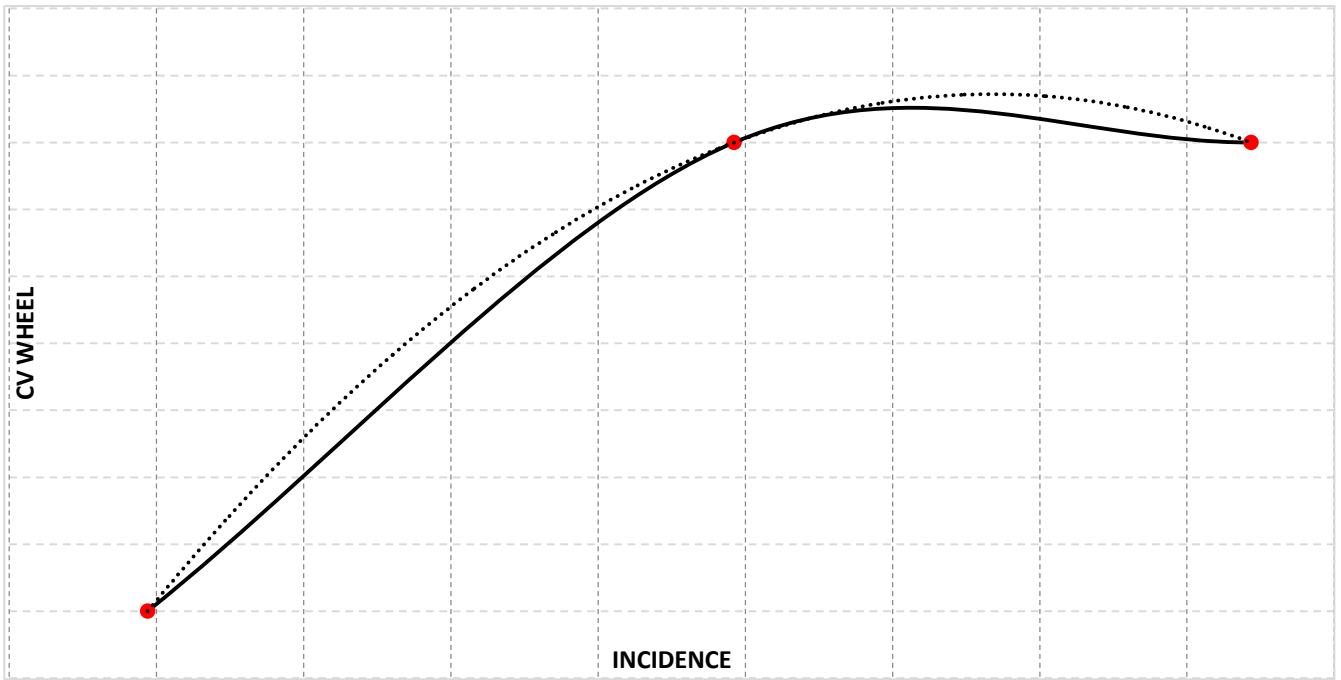


Figure 7-7 Graph of incidence related to the Cv wheel

$$-0,00001876 * i^2 + 0,00031492 * i + 0,90012264$$

✓ WHEEL DEVIATION ANGLE

For the wheel deviation angle, I act in the same way I did for CV wheel.

So, I take the data, order them and make the chart of the parameter related to the incidence.

	Incidenza	Relative Mach	Deviation
208	-6,448	0,345	9,1
208+2	12,02	0,284	18,5
188+2	17,7	0,386	15,2
208-2	-20,3	0,409	4,9
188	-0,380	0,406	7,5
178+2	17,17	0,413	15
188-2	-16,94	0,422	3,7
178-2	-15,02	0,431	3,7
178	2,512	0,426	7,3

Table 9 Wheel deviation angle for HP

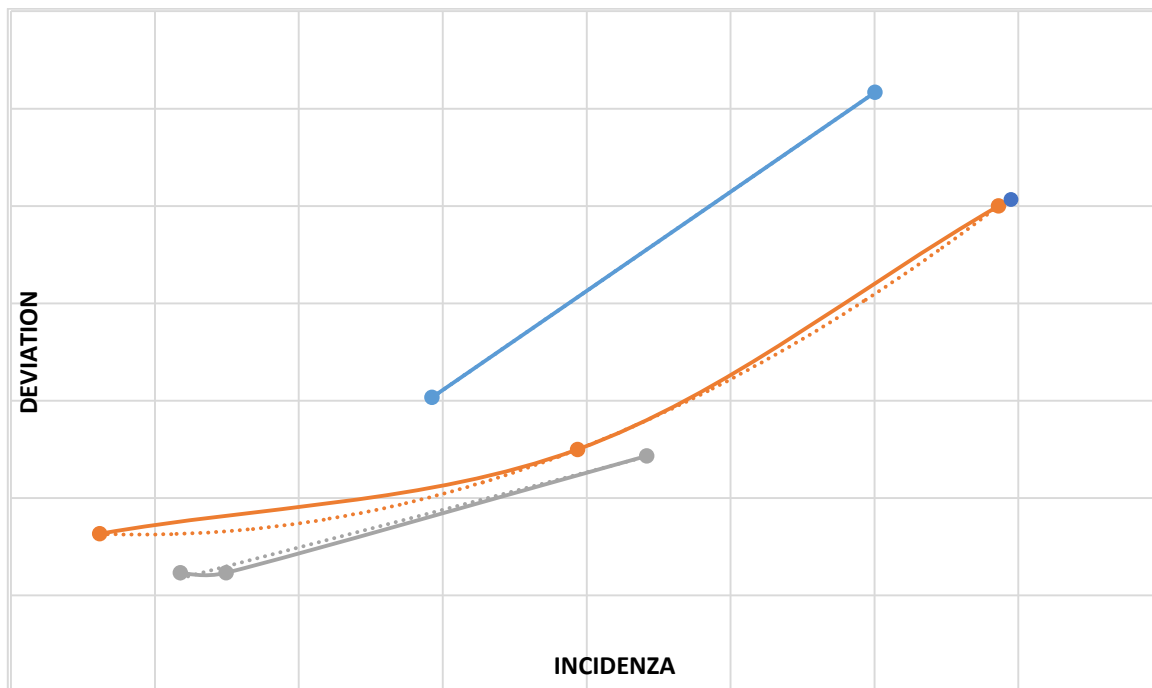


Figure 7-8 Graph of incidence related to the wheel deviation angle

As for the case of the CV wheel, I try to find even the correlation of the parameter with the relative Mach, using the coefficients of the lines and the Average Mach.

	C1	C2	C3
0,3385	-0,045	0,760	15,880
0,4097	0,007	0,294	7,610
0,4266		0,193	6,795

Table 10 Coefficients and average Mach values

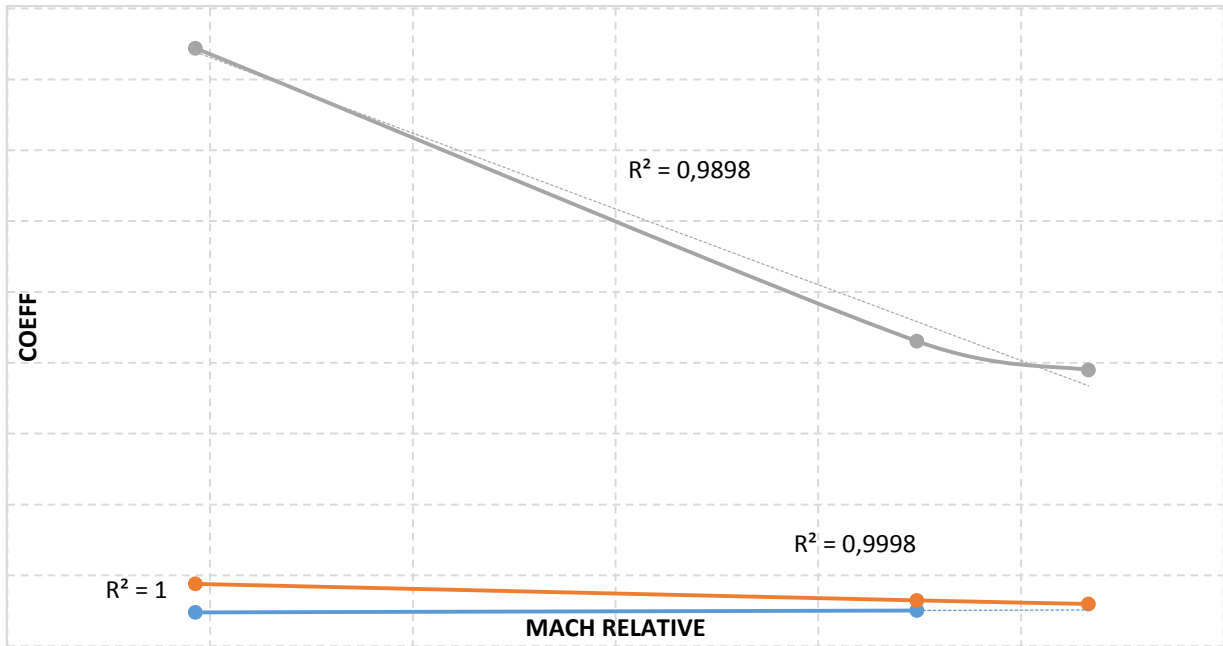


Figure 7-9 Graph of the relative Mach related to the coefficients

These equations being close to zero could give some serious problem of stability, for this reason we avoid the dependence to the Mach, and we just keep the dependence with the Incidence.

Even in this case we make the same reasoning done for the coefficient flow of the wheel, and we take only the median line of the figure 7-8.

As before, the point that create some problem is the 188+2.

We have decided, together, to exclude that point in these graphs, and eventually if the final results won't be satisfactory, that point will be studied deeper.

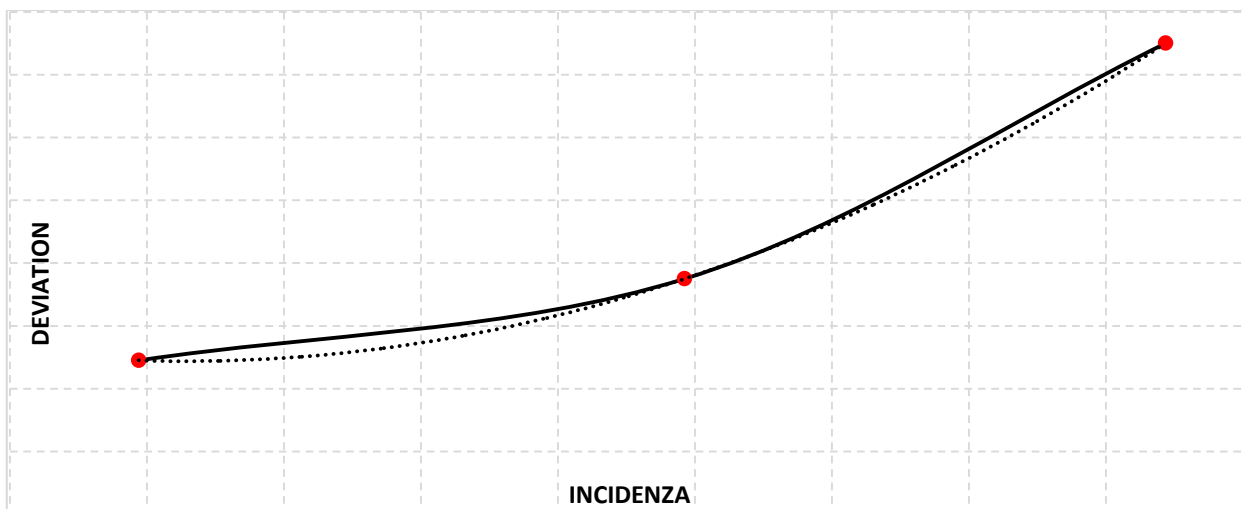


Figure 7-10 Graph of incidence related to the wheel deviation angle

$$0,00792110 * i^2 + 0,29434202 * i + 7,61093681$$

So, for making a brief summary, the relationships are the sequent, for the high-pressure case and for the low-pressure one:

HP

PARAMETER	EQUATION	RELIANCE
ξ NOZZLE	$(0,000004333) * IGV^2 - (0,0001333) * IGV + 0,067166667$	IGV
ξ WHEEL	$(0,00000057) * i^2 - (0,00379197) * i + 0,3552439$	Incidence
CV NOZZLE	0,976	Constant value
CV WHEEL	$(-0,00001876) * i^2 + (0,00031492) * i + 0,900122$	Incidence
Wheel dev angle	$(0,00792110) * i^2 - (0,29434202) * i + 7,61093681$	Incidence

Table 11 High pressure summary

These equations found are valuable for this case with this geometry. If the geometry would change, for finding out the equations we should make the same steps, but naturally with different values, and obtaining different equations.

LP

PARAMETER	EQUATION	RELIANCE
ξ NOZZLE	$(0,0000183) * IGV^2 - (0,00442853) * IGV + 0,36719509$	IGV
ξ WHEEL	$(0,000247) * i^2 + (0,005046) * i + 0,272977$	Incidence
CV NOZZLE	0,971	Constant value
CV WHEEL	$(0,00003935) * i^2 + (0,00098446) * i + 1,03097439$	Incidence
Wheel dev angle	$(0,04816233) * i + 5,11790717$	Incidence

Table 12 Low pressure summary

7.5. VERIFICATION AND COMPARISON

Once every equation, with its respective dependence has been found, we can recalculate the parameters and so make a comparison with the one of the CFD.

I will only report the values of the high pressure.

CFD

	Csi Nozzle	Csi wheel	Coeff. Flow nozzle	Cv wheel	Wheel deviation angle
178	0,082	0,3295	0,976	0,91	7,3
188	0,083	0,3538	0,976	0,9	7,5
208	0,086	0,3779	0,976	0,88	9,1
178-2	0,1	0,2612	0,976	0,905	3,7
188-2	0,1	0,2539	0,976	0,89	3,7
208-2	0,1	0,2785	0,976	0,886	4,9
178+2	0,119	0,4268	0,976	0,9	15
188+2	0,119	0,4397	0,976	0,96	15,2
208+2	0,125	0,4169	0,976	0,89	18,5

MODEL

	Csi Nozzle	Csi wheel	CV nozzle	Cv wheel	Wheel deviation angle
178	9,72E-02	0,3464	0,976	0,9006	8,182
188	9,72E-02	0,3541	0,976	0,9	7,52
208	9,72E-02	0,3386	0,976	0,8984	6,471
178-2	0,1168	0,2824	0,976	0,8863	4,892
188-2	0,1167	0,2801	0,976	0,8865	4,89
208-2	0,1167	0,268	0,976	0,8829	5,037
178+2	8,20E-02	0,4263	0,976	0,8995	15,87
188+2	8,20E-02	0,4228	0,976	0,8998	15,34
208+2	8,20E-02	0,4108	0,976	0,9007	13,56

DIFFERENCE

	Csi Nozzle %	Csi wheel %	CV nozzle %	Cv wheel %	Wheel deviation angle %
178	18,54	5,13	0,00	1,03	12,08
188	17,11	0,08	0,00	0,00	0,27
208	13,02	10,40	0,00	2,09	28,89
178-2	16,80	8,12	0,00	2,07	32,22
188-2	16,70	10,32	0,00	0,39	32,16
208-2	16,70	3,77	0,00	0,35	2,80
178+2	31,09	0,12	0,00	0,06	5,80
188+2	31,09	3,84	0,00	6,27	0,92
208+2	34,40	1,46	0,00	1,20	26,70

Table 13 Difference values

Looking at the table of the difference values, we can notice an important percentage difference in the “Csi nozzle”, and “Wheel deviation angle” values.

For what concern the nozzle coefficient of losses, we are treating values that are small, so even if the percentage difference seems to be huge, we are speaking of small values.

The high difference foreseen in the “wheel deviation angle” value, for almost every point, will influence only in a small way the final outputs not causing any particular problem.

So, as suggested by GE expert we can accept these values, and analyze the percentage difference in the final output, which will give us the conception of the work done.

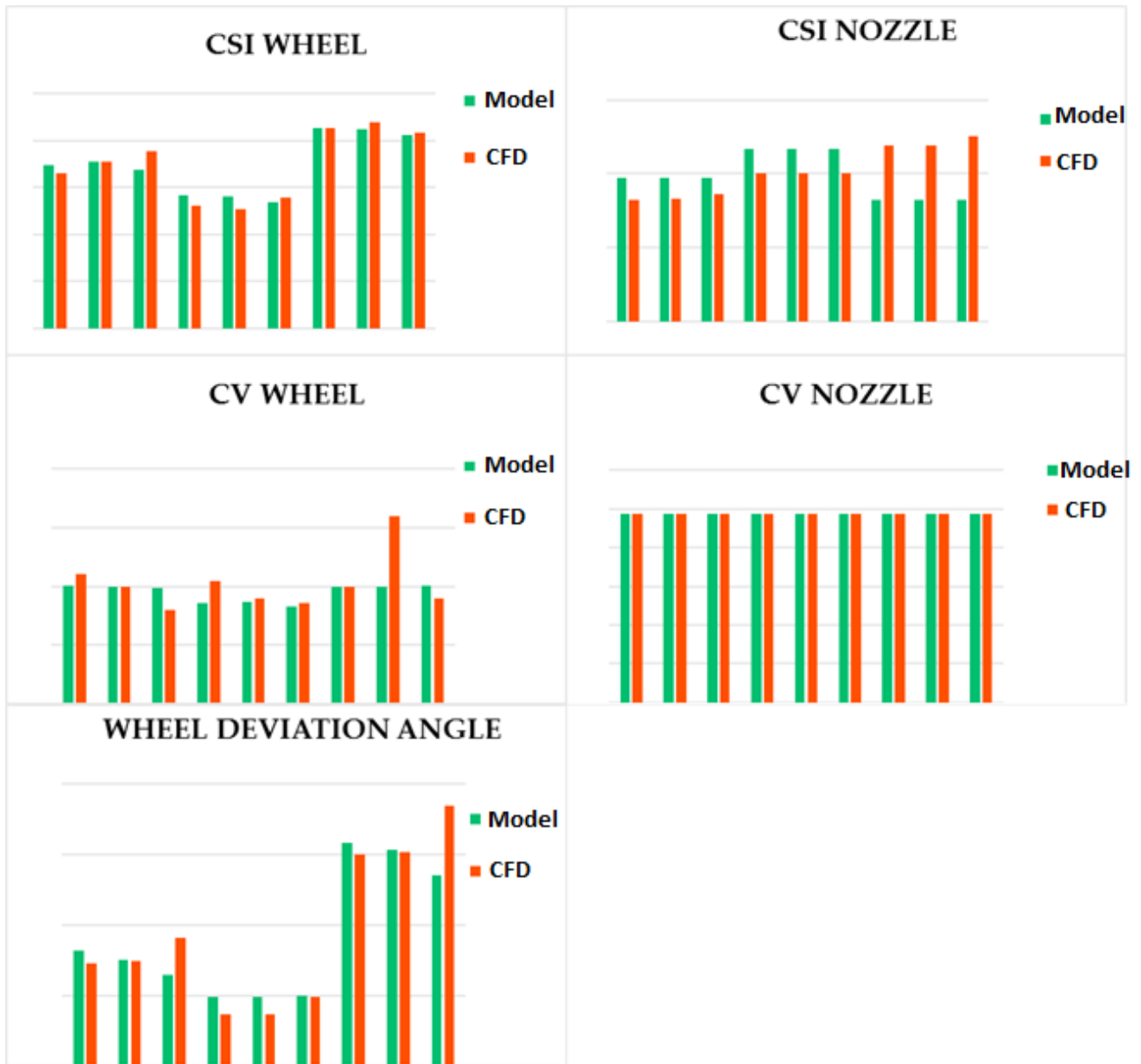


Figure 7-11 Model vs CFD comparison

Later on, inserting the equations found into the Hysys program, I can match the different values of eta, mass flow and power.

CFD

	ETA	MASS FLOW	POWER
178	86,18	116	7549
188	86,47	116	7300
208	85,3	116	6699
178-2	85,8	143,3	9305
188-2	86,39	143,2	9053
208-2	86,75	143,2	8477
178+2	83,96	88,1	5570
188+2	82,57	88,1	5310
208+2	80,64	88,1	4796

MODEL

	ETA	MASS FLOW	POWER
178	85,9	116	7526
188	86,54	116	7305
208	86,4	116	6797
178-2	83,69	143,3	9063
188-2	84,62	143,2	8856
208-2	85,17	143,2	8322
178+2	85,14	88,1	5648
188+2	84,51	88,1	5403
208+2	83,74	88,1	4964

DIFFERENCE

	ETA	MASS FLOW	POWER
178	-0,325960419	0	-0,305607228
188	0,080887451	0	0,06844627
208	1,273148148	0	1,441812564
178-2	-2,521209225	0	-2,670197506
188-2	-2,091704089	0	-2,224480578
208-2	-1,855113303	0	-1,862533045
178+2	1,385952549	0	1,38101983
188+2	2,295586321	0	1,721265963
208+2	3,701934559	0	3,384367446

And finally, the respective graphs

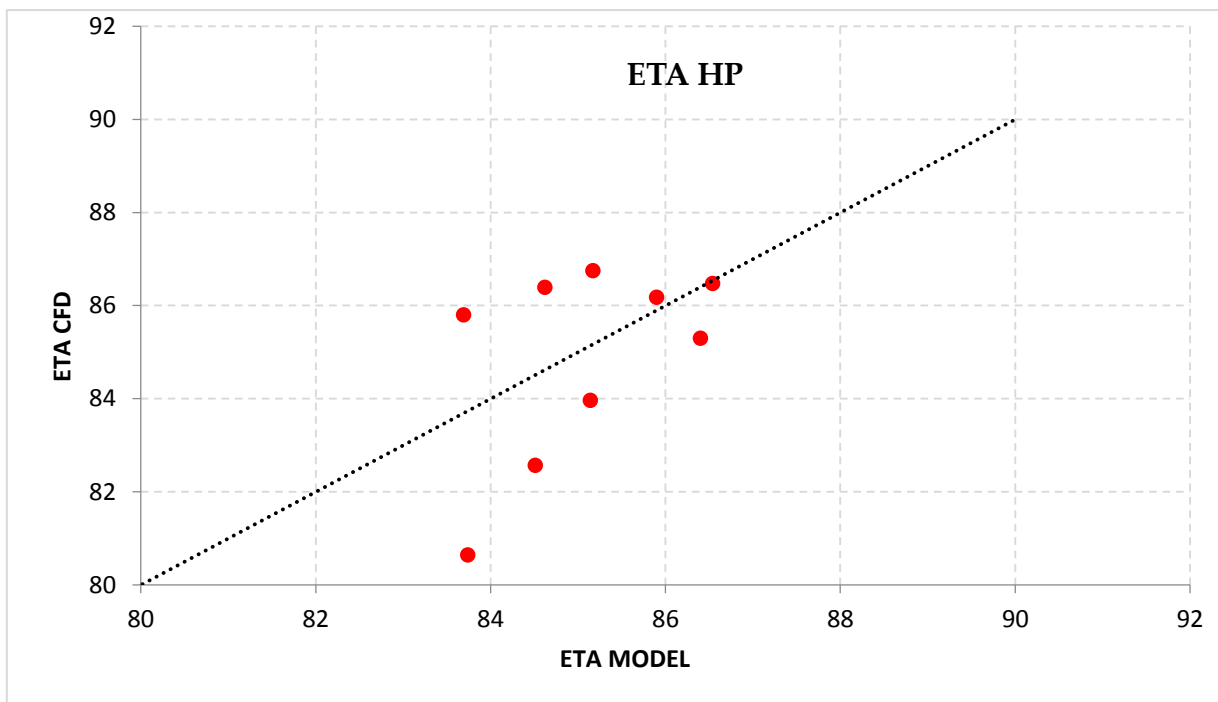


Figure 7-12 Model vs CFD comparison for eta

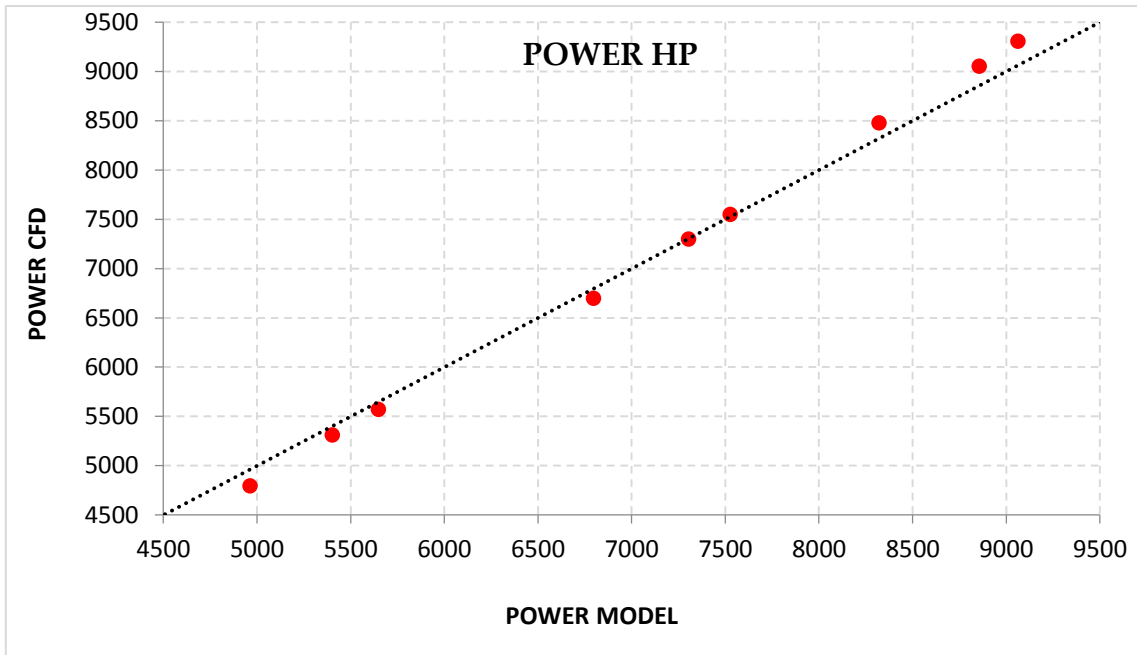


Figure 7-13 Model vs CFD comparison for the power

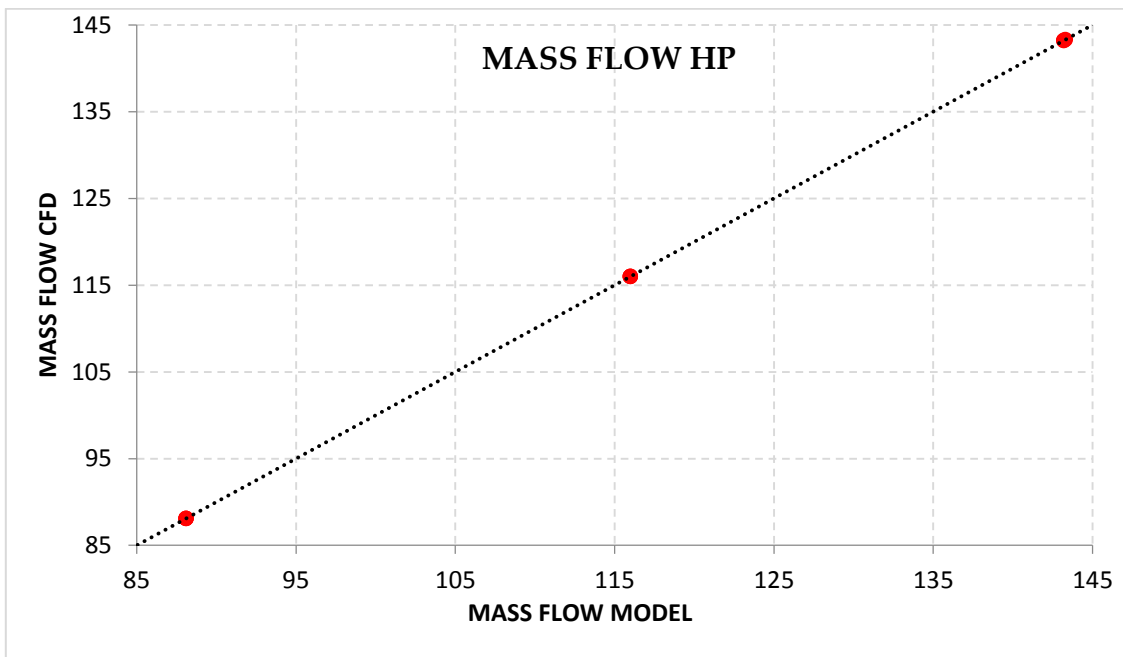


Figure 7-14 Model vs CFD comparison for the mass flow

Looking at the graphs related to the ‘Power HP’, ‘Eta HP’, and ‘Mass flow HP’ we can see that the difference between model and CFD is small.

Analyzing the percentage difference, we can understand if the equations found for the tuning parameters of the alternative model are valuable or not.

These three values, which are the output of the map generator, are of fundamental importance, and the maximum difference acceptable between the CFD value and the model value can be of 3%. If the difference would be higher the result could not be accepted.

For what concern the ‘mass flow’ the results are perfectly equal, and for the efficiency the difference is small.

Taking in consideration the gas power, we have a higher difference for some points, sometimes is over estimated, other times sub estimated, but anyway the values always fall in the acceptance field, so they do not cause any problem.

The point with the highest difference is the one with the highest counter pressure, and lowest %IGV, so we are speaking of a limit case.

7.6. CONCLUSION

Studying the graphs related to the model and CFD values, we can prove that the results are all comparable, except the ‘wheel deviation angle’.

The value of the C_v wheel doesn’t depend absolutely on the %IGV, as is easily understandable from the formula where both numerator and denominator depend on the wheel area, that doesn’t change with the different percentage of the vane. It changes with the counter-pressure.

For what concern the value of the C_{si} wheel, it depends linearly to the counter pressure. This is easily understandable from the formula, that contains the value P_{02} rothalpic, that increases when increases the pressure at the outlet of the wheel (P_2).

This can’t be affirmed for the C_{si} nozzle, the values of P_1 and P_{01} increase of the same quantity with the increase of P_2 , and so the value of the parameter doesn’t change with the counter pressure. It only changes with the %IGV.

This difference between the losses in the nozzle and in the wheel, is explicable observing that in these two sections of the expander are present different types of losses. In the nozzle, there are mainly losses for friction, while in the wheel they depend to the incidence (thickening of the boundary layer).

The wheel deviation angle instead increases with the decrease of the %IGV, that is naturally connected with the mass flow.

If the mass flow which flows along the nozzle decreases, the difference angle between the blade and the flow that passes over it increases.

We can affirm to have found a *valuable model* that describes the behavior of a turboexpander, using 5 calibration parameters described by equations. We have validated an alternative model for analyzing points where the CFD is not present, starting from some CFD stationary data.

The next step will be to use the performances maps for improving the prediction of the behavior of the total gas power of the turboexpander.

8. MAP CREATION

Once created the performances maps that better represent the behavior of the two stages of the turboexpander, the next step of my work would be of using these maps for modeling the outputs.

As we have seen before there are three outputs (Power, Eta, Mass flow), but the one I'm more interested in is the total gas power.

The equation of the total gas power that was used in the previous Hysys dynamic model was calculated in an analytical way.

Was used a flow function, a function that describes parameter related to other parameters. This function was not so accurate, for this reason the result of the total gas power had an uncertainty. It was calibrated for the nominal point, but for what concern the off-design point, it was improvable.

For modeling the total gas power, we are going to use the stationary model.

By this device we can study the model for understanding the behavior of the adimensional torque related to %IGV and u/c .

We will find an equation of the adimensional torque as function of u/c and of the percentage of inlet guided vane. The equation must be found for being inserted in the dynamic model, and having a more complete overview of the Turboexpander behavior.

The steps I followed for calculating the maps, always using the Hysys program, are:

1. I take one of the stationary model with %IGV equal to 100.
2. Change the value of u/c giving a value to it equal to: $\{u/c - 1,1*u/c - 1,2*u/c\}$. I give these values to u/c because I want to study its behavior at the boundaries. For reaching this value I change «pressure static 2». Once reached the right value I note the value of «pressure diffuser exit».
3. Change the value of %IGV. We take in consideration a range of it from 20 to 140; naturally changing this value the «pressure diffuser exit» will change.
4. Change the «static p at wheel exit», until the «pressure diffuser exit» will reach its initial value.
5. Control that the «Csi wheel» parameter would have the right value.

The opening of the inlet guided vane goes from 20 to 140. This is the aerodynamical opening, while the mechanical opening goes from 0 to 100.

The aerodynamical opening is the theoretical opening, used for the design, and in the theoretical calculation. The mechanical one instead is the practical opening.

In this way, I'm going to create a lot of different models with three values of u/c , and for each one of them I have different values of %IGV.

For every model I build, I have to take in consideration three values, which will be used in the creation of the maps

- **Eta** → Total to total isentropic efficiency

- **Tau** → $\tau = \frac{\eta}{2} * \left(\frac{U}{C}\right)^{-1}$
- **u/c** → Tangential speed / absolute isentropic speed

The equation of Tau is calculated from the sequent equations, starting from the torque value(T):

$$T = \frac{P}{\omega} = \frac{P}{P_{is}} * \frac{P_{is}}{\omega}$$

$$T = \eta_{tt,is} * \dot{m} * \frac{\Delta h_{tt,is}}{\omega} = \eta_{tt,is} * \dot{m} * \frac{c_{is}^2}{2 * \left(\frac{u}{r}\right)}$$

$$T = \eta_{tt,is} * \frac{\dot{m}}{\left(\frac{u}{C}\right)} * \frac{c_{is}}{2} * r = \dot{m} * r * c_{is} * \frac{\eta_{tt,is}}{2 * \left(\frac{u}{c_{is}}\right)}$$

$$\tau = \frac{T}{\dot{m} * r * c_{is}} = \frac{\eta_{tt,is}}{2 * \left(\frac{u}{c_{is}}\right)}$$

T: Torque

τ : Adimensional torque

\dot{m} : Mass flow

P: Power

ω : Angular velocity

r: Radius

c: Isentropic speed

u: Tangential speed

$\eta_{tt,is}$: Total to total isentropic efficiency

So, as done for the static model, I will only report the results for the HP.

For every table I create, I have even made a graph of the behavior of the efficiency related with the different %IGV, for taking control of the curve it creates.

The normal behavior should be of growth of the efficiency with the growth of the %IGV, until it reaches a perfect value; later, it decreases with the growth of the opening of the inlet guided vanes, due to the losses.

(U/C)

%IGV	30	40	50	60	70	80	100	110	120	130	140
DH_{tt,is}	74,21	74,21	74,21	74,21	74,21	74,21	74,2	74,21	74,2	74,21	74,21
ETA	78,207	79,083	80,260	81,589	82,867	84,003	85,809	85,651	84,3	81,26	73,59
U	239,9	239,9	239,9	239,9	239,9	239,9	239,9	239,9	239,9	239,9	239,9
Cis	385,2	385,2	385,2	385,2	385,2	385,2	385,2	385,2	385,2	385,2	385,2
U/C	0,622	0,622	0,622	0,622	0,622	0,622	0,622	0,622	0,622	0,622	0,622
Mass flow	34,81	46,41	58,01	69,62	81,22	92,82	116	127,6	139,2	150,8	162,4
Tau	0,628	0,635	0,644	0,655	0,665	0,674	0,689	0,687	0,677	0,652	0,590

Table 14 Values for $u/c = 1$

1,1*(U/C)

%IGV	30	40	50	60	80	90	100	110	120	130	140
DH_{tt,is}	61,32	61,34	61,28	61,33	61,32	61,32	61,35	61,32	61,32	61,32	61,32
ETA	73,579	76,05	77,970	79,807	83,423	84,510	85,101	85,816	86,129	85,275	83,496
U	239,9	239,9	239,9	239,9	239,9	239,9	239,9	239,9	239,9	239,9	239,9
Cis	350,2	350,3	350,1	350,2	350,2	350,2	350,3	350,2	350,2	350,2	350,2
U/C	0,684	0,684	0,685	0,684	0,684	0,684	0,684	0,684	0,684	0,684	0,684
Mass flow	34,81	46,41	58,01	69,62	92,82	104,4	116	127,6	139,2	150,8	162,4
Tau	0,537	0,555	0,569	0,582	0,609	0,616	0,621	0,626	0,628	0,622	0,609

Table 15 Values for u/c multiplied for 1,1

$$1,2*(U/C)$$

%IGV	30	40	50	60	70	80	100	110	120	130	140
DHtt, is	51,6	51,6	51,6	51,6	51,6	51,61	51,59	51,61	51,58	51,59	51,59
ETA	69,73	72,703	75,15	77,03	78,65	79,94	81,24	81,599	81,759	81,552	81,337
U	239,9	239,9	239,9	239,9	239,9	239,9	239,9	239,9	239,9	239,9	239,9
Cis	321,3	321,3	321,3	321,3	321,3	321,3	321,2	321,2	321,2	321,2	321,2
U/C	0,746	0,746	0,746	0,746	0,746	0,746	0,746	0,746	0,746	0,746	0,746
Mass flow	34,81	46,41	58,01	69,62	81,22	92,82	116	127,6	139,2	150,8	162,4
Tau	0,466	0,486	0,503	0,515	0,526	0,535	0,543	0,546	0,547	0,546	0,544

Table 16 Values for u/c multiplied for 1,2

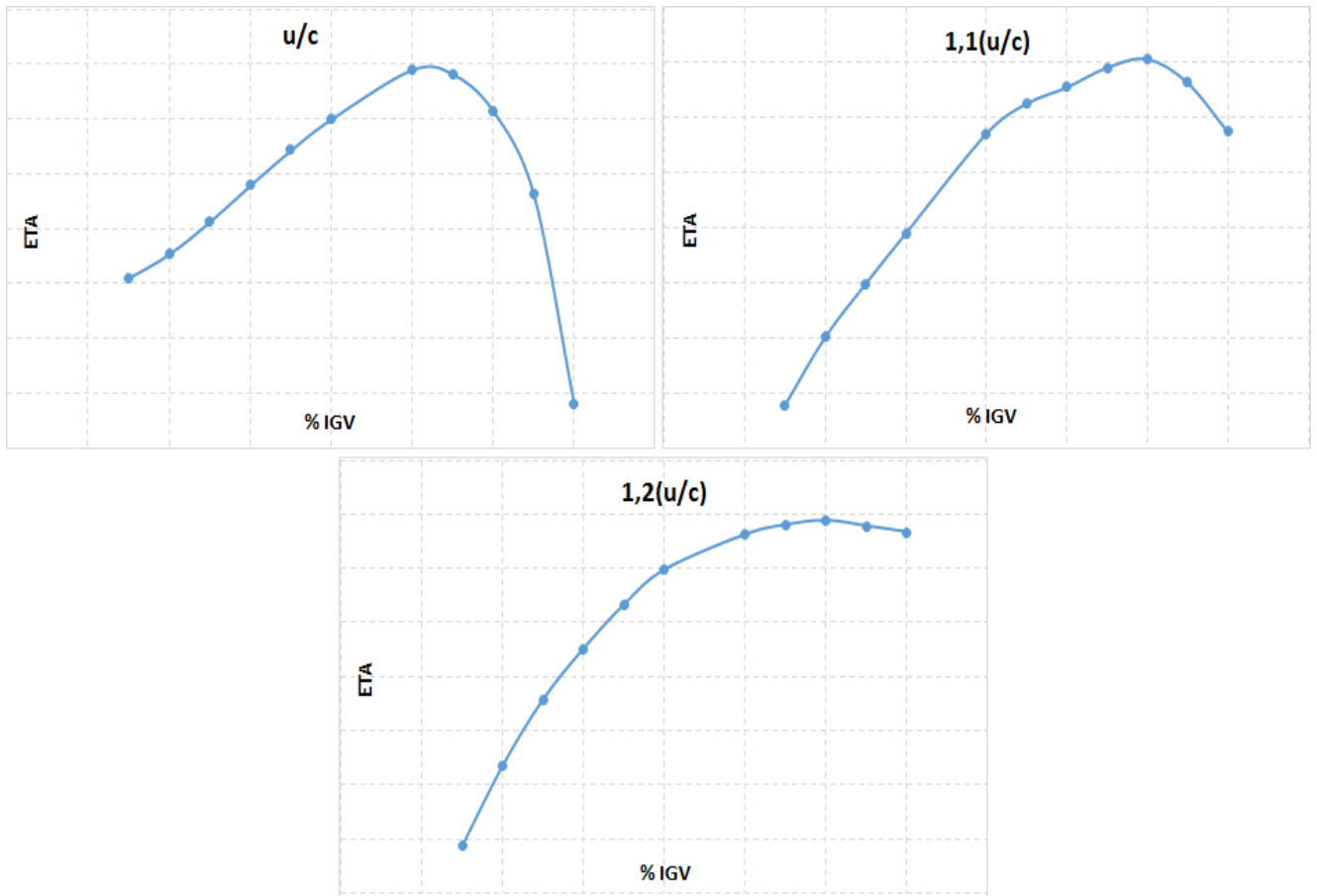


Figure 8-1 %IGV related to Eta, changing the u/c value

As we can see from the graphs, every line follows the normal behavior of the yield related to the opening of the inlet guided vane.

Once we have noted the values of tau and u/c we go ahead doing their graph, related with the growth of the %IGV, and using excel we find and annotate the formulas of every straight line.

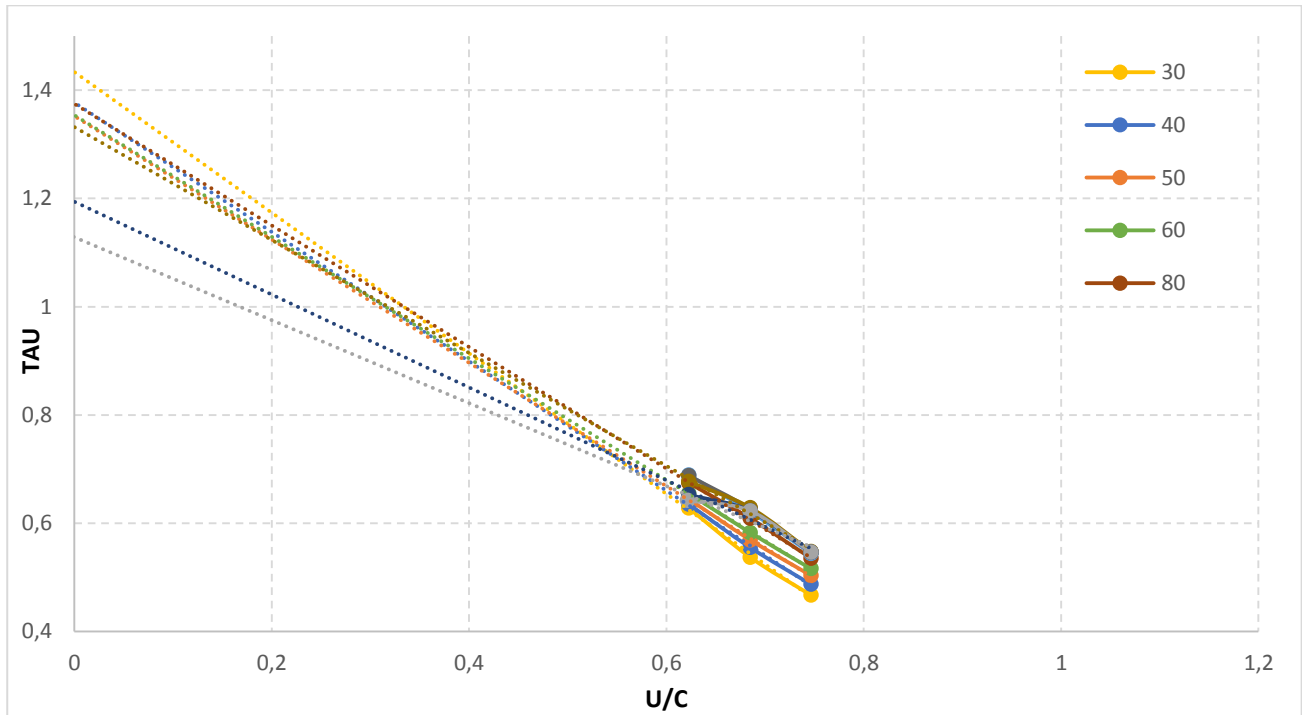


Figure 8-2 Graph of U/C related to Tau for different inlet guided vanes opening

Looking at this graph, we can note that the trendline for the limit cases has a direction a little bit different from all the other trendlines, that have similar behavior.

As we have seen in the graphs and in the conclusions of the previous chapter, the gas power is foreseen with a small uncertainty (lower than 3%) with %IGV between 75 and 120, so naturally increasing over 120 or decreasing below 75, the uncertainty will increase.

Being “tau” connected to the gas power, is explained why at those %IGV the trendlines do not have the same direction of the others.

As suggested by GE expert, we can even not take care of those cases for some simple reasons.

In the next step, we are not going to use the different values of tau for %IGV equal to 0, but we will use a unique one.

The other reason is that these cases analyzed are almost unique.

Rarely a plant need to open the nozzle vane at its maximum opening (130-140), or to almost close them totally (30), so we are not interested in the perfect design of tau at those values.

In this way, we have understood that when we are strongly off-design, our map generator is not able to validate perfectly the behavior of the expander.

Theoretically when the value of u/c is equal to 0, the value of τ should be the same for every opening percentage of the inlet guided vane.

This happens because, when $u=0$ even the angular speed ω will be equal to 0, and this means that the rotor wouldn't rotate.

Not rotating, the value of "tau" is due to a nominal couple. For finding its value I find the value of every straight line when u/c is equal to 0, and then I make an average.

We need to know the value of the nominal couple for studying better, eventually, the start-up of the plant. With $\omega = 0$ the couple is proportional to $\sqrt{\Delta h}$.

The reason why we are going to use the couple, and no other values, as for example the efficiency, is that the value of the couple is fundamental for creating a robust dynamic model, so is necessary this study of the couple.

HP average $\tau = 1,378$

LP average $\tau = 1,404$

Now I can rewrite every equation using the initial point value, and the point I've just found, where they are supposed to converge.

In this graph, we can see the difference between the new equations, represented by the lines, and the values of the old equations of the previous graph.

Of the previous graph I've just taken the points of u/c studied previously for making a comparison. As we can see the difference between the equations is small.

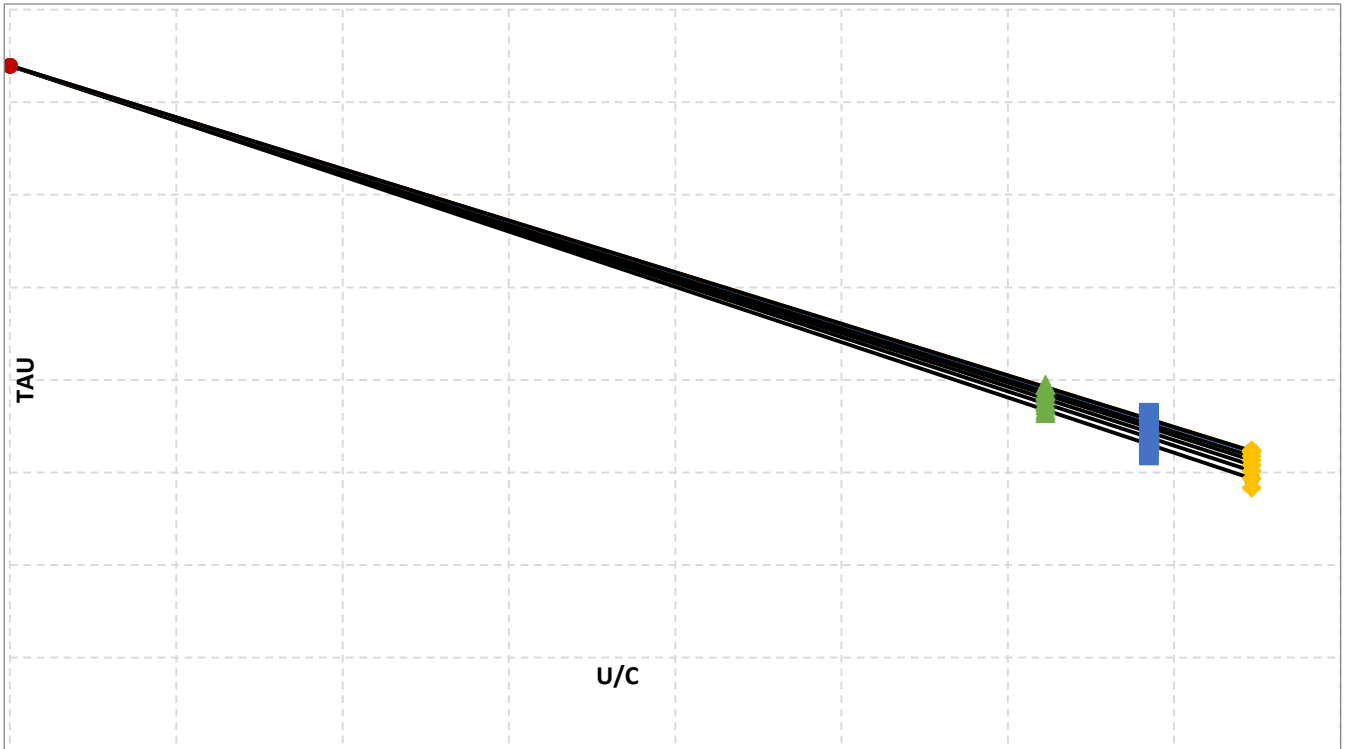


Figure 8-3 Graph of U/C related to τ

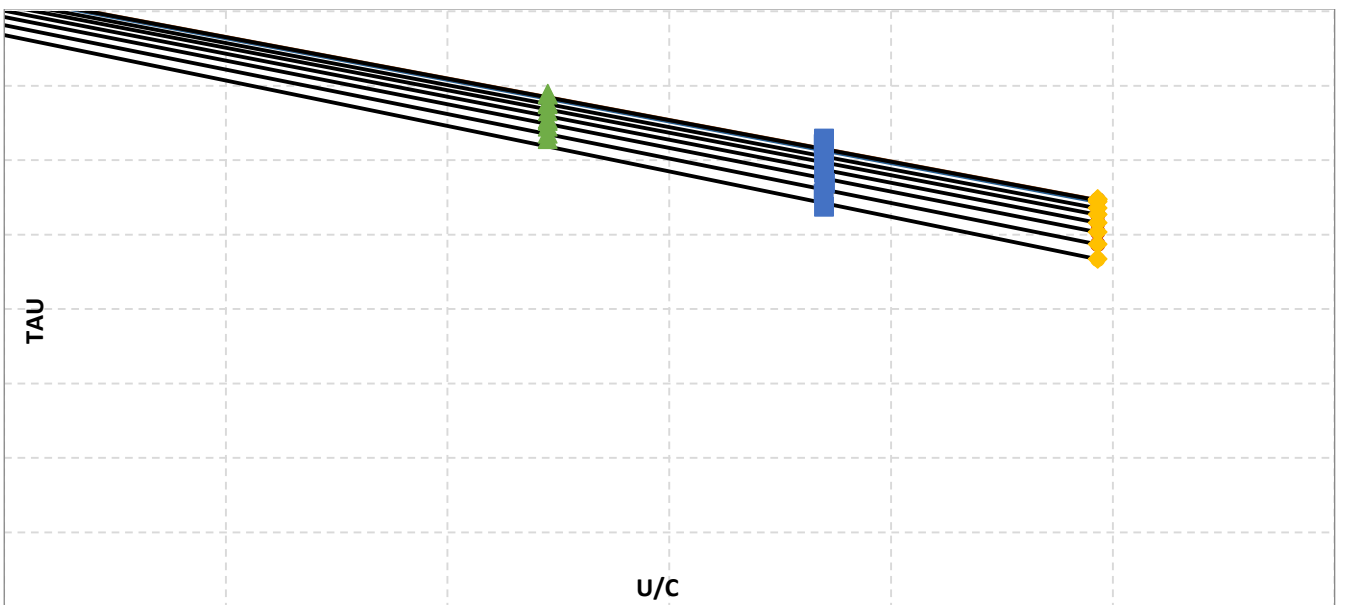


Figure 8-4 Graph of U/C related to τ zoomed

Now for creating the map we rewrite the value of “tau” using this formula:

$$\tau = a - b(y) * x$$

- **a** → Value of tau when u/c is equal to 0
- **b** → Slope of the line, which depends on
- **y** → %IGV
- **x** → u/c

We are going to use an equation like this because permits us to interpolate all the values in a perfect way.

For calculating the slope of the line, I make a graph between the angular coefficients of the equations found previously and the %IGV.

With excel I can calculate the value of the trendline, that is necessary for finding the equation of the slope. The equation found in the figure 8-5 will be the angular coefficients.

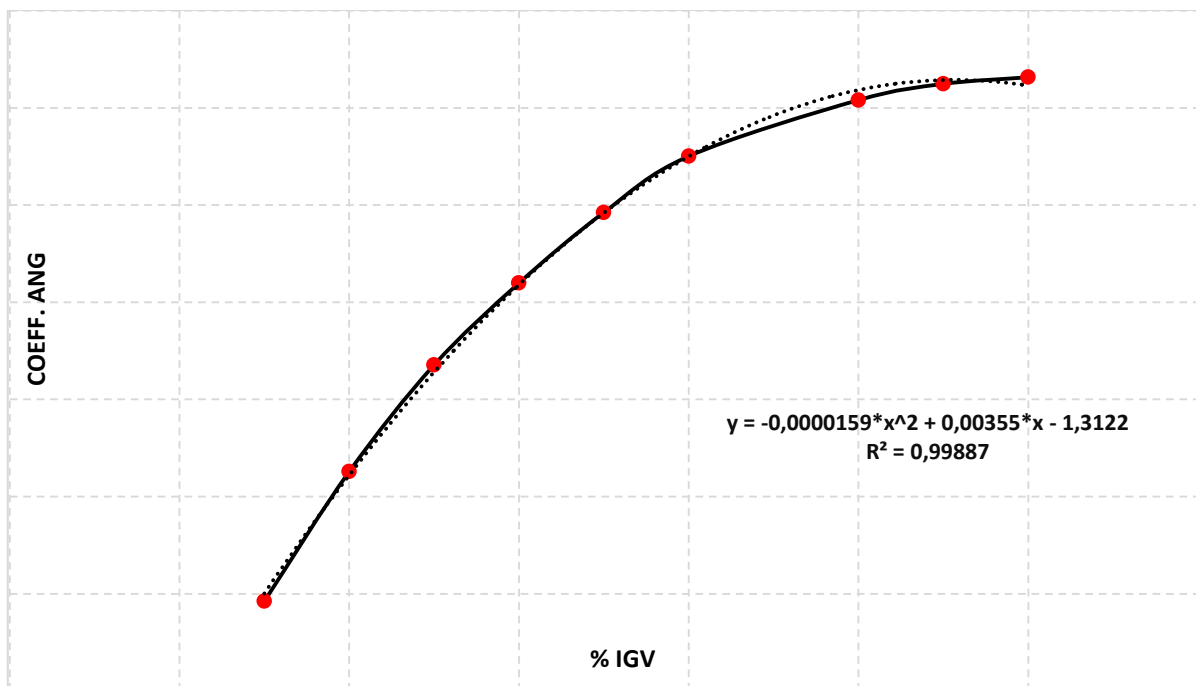


Figure 8-5 Graph of the angular coefficients related to the %IGV

Finally, we can write the final equation of “tau”, for both high-pressure and low-pressure expanders.

HP → $\tau = 1,379 + (-0,000015 * IGV^2 + 0,0035 * IGV - 1,3122) * U/C$

LP → $\tau = 1,4041 + (-0,000021 * IGV^2 + 0,00494 * IGV - 1,4053) * U/C$

For understanding if the equation is correct, I make the comparison between the “tau” value of the equation and the “tau” value of the initial CFD.

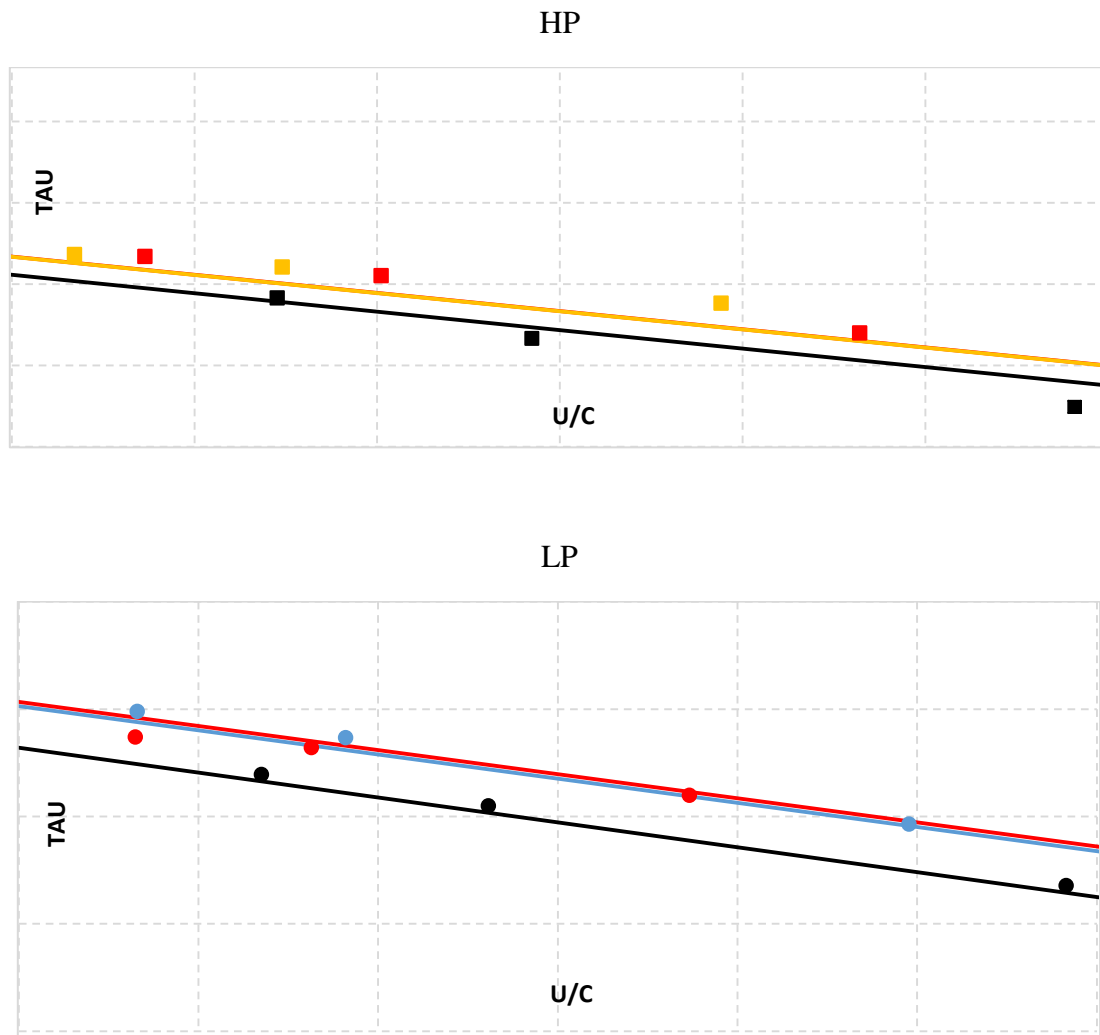


Figure 8-6 u/c vs Tau for high and low pressure

The straight lines in the figure 8-6 are derived by the new equations found, and are calculated giving different values to the %IGV (20-140) and u/c, while the points we can see, are the values of the CFD for the different percentage of inlet guide vanes.

The comment we can make analyzing these graphs is that the model validates the CFD, being the points near the straight lines, and being the numerical difference small.

HP

IGV	U/C _{is}	TAU_OLD	TAU_NEW	DIFFERENCE %
100	0,627	0,686	0,678	1,193
100	0,640	0,675	0,664	1,614
100	0,666	0,640	0,635	0,765
123,4	0,623	0,688	0,682	0,52
123,4	0,634	0,680	0,670	1,499
123,4	0,658	0,658	0,643	2,263
75,93	0,634	0,661	0,659	0,347
75,93	0,648	0,636	0,643	1,068
75,93	0,678	0,594	0,609	2,556

Table 17 Values of adimensional torque for high pressure

LP

IGV	U/C _{is}	TAU_OLD	TAU_NEW	DIFFERENCE %
100	0,586	0,748	0,743	0,641
100	0,598	0,736	0,730	0,773
100	0,629	0,696	0,695	0,043
124	0,586	0,736	0,746	1,248
124	0,596	0,732	0,735	0,409
124	0,617	0,709	0,711	0,225
73	0,593	0,722	0,716	0,899
73	0,606	0,703	0,701	0,298
73	0,638	0,648	0,664	2,388

Table 18 Values of adimensional torque for low pressure

As we can see from the two tables, both for the LP and HP expanders the difference between the tau of the CFD, and the tau calculated using the equation is small, always lower than 2%.

Now that we are sure of the functionality of the equations we can insert them in the dynamic model.

9. DYNAMIC MODEL

Now that have been found the new equations describing the behavior of Tau for both High pressure and Low pressure expanders, we can work directly on the dynamic model.

This will cause a different way of approaching the work.

While in the static model we were working, and studying, singularly the two expanders with every single stage (nozzle, wheel and diffuser) divided one from the other, now we have to work on the whole turboexpander.

Every small change that will be done on the turboexpander will influence the whole heat recovery cycle.

In the dynamic model the turboexpander is composed by a unique block, so we cannot change anymore, as before, intermediate values between the two expanders. We are going to treat the two expanders as a unique box.

This difference will naturally complicate the way of modifying the model.

Is important to highlight that, the dynamic model is not used for studying the intrinsic dynamic between the devices of the whole cycle, but only for replicating actions done in the field site, for obtaining a new stationary state.

We introduce a disorder, and once every value has changed, we wait until is reached another stall phase. We are not going to analyze the transitory, but only the final result.

I haven't dealt with the dynamic part of the model, so all the part of the transitory has not been faced up, even because the dynamic part wouldn't be inherent with my work of thesis.

Once modified the model I make a comparison between the results of my model and the data field.

Lots of values are available, for different inlet turboexpander pressures and different percentage of inlet guided vane opening.

Along the whole day are measured lots of data, from 9 in the morning until 19 in the night, every 15 seconds. In this way, we are able to understand how the data change along the whole day, and what is its behavior.

Many data are collected and the one I'm more interested in are:

- Suction Pressure and suction Temperature HP and LP.
- Discharge pressure and discharge temperature HP and LP.
- Mass flow for HP and LP.
- Expander efficiency for HP and LP.
- Expander gas Power for HP and LP.

In the plant these data are measured in different ways.

For measuring temperature are used thermocouples. For example, in the piece of piping between HP and LP are inserted 4 thermocouples, positioned at 90 degrees one to each other, and another one that is a "well thermocouple". Thermocouples are inserted in wells for reason of maintenance, capacity and strenghtness.

Thermocouple are widely used because are economics, standardized, easy to substitute, and can measure a high range of temperatures. The measurement must be done in a hot zone, where the temperature is different from the cold zone, for actuating the compensation.

A problem of these objects is the accuracy. Being these devices nonlinear, is hard to obtain systematic errors lower than 1 Celsius. (J. M. Kallfelz, 2013)

The mass flow is measured using a drilled orifice, where passes the liquid or gas flow.

When the liquid flows, assumes a speed and a pressure, and when it reaches the orifice, the fluid is forced to pass through it. The maximum point of convergence is just after the hole, and is called point of “contracted vein”.

Naturally passing through this point, the values of pressure and speed, change.

Once the fluid passes the point of “contracted vein” pressure and speed change once more.

Measuring the difference of pressure of the fluid between the normal size of the pipe and the “contracted vein” point, we can obtain both mass flow and volumetric flow.

The total power is calculated using a wattmeter. The wattmeter is an instrument which measures the active electrical power generated on an electrical section It is positioned just after the generator, and calculates the power. (D. B. Mann, 1983)

The efficiency is calculated using the formula $\eta = \tau * 2 * \frac{U}{C}$

The pressure is calculated using transducers, which are able to measure the pressure of the working fluid.

Are located many transducers in the whole system, but now we are interested in the ones located before and after the high and low pressure expanders. The transducers are not on the pipe, but far from them.

They are connected to the piping through a “tubing”, which is a tube of 10 mm made of steel, that connects the transducer with the pipe, and the gas flows until the instrument through a small hole of 4 mm.

Analyzing the turboexpander in the complete Hysys model I have followed the following steps:

1. Add in the calculation page the value of $C_{is} = \sqrt{2\Delta h_{is}}$
2. Change the formulation of Tau, and introduce the equation found with the map creation.
3. Change the formula for finding the Torque $T = \tau * m * r * \sqrt{2\Delta h_{is}}$
4. I set the value of IGV as the one of the field data, and then change HP and LP.
5. Compare the values of the dynamic model with the one of the field data. The values I’m interested in are Total power and secondly efficiency.

For understanding the perfect modulization of the whole plant we should understand how the %IGV of the high-pressure and low-pressure expanders are connected.

In the previous model the LP opening was described by a practical equation which had been tested on similar plants.

But that equation wasn’t reliable for turboexpanders of different plants, and gave some uncertainties in the results. For this reason, I’ve decided to re-write it for this plant. During the test of the plant,

usually, the change of the %IGV is manual, so the operator can change as prefers the opening of the guided vanes, for understanding how the machine behaves, and for finding the ideal point of the LP opening related to the HP opening.

But once the plant starts working, the operator is not going to change manually anymore the %IGV, because they are controlled by a control system.

The % IGV is strictly connected to the total gas power. If we want to increase, or decrease the power, we must act over the opening of the inlet guided vane of the HP.

The LP opening instead, are fundamental for dividing the gas power between the HP and the LP.

I've tried to find a unique law that would have connected them, using the nominal map.

This map reports the pressure at the condenser and the opening of the inlet guided vane of the HP, with the opening of the inlet guided vane of the LP.

In this nominal map, the percentage used for indicating the opening of the IGV is the "mechanical" opening, so it goes from 0 to 100.

Are available even the maximal and the minimal map, which tell us the field of clearance of the %IGV where we can move.

All the values of these maps are data field, that have been tested.

For finding a good equation, I have analyzed many values changing 3 different pressures at the condenser, and analyzing the HP percentage of IGV from 15% to 80%.

In this way, I've found the equation that connects the HP opening with the LP opening for all the different pressures.

Usually after a certain opening value, between 70% and 80%, the initial pressure goes below the limit pressure, so there are not any more reliable results.

The values below 15% and over 80% are not calculable, because in those cases the plant can't work in good conditions, caused by the vibrations of the wheel that occur at some %IGV.

This method for finding the equation of the LP %IGV can be used for every other plant, but naturally the equation will be different.

$$P_{\text{cond}} = 1,36 \text{ bar}$$

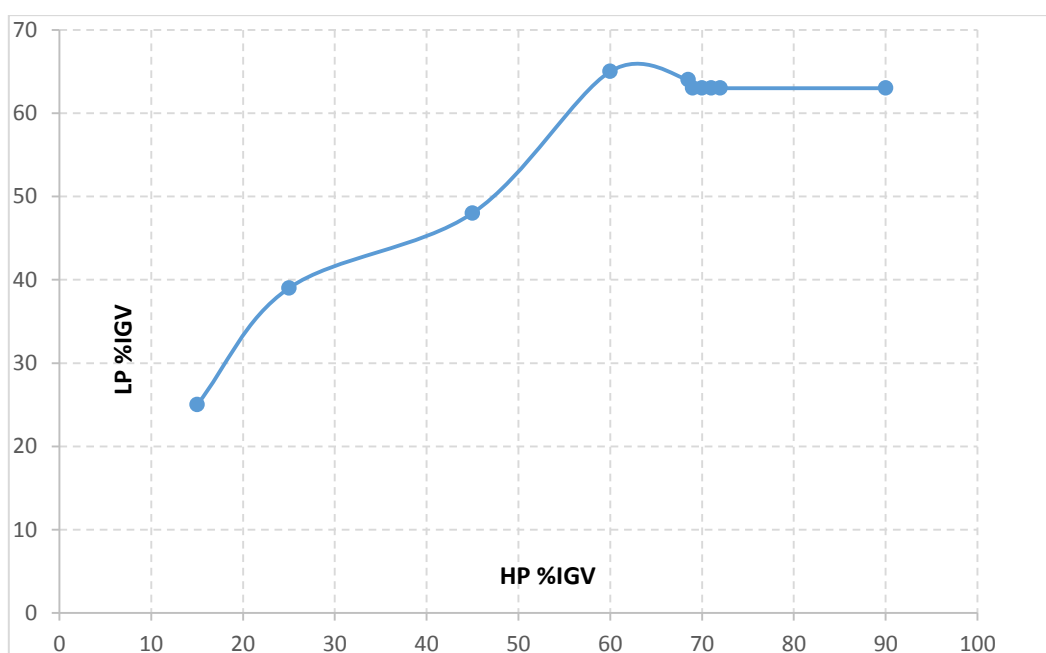


Figure 9-1 Behavior of LP %IGV related to HP %IGV and $P_{\text{cond}} = 1,36 \text{ bar}$

$P_{cond} = 1,62 \text{ bar}$

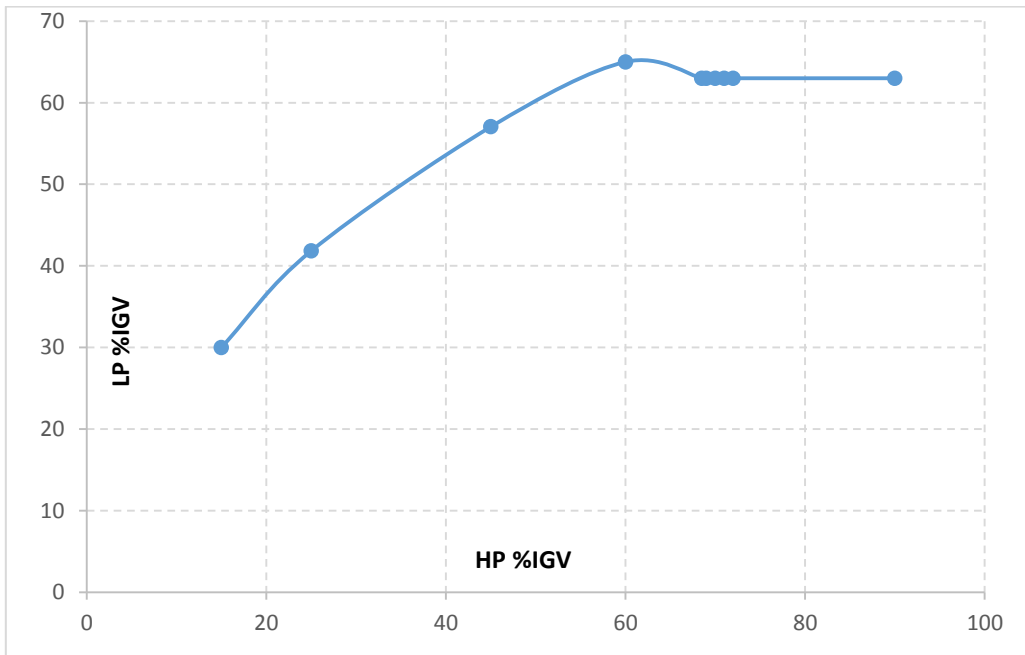


Figure 9-2 Behavior of LP %IGV related to HP %IGV and $P_{cond} = 1,62 \text{ bar}$

$P_{cond} = 2,10 \text{ bar}$

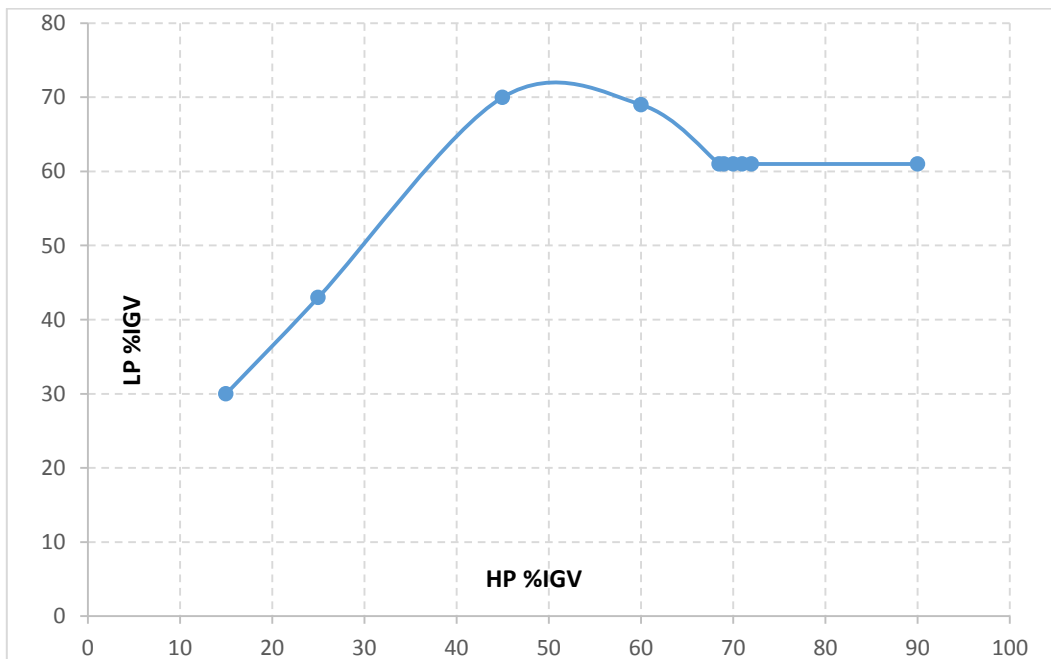


Figure 9-3 Behavior of LP %IGV related to HP %IGV and $P_{cond} = 2,10 \text{ bar}$

Looking at the different graphs we can see that the maximum opening of the LP corresponds to the opening of 62% of the HP expander, in the first two graphs, while in the third one the maximum opening of the LP is 50%.

After the value of 70 we have always the same value of LP opening, for all the graphs.

Increasing the value of %IGV of the HP, the pressure at the inlet (P_{00}) decreases, and after the nominal point the value goes below the limit layer.

Being that the plant can't work in good condition, due to the vibrations, on the field hasn't been tested the turboexpander for %IGV of the HP higher than 70.

This is the reason why we have always the same value. The same thing can be said for all the values below 15%.

Once found the equation for every case, I make the average of the three equations for having a unique one that connects HP and LP.

The equation is:

$$\text{Meccanical } IGV_{LP} = -0,00594 * IGV_{HP}^2 + 1,0141 * IGV_{HP} + 20,650$$

Now we can insert this equation in the model.

Later, I have analyzed 5 different points, matching the different results between the model and the field measurement.

I have chosen these points, trying to have different values of IGV in order to understand if the improvement of the model would be a casual behavior, or not.

	%IGV HP	P_2
1	45	1,88
2	45	2,88
3	60	2,13
4	68,5	1,44
5	71,81	1,373

Table 19 5 points of analysis

As explained before, for every point are measured values every 15 seconds, from 9 in the morning until 19 in the evening.

Naturally during the whole day, the values of %IGV, both HP and LP, change, and the same thing can be said for the P_{00} , and for other values.

How to decide which values should be taken?

Are available lots of graphs. The most significant graphs to be taken in consideration are the vibrations of each expander, the LP wheel vibrations, the HP wheel vibrations, the HP and LP power, and the axial thrust.

We have to choose the %IGV of HP and P_2 in order to have the lower values of vibrations, for not ruining the expander, and for having the better performances.

9.1. DATA MATCH

Once inserted the % IGV, that modifies the inlet pressure, and having modified the pressure at the exit of the wheel, I can make the comparison between the old model and the new model values compared with the data field.

For modifying the outlet pressure of the low-pressure wheel, we modify the exchange coefficient (U) of the condenser. This factor contains all the conduction factor of heat.

$$Q = U * A * \Delta T$$

We can change the value $U*A$, where A is the area of the condenser. Increasing $U*A$, and checking that Q doesn't change, ΔT decreases, and if it decreases even the pressure decreases. Changing this data naturally change even the rest of the system but all the data are under control, thanks to the use of solvers.

In the tables, there are different values, and for every value we have the data field, the model measurement, the difference between them and finally the percentage difference.

Naturally the comparison will be done between the old model and the new one, for understanding if the changes brought have improved the model.

For understanding if the model modified is better or not than the previous one we should check the total gas power.

Is important to underline that the total gas power is not the total power produced by the plant.

The total power produced will be a little bit lower.

The total gas power is produced by the high-pressure wheel and by the low-pressure wheel, then passes through the gear box, a box of gears that connects the wheel to the generator, and then to the generator, and naturally we will have some losses.

So, the total power is calculated multiplying the total gas power with the efficiency of the gear box, and the efficiency of the generator.

$$P_{gen} = P_{gas} * \eta_{gen} * \eta_{gb}$$

η_{gen} = Efficiency of the generator

η_{gb} = Efficiency of the gear-box

P_{gas} = Power of the gas

P_{gen} = Power of the generator

This is the most important value, that make us understand if the model has improved or not. For what concern the single gas power of high pressure and low pressure, we can't completely trust on the data field, so we can't make an appropriate comparison. This happens because the thermocouples placed on the pipe between the two expanders measure the temperature with an uncertainty of 5-6 °C, and so changing the intermediate temperature, the power and efficiency of the single expander is not calculated in the correct way, and should be re-equalized.

In this section of the pipe there are 4 thermocouples, and all of them measure the same temperature, with a difference between 0-1 °C.

		NEW MODEL			OLD MODEL		
		UNITS	REF VALUE	HYSYS MODEL	UNITS	REF VALUE	HYSYS MODEL
% 45 IGV HP $P_2 = 1,88$	Tot gas				Tot gas		
	Power	kW	9431	7680,10	Power	kW	9431 6238
% 45 IGV HP $P_2 = 2,88$	Tot gas				Tot gas		
	Power	kW	9431	6641,86	Power	kW	9431 3334,003
% 60 IGV HP $P_2 = 2,13$	Tot gas				Tot gas		
	Power	kW	11413	10730,27	Power	kW	11413 9740,25
% 68,5 IGV HP $P_2 = 1,44$	Tot gas				Tot gas		
	Power	kW	16136	15433,35	Power	kW	16136 14435,06
% 71,81 IGV HP $P_2 = 1,373$	Tot gas				Tot gas		
	Power	kW	15325	15720,16	Power	kW	15325 15759,32

Table 20 Total power data match

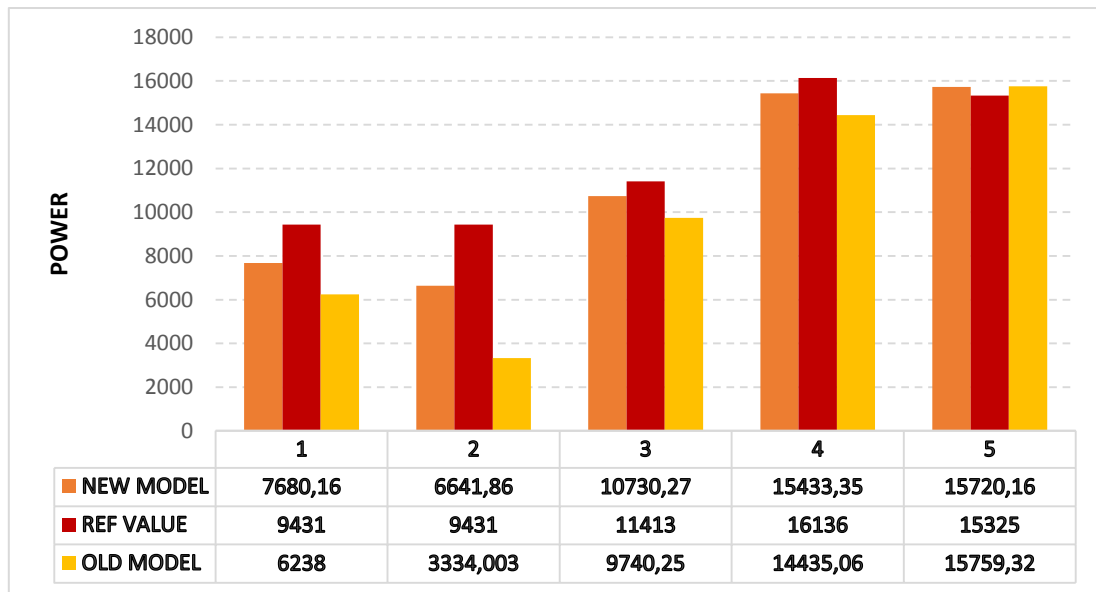


Figure 9-4 Power scheme

For all the cases taken in consideration, the total gas power calculated by the new model is predicted better than the old model.

In some cases, that are strongly off-design, as for example when the %IGV = 45 and $P_2 = 2,88$ bar, the value of the total gas power measured is strongly improved, but anyway, even if improved, we can't define that value satisfactory.

For what concern the point with a %IGV value of 60, or 68.5, which are both values near the nominal point, the old model predicts the total power with a low uncertainty, while the new one improves this uncertainty.

In the nominal point (71,81), as we can see from the table, the total gas power predicted by the new Hysys model is better than the one predicted by the old Hysys model, related to the reference value. This improvement has been possible because the new equation, that we have inserted of the adimensional torque, that modifies the total power gas, has been settled analyzing CFD values with a percentage opening of the inlet guided vanes of the HP between 75 and 120 (we are speaking of aero opening).

At this point we can affirm that the old model was well designed for predicting the values at the nominal point, but when we are going to predict the behavior of the turboexpander far from it, the model begins to have some problems.

The new model predicts, as well as the old one, the values at the nominal point, but predicts better the points near the nominal point.

For what concern the %IGV that are powerfully off-design, the value of the total gas power is predicted better, but anyway, the value is far from being reliable.

What we have obtained is a good improvement for the prediction of the total gas power, but anyway the model should be still re-analyzed and improved, for being able to predict the values even in off-design situation.

9.2. BEHAVIOR OF THE POWER RELATED TO THE IGV

Once changed the formula for calculating the total power, for completeness we will try to evaluate how it changes in the interval of %IGV.

We keep constant the pressure at the condenser, for example equal to $P_{cond} = 1,44$, and analyze the change of the initial pressure and of the total power.

We are going to make this analysis even if we do not have the values of the data field for all these different percentage opening of the inlet guided vanes.

The value of the pressure at the condenser is kept always equal because this pressure is connected to the temperature of the refrigerant fluid.

So being the temperature of the fluid refrigerant (air in this case) always the same, even the condenser pressure keeps constant.

For what concern, the mechanical opening of inlet guided vanes we take 6 values, even if, as said before, the last two values, which have an high value of %IGV, are only used for making a theoretical case.

Only in rare situations the percentage of opening of the IGV overcomes a value between 70-80 %, and when that value is overcome, the pressure at the inlet of the HP decreases.

A controller has been thought in order to block the %IGV opening, for not stopping the whole plant.

We will only change the opening of the inlet guided vane of the high pressure expander, because is connected to the percentage opening of the LP expander.

The % IGV are:

$$P_{cond} = 1,44 \text{ bar}$$

HP %IGV--MECH	HP %IGV--AERO	POWER	P_{00}
25	32,5	3734	40,05
50	65	10600	40,28
68,5	62,22	15230	40,09
77	100	15310	35,75
90	117	15100	32,27
100	130	14690	28,8

Table 21 Different power values for pressure at the condenser equal to 1,4 bar

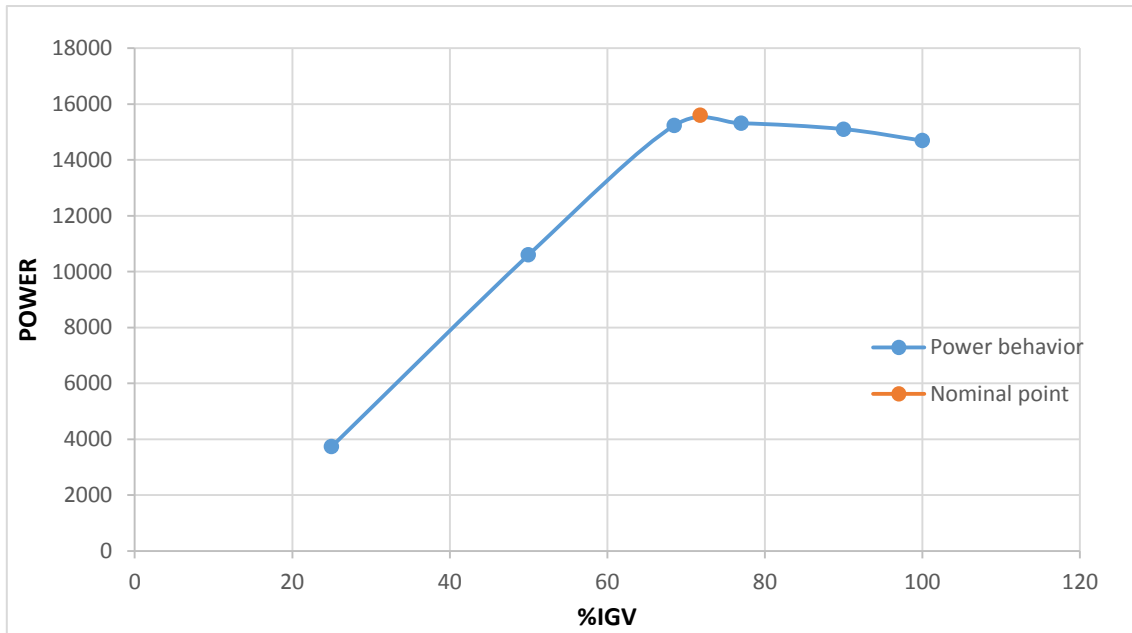


Figure 9-5 Graph of power related to %IGV with $P_{cond} = 1,44$

The total gas power value depends on, mass flow, eta and Δh .

As we know, increasing the %IGV we are going to increase the quantity of mass flow that enters in the nozzle.

At the same time, increasing the %IGV, and keeping the P_{cond} at the same value, the pressure at the inlet of the nozzle decrease. Decreasing the P_{00} will even decrease the value of the enthalpy.

From the graph, we notice that we have a constant grown of the total power with the increase of the %IGV until this last value reaches the quantity of 69%. Once passed that value the total power begins decreasing slowly.

One of the causes is an increase of losses after a certain layer; in fact, to the usual losses are added even secondary losses.

But the main cause is due to the efficiency. As we can see from a graph that has been made taking in consideration data field, monitoring the values of efficiency and mass flow for both HP and LP, when the mass flow overcomes a value, the efficiency begins decreasing.

It increases until that value and then it decreases.

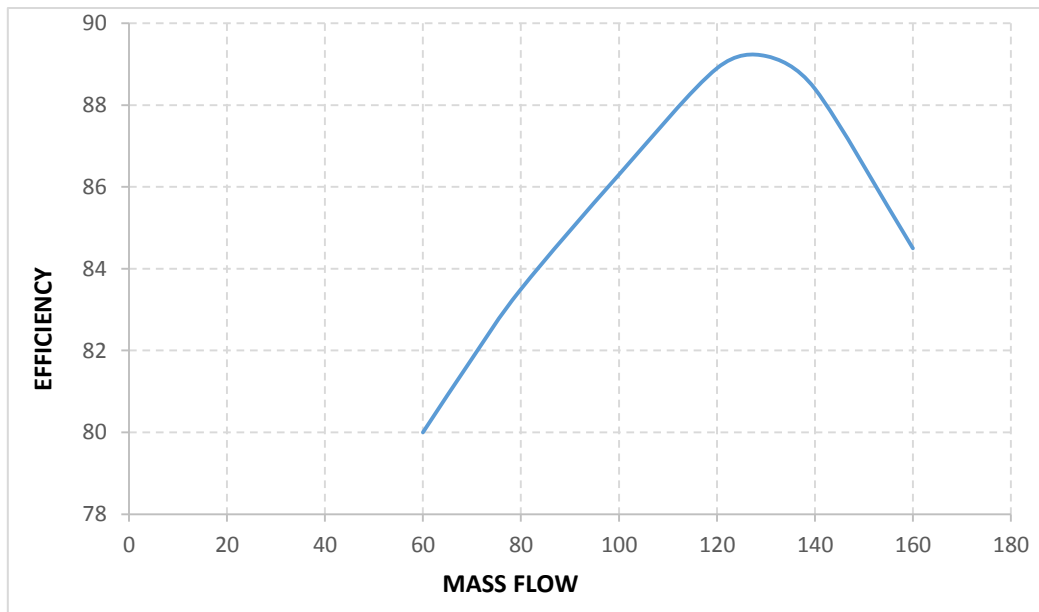


Figure 9-6 Graph of the mass flow related to the efficiency

The value of mass flow after which the efficiency decreases, corresponds to the % IGV of 70.

The total gas power value, as said before, depends on mass flow, eta and Δh .

When the %IGV increases, until the value of 70%, the mass flow and eta increase, while Δh decreases. After that limit value only the mass flow increase, while Δh and eta will decrease.

For this reason, the total gas power increases until the value of 70% and then decreases.

9.3. CONCLUSION

We can affirm that the work done has given the expected results, being now the model able to calculate more precisely the total gas power.

The main result of the activity has been the definition of a standard format for creating the turboexpander maps for the dynamic simulation.

I can assert to have found an equation of the adimensional torque, dependent from two factors, that predicts the value with a lower uncertainty, given the geometry of the turbine:

- 1) We start from the CFD, the primary source, which is used for settling the static model.
- 2) Once settled the static model (map generator), I make different tables changing values of $[u/c]$ and $[\%IGV]$.
- 3) Take note of the values of τ related with $[u/c]$, for every single percentage opening of IGV, obtaining different equations which have different values for $u/c=0$.
- 4) I find out a unique value of τ for $u/c=0$, making the average of the previous values of τ for that point. Once obtained it I can rewrite every single equation making the straight-line pass through the final unique point and the initial points.
- 5) We find out the equation $\tau = a - b(y) * x$

We have even proved that the behavior of the gas power related to the $\%IGV$ is reliable and believable, even if we do not have any data field to compare with.

We notice that after the implementation, the Hysis model provides gas power values that are reasonable, in an interval that goes from the maximum operativity until the minimum.

One of the most important results we have is that the turboexpander behaves in a continuous way, without variations of torque related to the $\%IGV$.

10. FINAL CONCLUSIONS

The first objective of the work was the validation of an alternative stationary model, and the creation of performances maps for analyzing some points where the CFD is not done, and we can affirm to have found a valuable model that describes the behavior of a turboexpander using 5 calibration parameters described by equations.

We have validated the alternative model for analyzing points where the CFD is not present, starting from some CFD stationary data.

For what concern the second part of the work, the objective was to find a method to model the outputs with transference function, in off-design conditions, concentrating our attention on the total gas power, and to make a comparison with data field obtained from experimental campaign on a real plant.

We can affirm that the work done has given the expected results, being now the model able to calculate more precisely the total gas power.

The main result has been the definition of a standard format for creating the turboexpander maps for the dynamic simulation, as explained in detail in the conclusion of the chapter 9.

I can assert to have found an equation of the adimensional torque which predicts the value with a lower uncertainty, given the geometry of the turbine.

We have even demonstrated that the behavior of the gas power related to the %IGV is reliable and believable, even if we do not have any data field to compare with.

We notice that after the implementation, the Hysis model provides gas power values that are reasonable, in an interval that goes from the maximum operativity until the minimum.

For what concern the future developments of my thesis work:

The model can be further improved, and this should be done using the same approach I have used with the other two outputs.

I had begun the same work with the mass flow but it has not been concluded.

11. APPENDIX: MASS FLOW

Once defined the equation of the adimensional torque, for having a total complete design of the turboexpander, I should define the mass flow related with the inlet guided vanes and with the u/c.

Until now we have considered the choked nozzle, so the Mach value in the throat equal to 1.

For completeness, I should find the link between IGV, u/c and the pressure between the outlet of the nozzle and the inlet of the wheel.

Previously we have always taken this data from the CFD.

My purpose is to find the value of the molar specific heat (C_p), calculating it using the formula related to the POD and P_{02} , and comparing it with the one calculated using a new formula related to IGV and u/c.

Once checked the molar specific heat percentage difference, I will be able to calculate the value of the pressure between nozzle and wheel (POD), and then even the mass flow in that point, that is not calculable in other ways.

As done before, I make the study for the nine points of the high pressure taking the values I need from the CFD post-processed data.

I need the sequent values:

- D_{2s} → Shroud diameter at wheel outlet.
- D_{2h} → Hub diameter at wheel outlet.
- ρ_{02} → Density at wheel outlet.
- ω → Tangential speed.
- D_1 → Inlet wheel diameter.
- POD → Intermediate pressure between nozzle and wheel.
- P_{02} → Total pressure at wheel outlet.

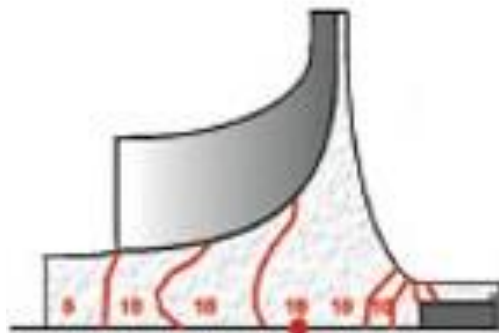


Figure 11-1 Wheel profile

In this way, I can calculate

$$Cp (1) = \frac{P_1 - P_{02}}{\frac{1}{2} * \rho_{02} * (u_1^2 - u_2^2)}$$

P_1 is the pressure previously called POD . The other values are calculated in this way:

$$u_1 = \omega * \frac{D_1}{2}$$

$$u_2 = \omega * \left(\frac{D_h + D_s}{4} \right)$$

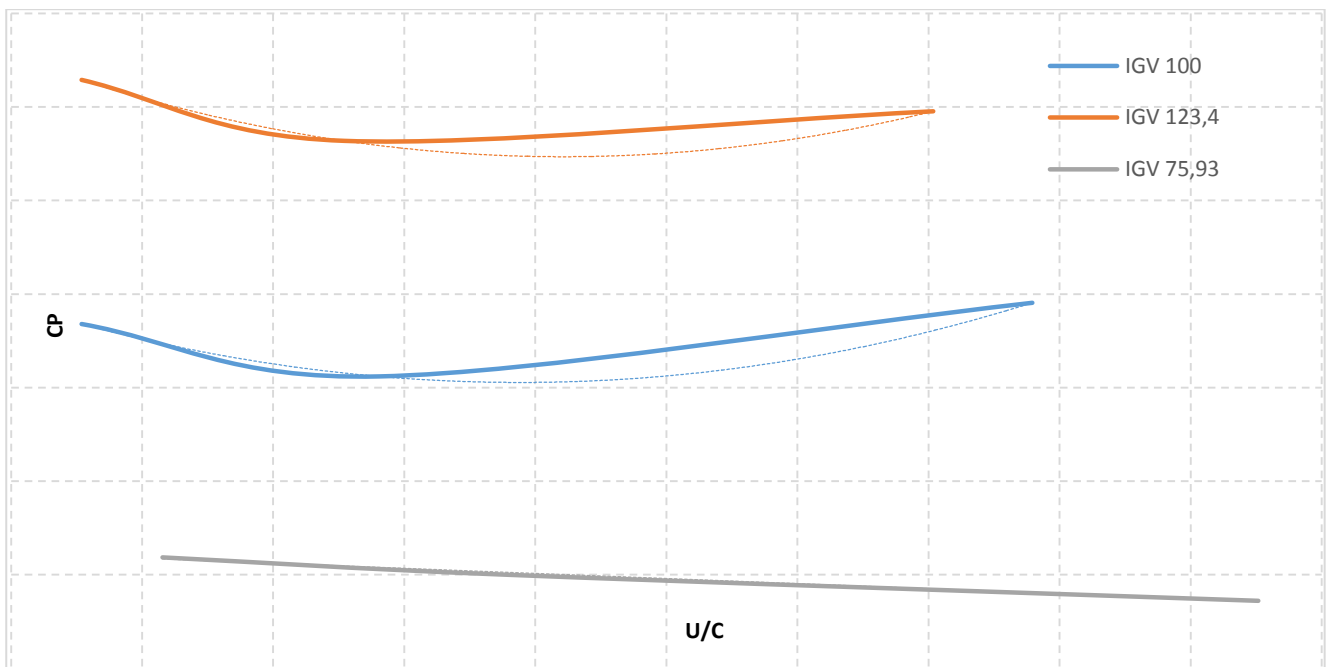


Figure 11-2 Graph of U/C related to Cp

I've graphed the values of u/c related to the values of Cp, taking in consideration the percentage of inlet guided vanes. I take note of the coefficients of the equations, and then I'll re-graph those values related to the IGV.

	C1	C2	C3
123	8469,861	-10575,5	3302,448
100	89,060	-121,674	42,767
76,85	22,959	-32,845	12,611

Table 22 Table of coefficients values related to the IGV

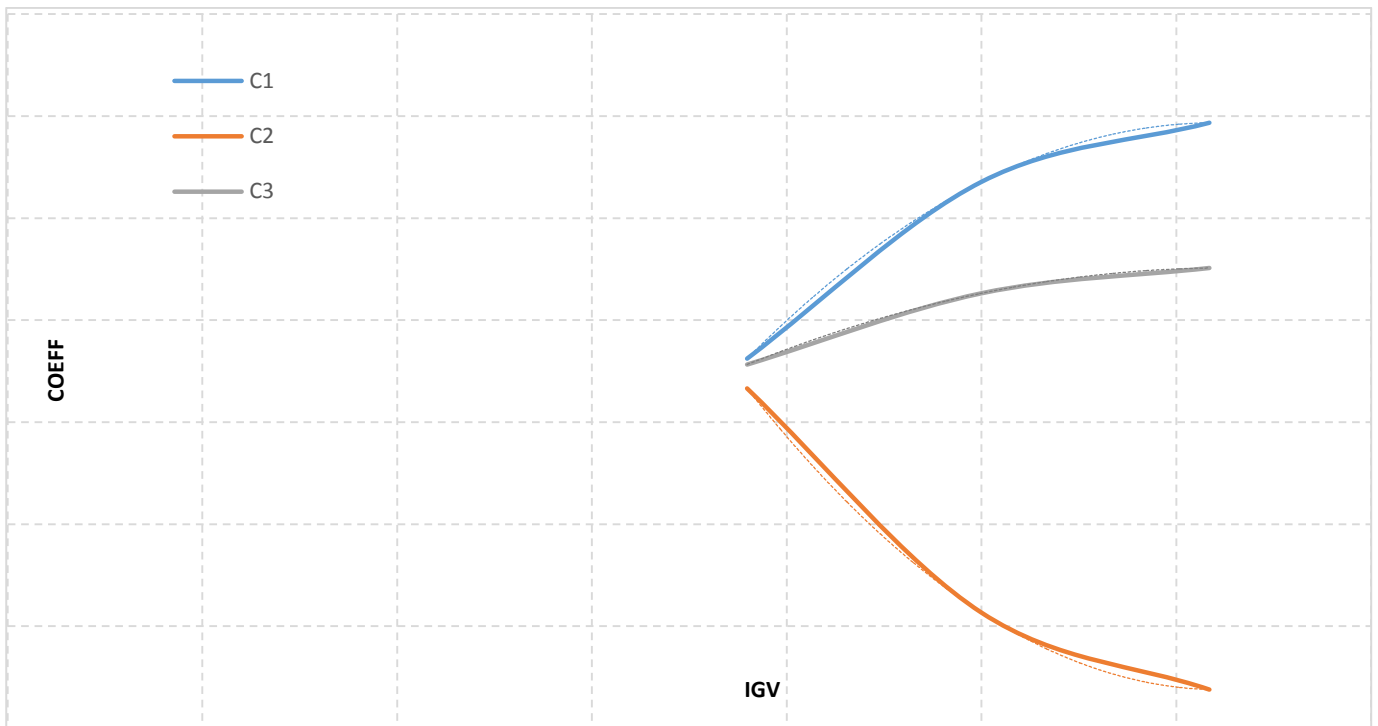


Figure 11-3 Graph of IGV related to the coefficients

Once having done even this graph, I take the values of the lines and finally I can write the definitive equation of the C_p related to IGV and u/c .

$$\begin{aligned}
 C_p(2) = & (-0,1989 * IGV^2 + 49,404 * IGV - 2579,55) * \left(\frac{U}{C}\right)^2 \\
 & + (0,2489 * IGV^2 - 62,048 * IGV + 3242,43) * \left(\frac{U}{C}\right) \\
 & (-0,0777 * IGV^2 + 19,482 * IGV - 1018,289)
 \end{aligned}$$

The values of $C_p(1)$ and $C_p(2)$ have only a small uncertainty, less than 3%, so we can affirm that the equation found is valid.

Now we are able to calculate the POD, using the inverse formula of $C_p(1)$, and in this way connecting the value of the pressure to the geometry of the turboexpander.

$$POD = P_1 = P_{02} + \frac{1}{2} * \rho_{02} * (u_1^2 - u_2^2) * C_p$$

We are able in this way, using input conditions, to calculate the intermediate pressure, and so even the mass flow.

For calculating the mass that flows through the nozzle, we are going to use the sequent equation, that includes other values as:

- $T_{00} \rightarrow$ Nozzle inlet temperature
- $R \rightarrow$ Gas constant
- $\gamma \rightarrow$ Coefficient of adiabatic dilatation
- $\varepsilon_{nozzle} \rightarrow$ Nozzle loss coefficient
- $C_v \rightarrow$ Nozzle flow coefficient
- $A_{geom} \rightarrow$ Nozzle geometrical area

$$\mathbf{m} = \frac{P_1}{\sqrt{RT_{00}}} * \sqrt{\frac{2 * \gamma}{\gamma - 1}} * C_v * A_{geom} * \sqrt{\left(\frac{P_{00}}{P_1} - \varepsilon * \frac{P_{00}}{P_1}\right)^{\frac{\gamma-1}{\gamma}}} * \sqrt{\left(\frac{P_{00}}{P_1} - \varepsilon * \frac{P_{00}}{P_1}\right)^{\frac{\gamma+1}{\gamma-1}}}$$

For finding this formula we make several transformations:

$$\mathbf{m} = \frac{P_{01}}{\sqrt{RT_{01}}} * \sqrt{\gamma} * A * \frac{M_1}{\sqrt{\left(1 + \frac{\gamma-1}{2} * M_1^2\right)^{\frac{\gamma+1}{\gamma-1}}}}$$

$$M_1 = \sqrt{\frac{2}{\gamma - 1} \left(\left(\frac{P_{01}}{P_1} \right)^{\frac{\gamma-1}{\gamma}} - 1 \right)}$$

$$\mathbf{m} = \frac{P_{01}}{\sqrt{RT_{01}}} * \sqrt{\gamma} * A * \frac{\sqrt{\frac{2}{\gamma-1}} * \sqrt{\left(\frac{P_{01}}{P_1}\right)^{\frac{\gamma-1}{\gamma}} - 1}}{\sqrt{\left(\frac{P_{01}}{P_1}\right)^{\frac{\gamma+1}{\gamma}}}}$$

$$\mathbf{m} = \frac{P_1}{\sqrt{RT_{01}}} * \sqrt{\frac{2\gamma}{\gamma-1}} * A * \left(\frac{P_{01}}{P_1}\right)^{1-\frac{\gamma+1}{2\gamma}} * \sqrt{\left(\frac{P_{01}}{P_1}\right)^{\frac{\gamma-1}{\gamma}} - 1}$$

$$\mathbf{m} = \frac{P_1}{\sqrt{RT_{01}}} * \sqrt{\frac{2\gamma}{\gamma-1}} * A * \sqrt{\left(\frac{P_{01}}{P_1}\right)^{\frac{\gamma-1}{\gamma}}} * \sqrt{\left(\frac{P_{01}}{P_1}\right)^{\frac{\gamma-1}{\gamma}} - 1}$$

$$\varepsilon = \frac{(P_{00} - P_{01})}{(P_{00} - P_1)} \rightarrow P_{01} = P_{00} - \varepsilon * (P_{00} - P_1) \rightarrow \frac{P_{01}}{P_1} = \frac{P_{00}}{P_1} - \varepsilon * \left(\frac{P_{00}}{P_1} - 1\right)$$

$$\mathbf{A} = C_v * A_{geom}$$

$$T_{01} = T_{00}$$



$$m = \frac{P_1}{\sqrt{RT_{00}}} * \sqrt{\frac{2 * \gamma}{\gamma - 1}} * C_v * A_{geom} * \sqrt{\left(\frac{P_{00}}{P_1} - \varepsilon * \frac{P_{00}}{P_1}\right)^{\frac{\gamma-1}{\gamma}}} * \sqrt{\left(\frac{P_{00}}{P_1} - \varepsilon * \frac{P_{00}}{P_1}\right)^{\frac{\gamma+1}{\gamma-1}}}$$

The inlet temperature is constant for every case, so as the gas constant and the coefficient of adiabatic dilatation. The other three values instead change with the change of the vanes. For being precise we calculate the pressure in the nozzle throat, where the Mach value is equal to 1.

$$\text{If } P_1 > P' \rightarrow P_1 = P_{OD}$$

Otherwise, if $P_1 < P'$

$$P_1 = \frac{P_{00}}{\left(1 + \frac{\gamma - 1}{2}\right)^{\frac{\gamma}{\gamma-1}}} = \frac{P_{00}}{\left(\frac{\gamma + 1}{2}\right)^{\frac{\gamma}{\gamma-1}}}$$

If the value of P_1 is lower than P' , in the equation of the mass flow we must substitute the pressure between nozzle and wheel with the pressure in the throat of the nozzle. Otherwise we'll leave the value of P_1 .

Acting like this we have now an equation of the mass flow dependent from the geometry of the turbine.

For understanding if the equation found is valuable we must compare it with the mass flow value of the CFD, and if the percentage difference is lower than 3%, it can be validated.

m	116,841	116,84	116,87	144,29	144,29	144,29	88,622	88,622	88,622
m_old	116	116	116	143	143	143	89	89	89
Difference %	0,720	0,720	0,751	0,894	0,894	0,894	0,426	0,426	0,426

Table 23 Percentage difference between the mass flow calculated in different ways

Being the difference lower than 3% for every one of the 9 cases, we can affirm that the equation is valuable.

Once the right equation has been found, we should work on the dynamic model, but unfortunately there has not been enough time for proceeding the work. This is certainly one of the future step to do for improving the model.

12.BIBLIOGRAPHY

- (s.d.). Tratto da General Electric.
- Benson, R. S. (1965). *An analysis of the losses in a radial gas turbine*.
- Block, H. (2001). Turboexpanders and process applications.
- Burrato, A. (2012). Development and applications of Oregon™, Waste Heat Recovery Cycle.
- Chen H., G. D. (2010). A review of thermodynamic cycles and 148 working fluids for the conversion of low-grade heat.
- D. B. Mann, J. A. (1983). Gas Orifice Meter Discharge Coefficients As Determined By Mass Flow Measurements.
- D. Y. Peng, D. B. (1976). A new two-constant equation of state.
- D.J., W. (1983). "Chlorocarbon emission scenarios: potential impact on stratospheric ozone.
- E. Macchi, M. A. (2016). Organic Rankine Cycle (ORC) Power System.
- E. Macchi, M. A. (s.d.). Valutazione di cicli termodinamici innovativi per applicazioni con caldaie a sali fusi alimentate a biomassa legnosa.
- E.H. Wang, H. Z. (2011). Study of working fluid selection of organic Rankine cycle (ORC) for engine waste heat recovery.
- Gaetano Chinnici, M. D. (2015). Analysis of biomass availability for energy use in Sicily.
- Gas., G. O. (s.d.). Waste heat recovery system for GE and other OEM gas turbines: Turboexpanders and process applications.
- General Electric, T. g. (s.d.). *Turboexpander-Generator*.
- Ghasemi, H. (2013). Modeling and optimization of a binary geothermal power plant.
- Hung T.C., S. T. (1997). A Review of Organic Rankine Cycles (ORCs) for the Recovery of Low-Grade Waste Heat.
- I. Papes, J. D. (2015). New insights in twin screw expander performance for small scale ORC systems from 3D CFD analysis.
- J. M. Kallfelz, R. K. (2013). Advanced reactors: Physics, Design and Economics.
- K. K. Botros, C. H. (2015). "Assessment of Recoverable vs Unrecoverable Degradation of Gas Turbines Employed in Five Natural Gas Compressor Station.
- Kang, S. H. (2013). Design and experimental study of an ORC and radial turbine using R245fa working fluid.
- M. Imran, M. U. (2016). Volumetric expanders for low grade heat and waste heat recovery applications.
- Muhammad Ihram, M. I.-S. (2015). Volumetric expanders for low grade heat and waste heat recovery applications.

- Oudkerk, J. F. (2015). Experimental performance of a piston expander in a small-scale organic Rankine cycle.
- Pedro J. Mago, L. M. (2007). An examination of regenerative Organic Rankine Cycles using dry fluids.
- Peng, R. F. (1986). Equations of state and Constitutive equations. *Journal of Rheology*.
- Quoloni, S. D. (2012). Working fluid selection and operating maps for Organic Rankine Cycle expansion machines.
- R. Capata, E. Z. (2014). Preliminary Design of Compact Condenser in an Organic Rankine Cycle System for the Low Grade Waste Heat Recovery.
- R. Vescovo, N. P. (2009). Applicazione di Cicli ORC a Recupero Termico da Processi Industriali. (s.d.). Radial expander design for an engine organic rankine cycle waste heat recovery system.
- Ramajia, J. (2012). R-22 refrigerant phase out and its repercussions.
- S. Quoilin, M. v. (2013). Techno-economic survey of organic rankine cycle systems. *Siemens Organic Rankine Cycle Waste Heat Recovery with Orc*. (s.d.).
- Soave, G. (1972). Equilibrium constants from a modified Redlich-Kwong equation of state.
- Sotirios Karellas, A. S.-D. (2014). Influence of supercritical orc parameters on plate heat exchanger design.
- Sunetra Sarkar, K. V. (2013). Influence of pitching angle of incidence on the dynamic stall behavior of a symmetric airfoil.
- Waals, J. D. (1988). On the continuity of the gaseous and liquid states.
- Weis, A. P. (2015). Volumetric expanders versus turbine- which is the better choice for small ORC plants?